STABILITY OF COARSE MINE WASTE DUMPS

TREVOR STUART HUGHES

A dissertation submitted to the Faculty of Engineering, University of the Witwatersrand, Johannesburg, in partial fulfillment for the Degree of Master of Science in Engineering.

JULY, 1984

D E C L A R A T I O N

I, Trevor Stuart Hughes hereby declare that this is my own unaided work and I have not submitted this dissertation to any other University for degree purposes.

THughes

2nd day of July 1984

ABSTRACT

It is economically desirable to build dumps of coarse mine waste as high as possible. A review of available literature indicated that a significant decrease in the strength of coarse material occurs at high stress levels. A literature survey was conducted to establish possible dump failure modes and methods of slope stability analysis appropriate to dumps.

Consolidated, drained triaxial tests on several mine waste materials have shown that above a normal stress of 1600 kPa, slight curvature of the Mohr strength envelope occurs. However, sample stability analyses show that there is little or no difference in factors of safety for typical dump slopes, obtained by using a constant average friction angle, or by using variable friction angles derived from a power equation which describes the curved strength envelope. Thus it is concluded that the curvature of the strength envelope, has little influence on the factor of safety of dump slopes.

ACKNOWLEDGEMENTS

I would like to express my appreciation to the following:

My supervisor, Professor G E Blight, whose assistance and advice I gratefully acknowledge.

Anglo American for financial assistance and the provision of material for laboratory work. Mr. Ken Lyle from Anglo American for assistance and advice.

The Council for Scientific and Industrial Research and the University of the Witwatersrand, Johannesburg for financial assistance.

Ed Braddock and Gary Bentel for guidance and assistance in the laboratory.

Jean McClean for her patience and friendship in typing this thesis.

Roberto, Stavros, Niko, Mike, Hans and Gary for their friendship and discussion.

My family and Claudine for love and encouragement.

TABLE OF CONTENTS

TABLE OF CONTENTS (Cont.)

TABLE OF CONTENTS (Contd.)

LIST OF FIGURES

LIST OF FIGURES (Contd.)

LIST OF FIGURES (Contd.)

LIST OF FIGURES (Contd.)

LIST OF FIGURES (Contd.)

LIST OF FIGURES (Contd.)

LIST OF TABLES

LIST OF TABLES (Contd.)

LIST OF TABLES (Contd.)

CHAPTER 1 : INTRODUCTION

South Africa has a large mining industry and every year large tonnages of waste material must be disposed of. Waste material consists primarily of two types;

- coarse waste (cohesionless)
- fine tailings (cohesive)

In this dissertation coarse mine waste dumps are considered. The purpose of this dissertation has been to investigate slope stability aspects of dumps with emphasis on the influence of dump height on the shear strength properties of the dump material and dump stability.

To predict the performance of a dump it is necessary to have knowledge of the waste material properties. In Chapter 2 available literature concerning the behaviour of cohesionless materials is reviewed. Trends in shear strength behaviour are discussed with respect to the following factors,

- relative density
- composition (grading)
- particle breakage
- particle size
- interparticle friction
- degree of saturation or water content
- intermediate principal stress

It is economically desirable to construct dumps as high as possible. Present stability analyses are based on the assumption of a linear relationship between the shear strength and the normal stress. In Chapter 2 evidence is presented which shows this assumption to be incorrect for many materials.

The type of instability and the most appropriate stability analysis for a waste dump depends upon a variety of factors. These factors vary from the method of construction to foundation conditions. The following modes of dump failure are discussed in Chapter 3;

- surface or edge slides
- shallow flow slides
- base/foundation failure
- block translation
- circular arc failure
- toe spreading
- blow out

A number of methods for calculating the factor of safety against slope failure of a dump are presented in Chapter 4. The methods use simple equations or stability charts, and tables and assume simplified conditions such as simple uniform slope geometry and uniform material properties. The simplified y=o method is recommended for use in slope stability analysis for dumps. The simplified methods presented are valuable because of their ease of use and potential for pin-pointing likely failure.

In order to investigate the relationship between shear strength and normal stress a programme of standard consolidated, drained triaxial tests has been carried out. The cell pressure was limited to a maximum of 2000 kPa (a normal stress on the failure plane at failure of approximately 3100 kPa). The results of the testing programme are presented and discussed in Chapter 5.

Sample analyses of typical dumps using the failure modes discussed in Chapter 3 and the y=o method of slope stability analysis (Chapter 4) are described in Chapter 6. The analysis uses the strength values obtained from the testing programme and discusses the influence of increasing dump height on factor of safety.

CHAPTER 2 : THE BEHAVIOUR OF COHESIONLESS MATERIALS

2.1 Material Evaluation

To predict the performance of a waste dump, knowledge of the properties of the waste and foundation material is required. Call[1] listed the performance characteristics and the associated material properties as follows:

Performance Characteristic	Material Properties
Stability	Shear strength, density
Settlement	Compressibility
Erodability	Grain size, weathering index
Drainage	Permeability

A more detailed list adapted from Call is contained in Table 1.

2.2 Deformation Characteristics of Cohesionless Materials

The mechanism of deformation in cohesionless material can be subdivided into 3 interdependent deformations;

- elastic deformations in particles and points of contact when the stresses are changed.

- permanent deformations in the form of rearrangement of particles as the particles are displaced in relation to each other and

- permanent deformation due to crushing of particles.

The sum of these deformations determines the volume change. At low stress levels the elastic deformations are small and crushing non-existent, but the influence of these two factors increases with increasing stress level. Bell[10] states that fracturing of particles

TABLE 1 : WASTE EMBANKMENT PERFORMANCE CHARACTERISTICS AND MATERIAL PROPERTIES

Performance Characteristic	Direct material Properties	Indirect Properties
Stability	Shear Strength	Substance Compressive Strength
	Angle of Repose	Substance Shear Strength
	Unit Weight	Specific Gravity
		Gradation
		Particle Shape
		Atterburg Limits
Settlement	Compressibility	
	Unit Weight	
	Void Ratio	Rock Type
		Mineralogy
Drainage	Transmissivity	Soil Classification
Erosion	Grain Size	
	Infiltration Capacity	
	Clay Dispersivity	
	Weathering Index	

in granular soils only becomes important when the stress level exceeds 3,5 MPa. However, this stress level must surely depend on the strength of the particles, soft particles crushing at stress levels much lower than that of hard particles.

Thus the internal shearing resistance of a granular soil is generated by friction developed when grains in the zone of shearing are caused to slide, roll, rotate and deform against each other. In dense materials particles have to move up and over one another during shear and hence the volume increases. This volume increase is associated with an increase in shear strength. The increase in strength is a function of the energy required to expand the material. When the dense sand is sheared, the principal stress difference reaches a peak or maximum, after which it decreases to an ultimate value $(\sigma_1 - \sigma_3)_{ult}$, refer to figure 1. The void ratio-stress curve shows that dense sand slightly decreases in volume at first from e_d (e - dense) and then dilates or expands up to e_{cd} (e_c-dense), where e_c is the critical void ratio. Casagrande[8] called the ultimate void ratio at which continuous deformation occurs with no change in principal stress difference the critical void ratio.

Conversely in loose materials the particles move into closer packing and the volume decreases. When the loose sand is sheared, the principal stress difference gradually increases to a maximum or the ultimate value $(\sigma_1 - \sigma_3)_{ult}$. Concurrently, as the stress is increased the void ratio decreases from e_l(e - loose) down to e_{cl}(e_c - loose), refer to Figure 1.

2.3 The Strength of Cohesionless Materials

As stated previously the strength of a granular soil is generated by the friction developed between the particles and their resistance to deformation. The shear strength that can be developed will thus depend on a variety of factors, some of these being the interparticle friction, the stress level in the material, relative density and the deformation properties of the material.

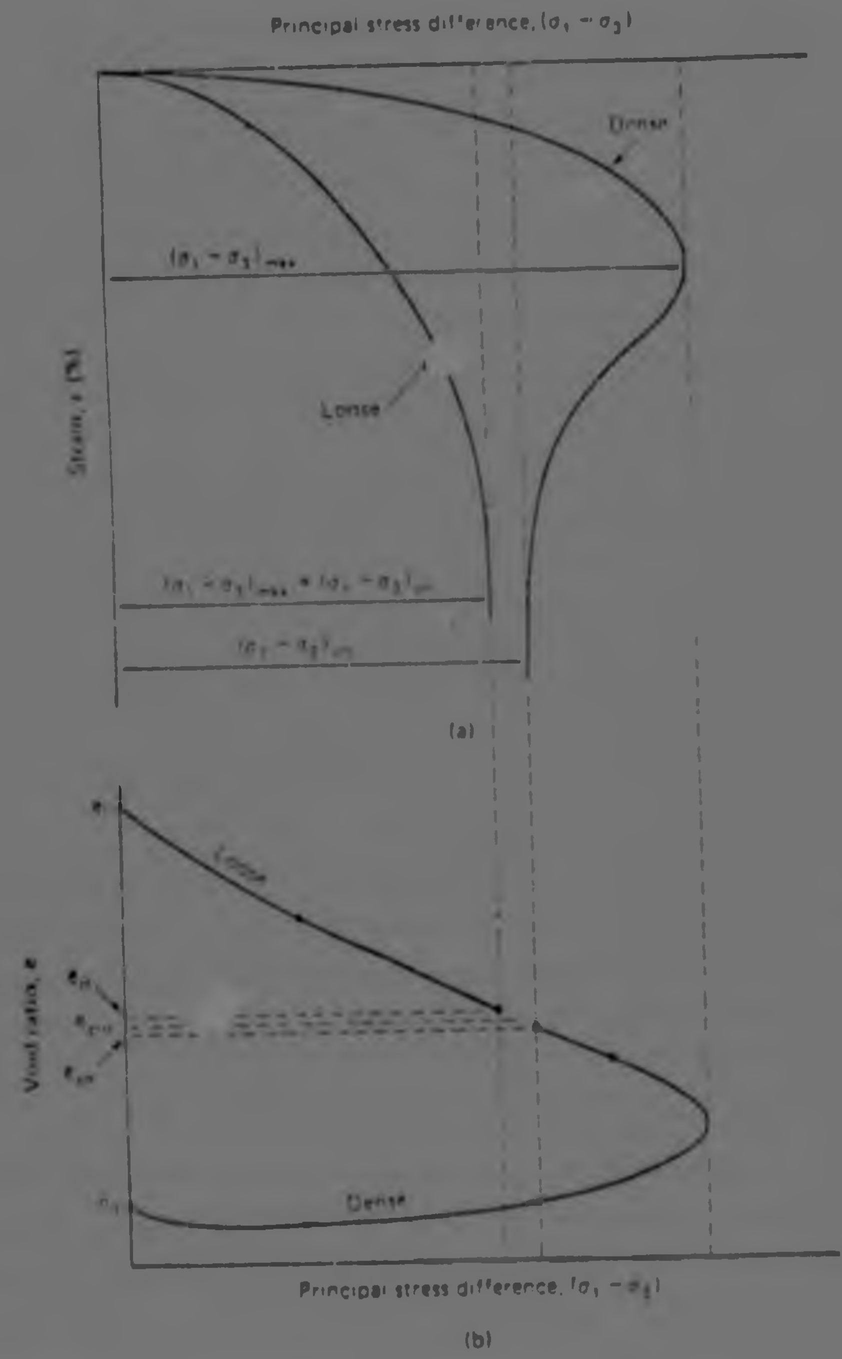

FIGURE 1 : Triaxial tests on "loose" and "dense" specimens of a typical sand : (a) stress-strain curves; (b) void ratio changes during shear

The shear strength of a soil can be calculated using Coulomb's shear strength expression;

$$\tau = c + \sigma \tan \varphi \qquad \text{..........................} \quad (1)$$

where τ is the shear strength
c is the cohesion
σ the normal stress
ϕ the friction angle

Granular material is often assumed to be cohesionless and hence,

$$\tau = \sigma \tan \phi \qquad \text{..........................} \quad (2)$$

Writing in terms of effective stress;

$$\tau = (\sigma - U) \tan \phi \qquad \text{..........................} \quad (3)$$

where U is the pore pressure.

Current stability analyses are based on the above linear equation and this appears to be a reasonable approximation. However, considerable evidence exists that the shear/normal stress relationship is non-linear and this matter will be discussed later in this section.

Marsal[2] performed a large number of triaxial tests on rockfill materials. Analysis of his results shows that gradation, certain physical properties of the grains, average particle dimensions and void ratio, are factors having significant influence on the shear strength. The action of water when an assembly of particles subjected to load is saturated, is not to be disregarded. Marsal came to the following conclusions:

1. The shear strength is larger in well-graded materials with a low void ratio.

2. Materials with similar gradations present an appreciable variation in their strength, probably due to intrinsic characteristics of the particles.

3. The strength of the material decreases as particle breakage increases.

Vesic[5] performed triaxial tests on medium-grained uniform quartz sand. From the preliminary investigations, Vesic found that the strength in the high pressure range (100-1000 kg/cm^2) was not affected by the initial void ratio, and that the strength envelope of this material in this pressure range passes through the origin. For lower pressures (10-100 kg/cm^2) it was found that the strength envelope was curved and the strength was dependent on the initial void ratio. Vesic plotted the secant friction angles ϕs, where ϕs is defined as

$$\phi s = \sin^{-1} \left(\frac{\sigma_1 - \sigma_3}{\sigma_1 + \sigma_3} \right) \quad \ldots\ldots\ldots\ldots\ldots\ldots\ldots \quad (4)$$

versus the mean normal stress at failure. From this diagram, figure 2 , it can be seen that there exists a mean normal stress, beyond which the curvatures of strength envelopes for all initial void ratios vanish and beyond which the shear strength of the sand is not affected by its initial void ratio. Vesic terms this the breakdown stress, because it represents the stress level beyond which all dilatancy effects disappear, and beyond which particle breakage becomes the only mechanism, in addition to simple slip by which shearing displacement in the slip planes becomes possible. Vesic found that this stress appeared to be affected by the numerical composition, gradation and particle shape.

FIGURE 2 : Secant angle of shearing resistance ϕ_s in function of mean normal stress data for different sands[5].

2.4 Curvature of the Mohr Envelope

As stated previously considerable evidence exists that the shear/normal stress relationship is non-linear. Leps[7] (1970) assembled published data readily available for individual large scale triaxial tests on gravels and rockfill. The friction angles as a function of the normal pressures across the failure plane, as deduced from the use of the Mohr diagram were plotted by Leps as shown in Figure 3. It can be seen from the figure that there is a significant decrease in the friction angle of sand, gravel and rockfill with an increase in the normal pressure. (The backup data for this plot is tabulated in Table A1 in Appendix A).

Marsal[2] performed large scale triaxial tests on rockfill materials and plotted the Mohr failure envelopes as shown in Figure 4. The curvature of the Mohr envelope is quite clear in this figure.

Bertacchi and Bellotti[9] (1970) did experimental research on materials for rockfill dams testing coarse granular materials using a triaxial cell with a diameter of 350 mm and a height of 700 mm. The results of their research, refer to figure 5, show the decrease in shear strength and the friction angle with an increase in the stress level.

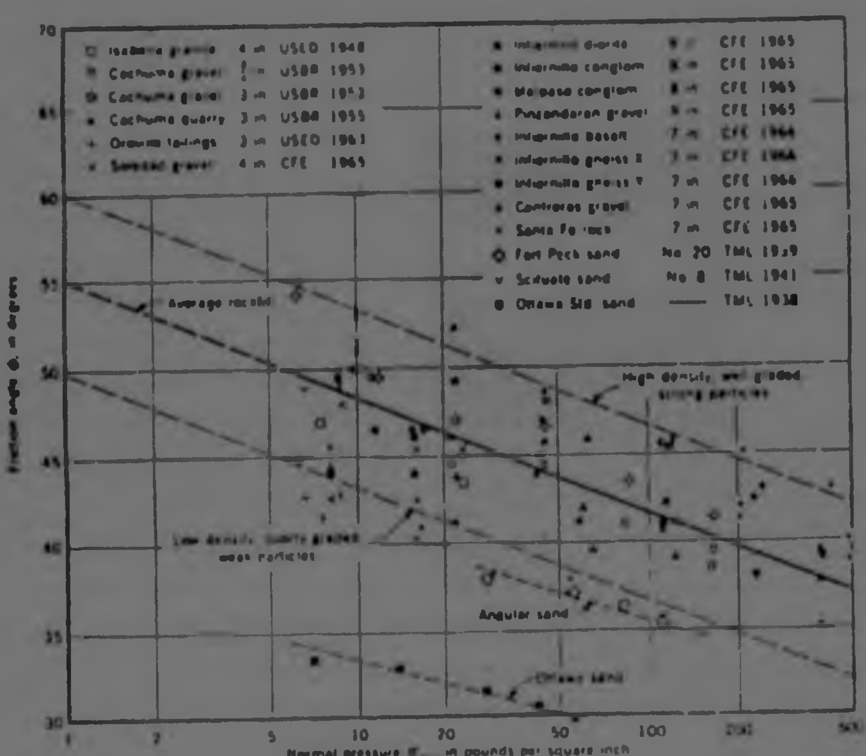

FIGURE 3 : Shearing strength of rockfill from large triaxial tests[7]

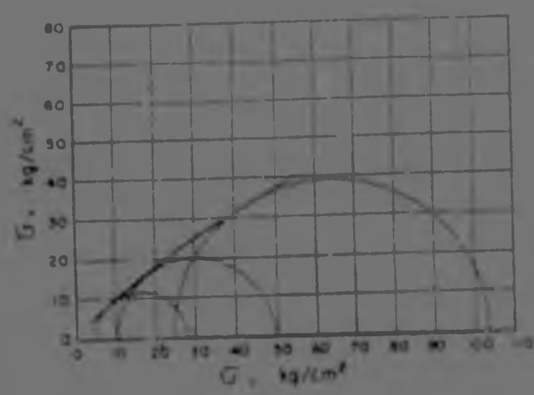

TYPICAL PARTICLES

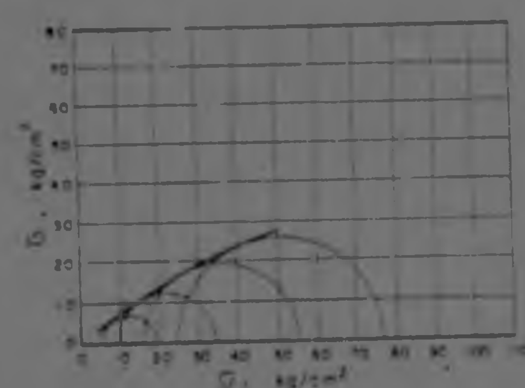

TYPICAL PARTICLES

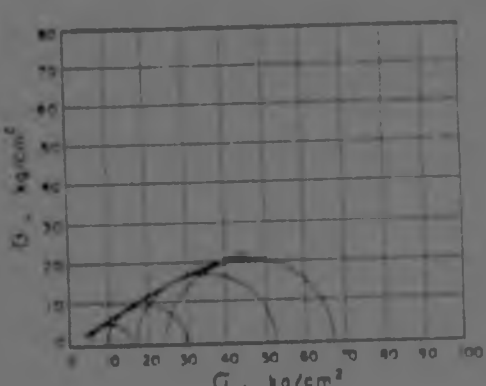

TYPICAL PARTICLES

FIGURE 4 : Marsal's Mohr circles

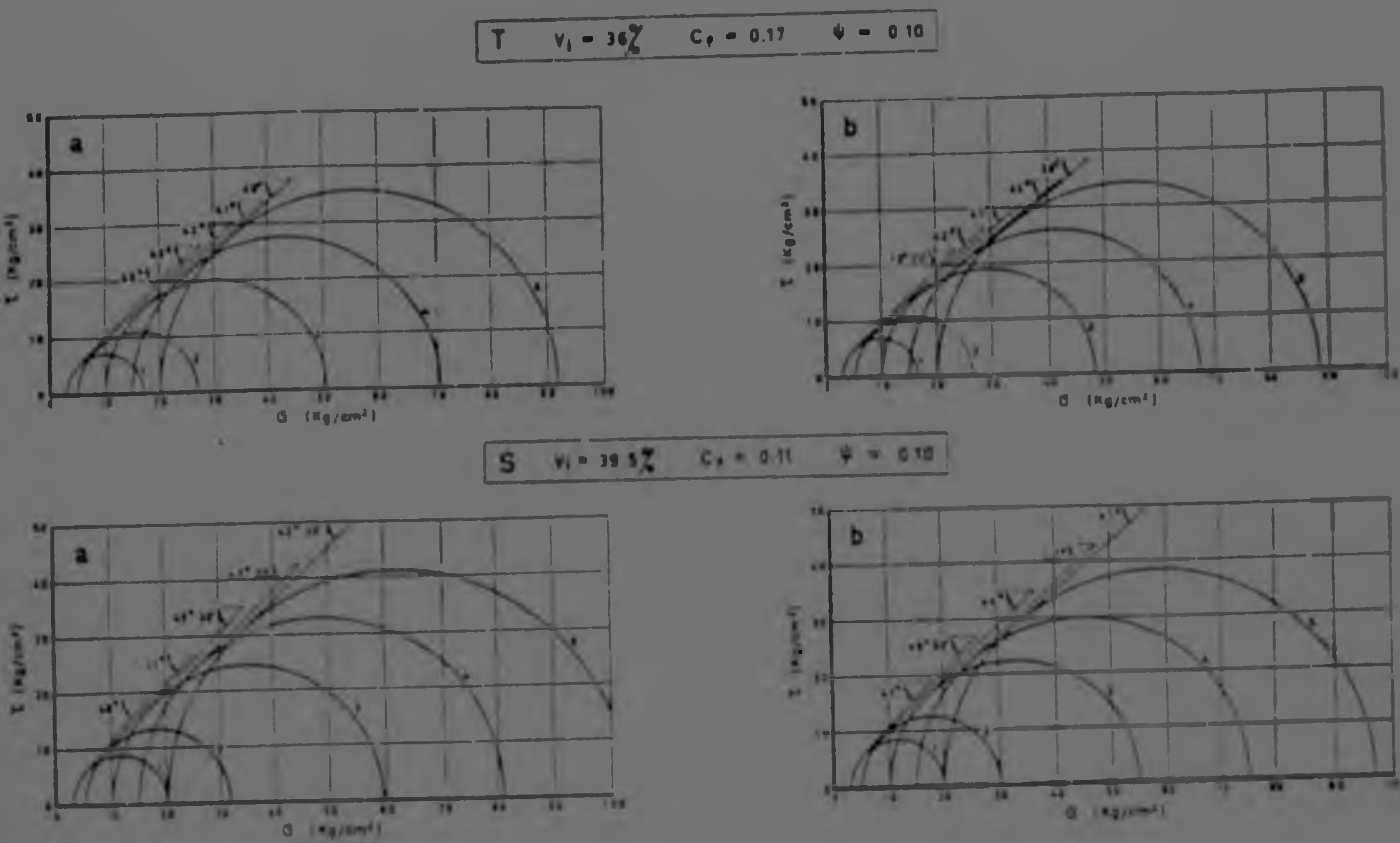

FIGURE 5 : Triaxial tests on 350 mm diameter 700 mm h. specimens, Mohr circles .

(a) Dry material
(b) Saturated submerged material
(T) Tonalite
(S) Serpentine
(σ) Normal tension

(τ) Tangential tension,
Grain-size grading :
0,2 to 35 mm
(V_i) rosity
(C_f) coefficient of grain shape
(ψ) Maximum ϕ particles to ϕ cell.

Banks et al[11] performed over three hundred triaxial tests to determine the decrease in the friction angle with increasing stress level. The results of this investigation are plotted in Figure 6.

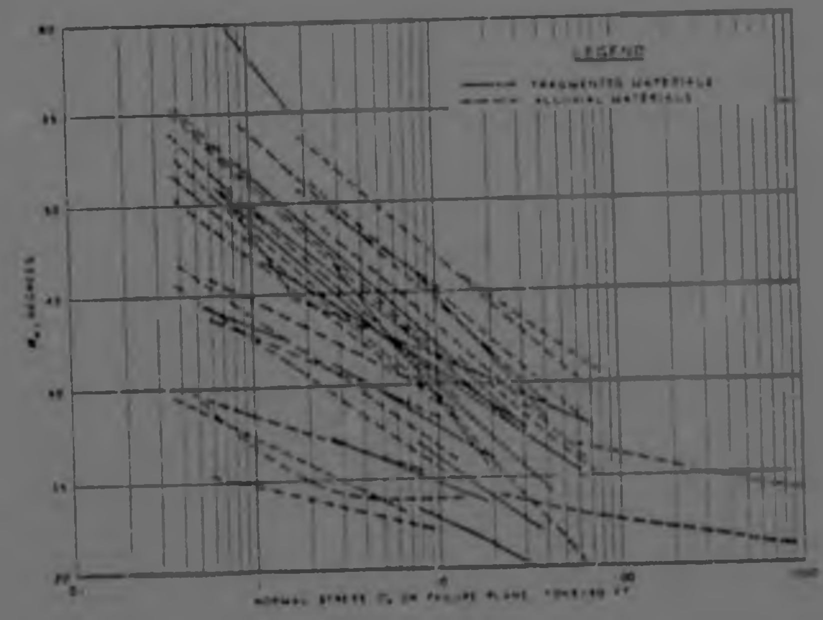

FIGURE 6[11]: ϕ_0 Versus σ_0, $\phi_0 = \sin^{-1}\dfrac{(\sigma_1-\sigma_3)_{failure}}{(\sigma_1+\sigma_3)_{failure}}$

With respect to sand, refer to Figure 2, there is also a definite decrease in the shear strength with increasing normal stress. However Vesic[5] was able to determine a critical normal stress level beyond which the friction angle attained a constant value. The Mohr figures shown in Figure 7 also show the non-linear relationship between shear strength and normal stress. The contribution of relative density to the strength can also be seen.

Bertacchi and Bellotti[9] suggest that the decreasing steepness of the envelope with increasing load indicates that the rounding off of surface roughness and the increasing presence of friction material between the particles determines a gradual reduction of the friction angle.

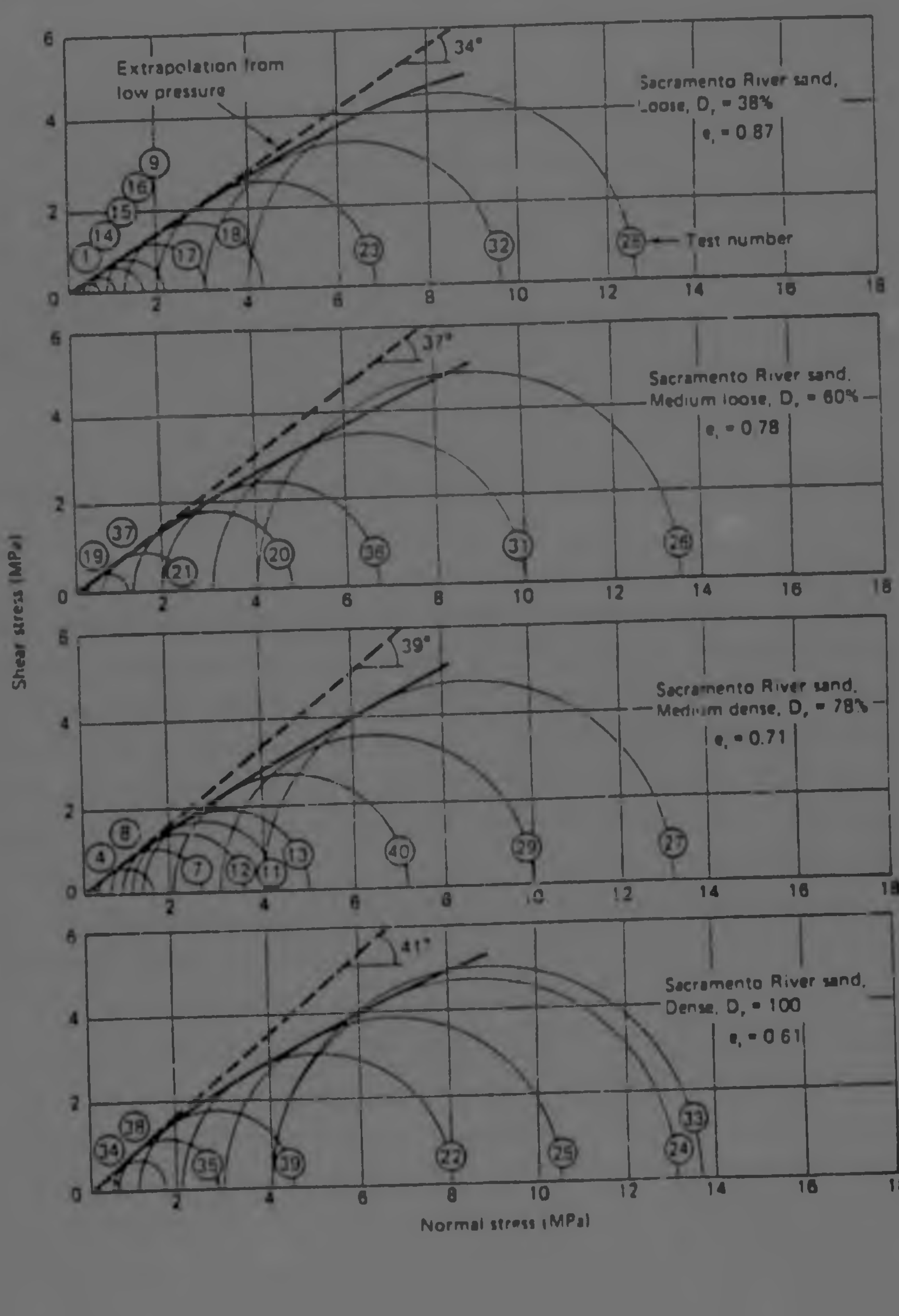

FIGURE 7 : Mohr circles and failure envelopes from drained triaxial tests, illustrating the effects of void ratio or relative density on shear strength (after Lee, 1965; also after Lee and Seed, 1967)[8].

De Mello[12] has suggested the relationships shown in Figure 8 for presently available data on curved strength envelopes in granular materials.

ROCK TYPE / REGRESSION	REF.
EL INFIERNILLO DIORITE $\tau = 1.10\,\sigma^{[illegible]}$	MARSAL 1967, 1971, 1975
[illegible] CONGLOMERATE $\tau = 1.27\,\sigma^{[illegible]}$	MARSAL 1971, 1975
[illegible] SAND + GRAVEL $\tau = 1.27\,\sigma^{[illegible]}$	MARSAL ET AL 1967
SAN FRANCISCO BASALT $\tau = 1.54\,\sigma^{[illegible]}$	MARSAL 1971
[illegible] CONGLOM. $\tau = 1.15\,\sigma^{[illegible]}$	GAMBOA & BENASSINI 1967
MALPASO CONGLOMERATE $\tau = 1.53\,\sigma^{[illegible]}$	MARSAL 1975

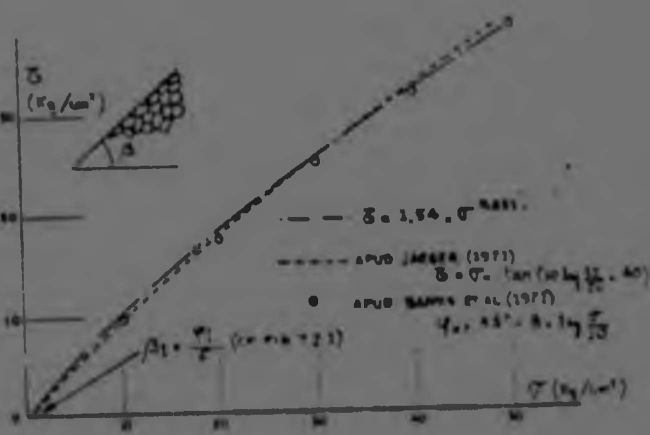

FIGURE 8 : Summary data on curved strength envelopes in granular materials[12].

For each of over three hundred triaxial tests performed by Banks, et al[11], the angle of maximum stress obliquity ϕ_o and the corresponding normal stress was developed. ϕ_o is as defined in Figure 9 (11) and is the slope of the line drawn through the origin of a Mohr diagram and tangent to the Mohr's circle (ϕ_o is equal to Vesic's ϕ_s (secant friction angle) shown in figure 2). The results shown in figure 6 indicate a relatively linear relation between ϕ_o and the common logarithm of σ_o. Thus from considerations of geometry, Banks expressed the relation as;

$$\phi_o = \phi_{ref} - F \log\left(\frac{\sigma_o}{\sigma_{ref}}\right) \quad \ldots\ldots\ldots\ldots\ldots\ldots \quad (5)$$

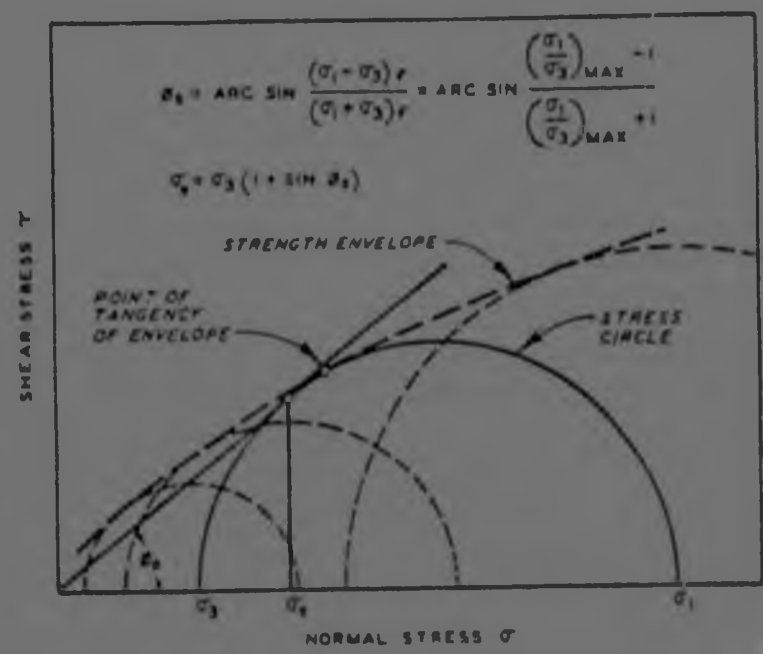

FIGURE 9 : Relation of ϕ_o to strength envelope for series of triaxial tests (11)

where ϕ_{ref} and σ_{ref} are arbitary reference values of ϕ_o and the normal stress respectively;

P is the index of change in ϕ_o with changing normal stress, or in effect, P is the change in ϕ_o corresponding to a change in σ_o of one cycle of the logarithmic scale.

Banks states that these parameters permit the results to be conveniently expressed in a single plot by assuming a value for either ϕ_{ref} or σ_{ref} as shown in Figure 10. In figure 10(a) the variation of P with σ_{ref} is shown for ϕ_{ref} assumed equal to 45^o, while in figure 10(b) the variation of P with ϕ_{ref} is shown for σ_{ref} assumed equal to 1 ton per square feet.

Banks has found that when the exponentially linearised test data are used in a computation of the shear strength at a point within a mass of cohesionless data, a curved strength envelope shown in Figure 11 is reconstructed. However, this reconstructed strength envelope will always fall below the envelope tangent to the Mohr stress circles shown in Figure 9. The difference between the two envelopes increases with increasing values of P and increasing normal stress.

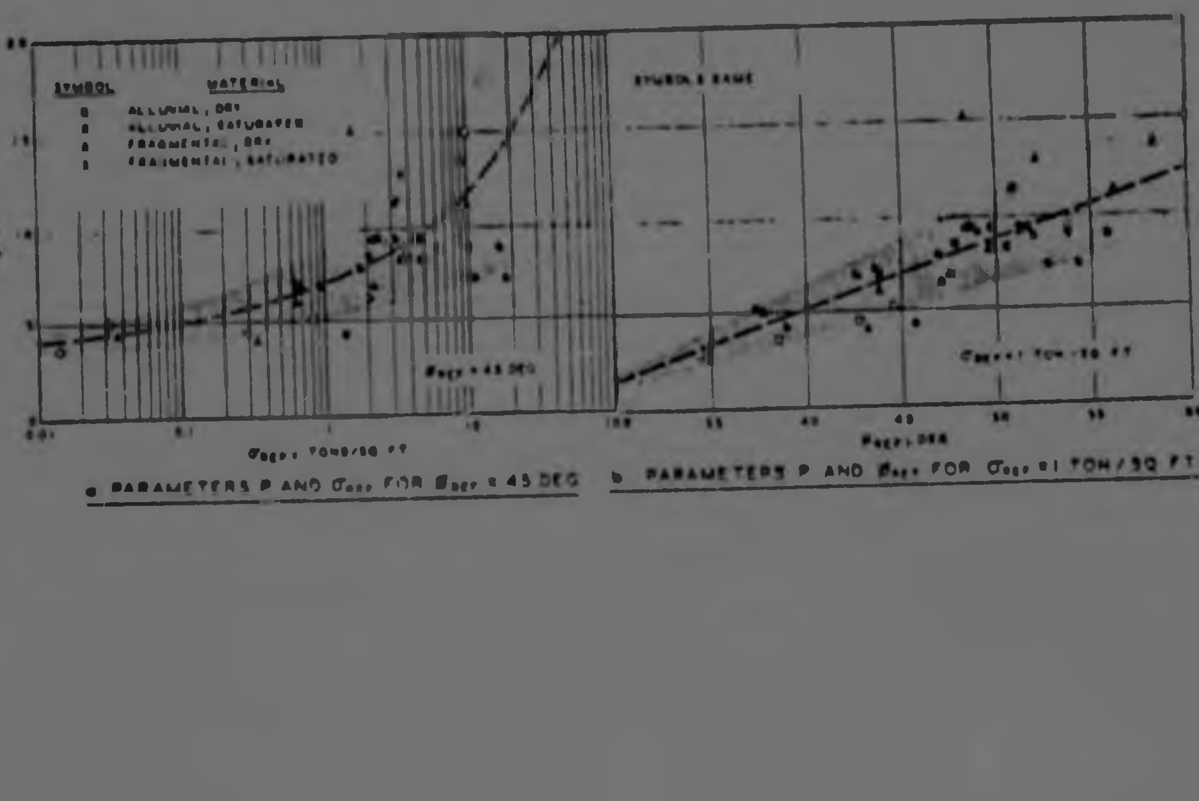

a PARAMETERS P AND σ_{ncp} FOR ϕ_{ncp} = 45 DEG

b PARAMETERS P AND ϕ_{ncp} FOR σ_{ncp} = 1 TON/SQ FT

FIGURE 10 : Strength parameter summary[11]

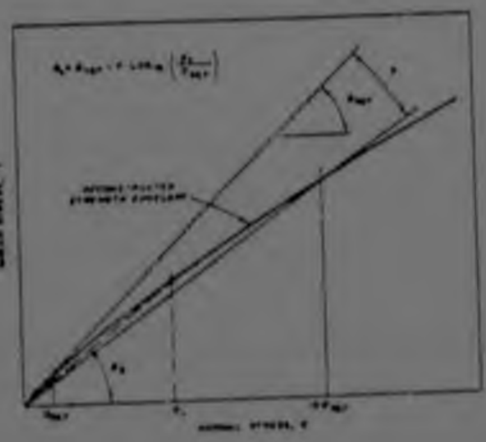

FIGURE 11 : Curved strength envelope parameters[11]

Available test data is sufficient only in indicating trends and from a review of this data the following tentative statements can be made about the behaviour of cohesionless material.

2.5.1 Relative Density:

At a given normal stress, increasing relative density results in an increased friction angle. Marsal's[2] data indicates that the maximum effect may be in the order of 3° to 4° at a normal pressure of 69 KPa declining to 1,5° at 3456 KPa. Figure 7 also indicates the importance of relative density as a factor influencing strength. The difference in behaviour between loose and dense soil is shown in Table 2 below.

TABLE 2 : EFFECT OF GRAIN SHAPE AND GRADING ON THE PEAK FRICTION ANGLE OF COHESIONLESS SOIL (after Terzaghi[14])

	Shape and Grading	Loose	Dense
1.	Rounded, uniform	30°	37°
2.	Rounded, well graded	34°	40°
3.	Angular, uniform	35°	43°
4.	Angular, well graded	39°	45°

The trend of a higher ϕ for denser soil can be explained by the phenomenon of interlocking and by energy considerations. Energy can be expended in two ways

i to overcome the frictional resistance between particles and

ii. to expand the soil against the confining stress.

The greater the density, the more the volume change that tends to occur during shear. Hence greater energy is expended to shear soil and thus a greater ϕ results.

2.5.2 Composition:

The composition of a granular soil influences the friction angle, indirectly by influencing e_o and directly by influencing the amount of interlocking that occurs for a given e_o. Improving the gradation of rockfill, provided it is not done with fines, is found to increase the friction angle at any given normal pressure. A better distribution of particle sizes appears to produce a better interlocking. A well-graded soil experiences less breakdown than that of a uniform soil of the same particle since there are more interparticle contacts.

Marsal[2] found that materials composed of well-graded and well-rounded particles were superior in their mechanical properties to uniformly graded angular rockfill materials. The table by Bell[10] shows the influence of composition clearly, refer to Table 2.

2.5.3 Particle Breakage:

Marsal[2] states that the most important factor affecting both the shear strength and compressibility, is the phenomenon of fragmentation undergone by a granular body when subjected to changes in its state of stress. Marsal concluded that particle breakage is a function of the mean intensity of particle contact forces and of the unconfined compressive strength of the rock particle.

This conclusion is substantiated by the results plotted in Figure 12. Material 1 was well graded and experienced little particle breakage. Material 3 was uniformly graded and experienced a large percentage of particle breakage. An intermediate situation is observed in Material 2. Material 1 experienced more interparticle contacts than Material 3 because of the nature of the gradings and hence had less particle breakage and probably a greater shear strength.

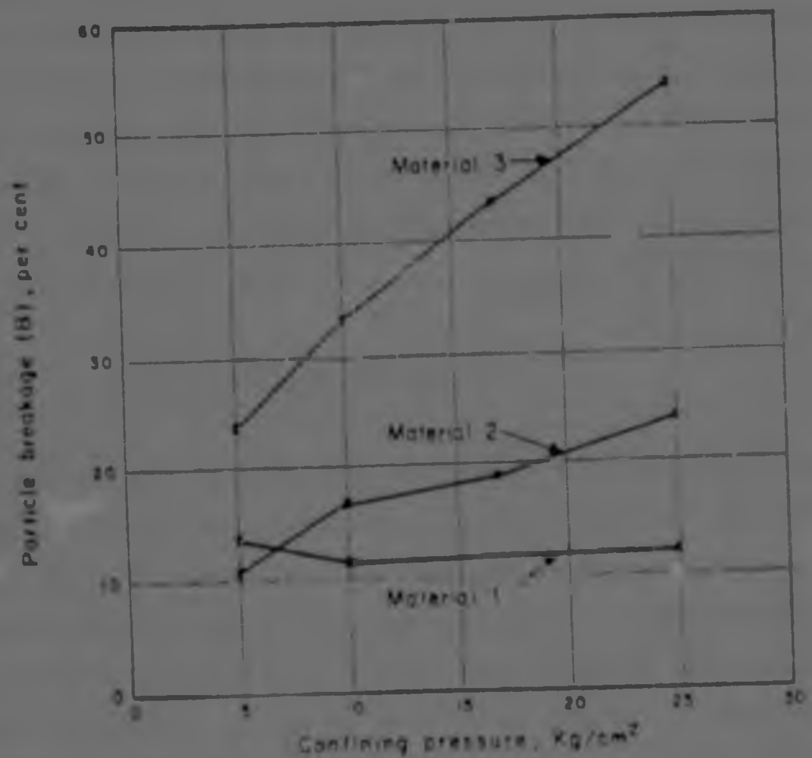

FIGURE 12 : Particle breakage in triaxial tests[7]

2.5.4 <u>Particle Size</u>:

Lambe and Whitman[4] state that the friction angle of sands with different particle sizes does not vary much. Greater initial interlocking exists for the larger particles, but this advantage is compensated for by the increased degree of particle crushing and fracture due to the larger contact forces. Holtz[illegible] states that fine sand and coarse sand at the same void ratio will probably have the same friction angle.

However, Bell[10] states that when speaking of granular soils in general, the larger the particle the higher the strength. This statement is supported by Figure 3 and the results tabulated in Table A1 in Appendix A.

The importance of crushing and the consequent curvature of the Mohr envelope, is greater for large particles such as gravel sizes and rock fragments. Crushing is initiated at smaller confining stresses due to increased contact forces.

Larsson[3] found that the maximum angles of friction measured in standard triaxial tests were 50° for gravel, 45° for sand and 40° for silt. Larsson concluded from this that the maximum positive dilatancy is dependant on the particle size. When coarse materials are sheared, the distance the particles in the shear plane are lifted perpendicular to the shear direction is dependant on the particle size. Bell[10] has given the following limits for the friction angles; gravels 35°-45°, sands 32°-42° and silts 32°-36°.

2.5.5 Interparticle Friction:

At low stress levels, the more angular the particles, the greater the interlock and hence the stronger will be the material. Inspection of Tables 2 and 3 show the influence of angularity. Marsal reports that 180 mm clean, hard, angular, quarried basalt, at normal pressures between 69-138 KPa, had friction angles 10° to 15° greater than those for 180 mm well rounded gravel. However, at increasing stress levels, the particles start to break and crush, so that the influence of particle shape decreases with increasing stress level.

Lambe and Whitman[4] state that unless a sand contains mica, mineral composition makes relatively little difference. This is confirmed by Marachi's[6] experiments in which he found that the angles of friction for all of the rockfill materials tested, were within a narrow range of a few degrees.

TABLE 3 : ANGLE OF INTERNAL FRICTION OF COHESIONLESS SOILS*

No. General Description	Grain Shape	D_{10} (mm)	C_w	Loose e	Loose ϕ(deg)	Dense e	Dense ϕ(deg)
1. Ottawa standard sand	Well rounded	0,56	1,2	0,70	28	0,53	35
2. Sand from St. Peter sand-stone	Rounded	0,16	1,7	0,69	31	0,47	37‡
3. Beach sand from Plymouth, MA	Rounded	0,18	1,5	0,89	29	-	-
4. Silty sand from Franklin Falls Dam site, NH	Subrounded	0,03	2,1	0,85	33	0,65	37
5. Silty sand from vicinity of John [illegible]n Dam, CO	Subangular to subrounded	0,04	4,1	0,65	36	0,45	40
6. Slightly [illegible]y sand from the shoulders of Ft.Peck Dam, MT	Subangular to subrounded	0,13	1,8	0,84	34	0,54	42
7. Sc[illegible]ed glacial sand, M[illegible]ester, NH	Subangular	0,22	1,4	0,85	33	0,60	43
8.‡Sand from beach of hydraulic fill dam, Quabbin Project, MA	Subangular	0,07	2,7	0,6	[illegible]	0,54	46
9. Artificial, well-graded mixture of gravel with sands No. 7 and No. 3	Subrounded to subangular	0,16	68	0,41	42	0,2	57
10. Sand for Great Salt Lake fill (dust gritty)	Angular	0,07	4,5	0,82	38	0,53	47
11. Well-graded, compacted crushed rock	Angular	-	-	-	-	0,18	60

* by A. Casagrande.

‡ The angle of internal friction of the undisturbed St. Peter sandstone is larger than 60o and its cohesion so small that slight finger pressure or rubbing, or even stiff blowing at a specimen by mouth, will destroy it.

‡ Angle of internal friction measured by direct shear test for No. 8, by triaxial tests for all others.

2.5.6 Degree of Saturation

Marsal[2] showed graphically, Figure 13, the degree to which saturation affects the strength. For Gneiss (Material 3), the dry frictional strength was found to be about 170% of the saturated case. For basalt (Material 1), the dry strength was about 120% of the saturated strength. However, Marsal has not described the type and procedure of test used in any detail. Holtz[8] states that the surface roughness has an effect on ϕ and that it has been found that wet soils show a 1° to 2° reduction in ϕ when compared to dry sands. The results of the triaxial tests by Bertacchi and Bellotti[9], refer to Figure 5 and Table 4, give a good indication of the degree of influence saturation has on rockfill.

In general, the literature consulted gives the idea that the behaviour of dry cohesionless soil, is virtually identical to the drained behaviour of cohesionless saturated soil.

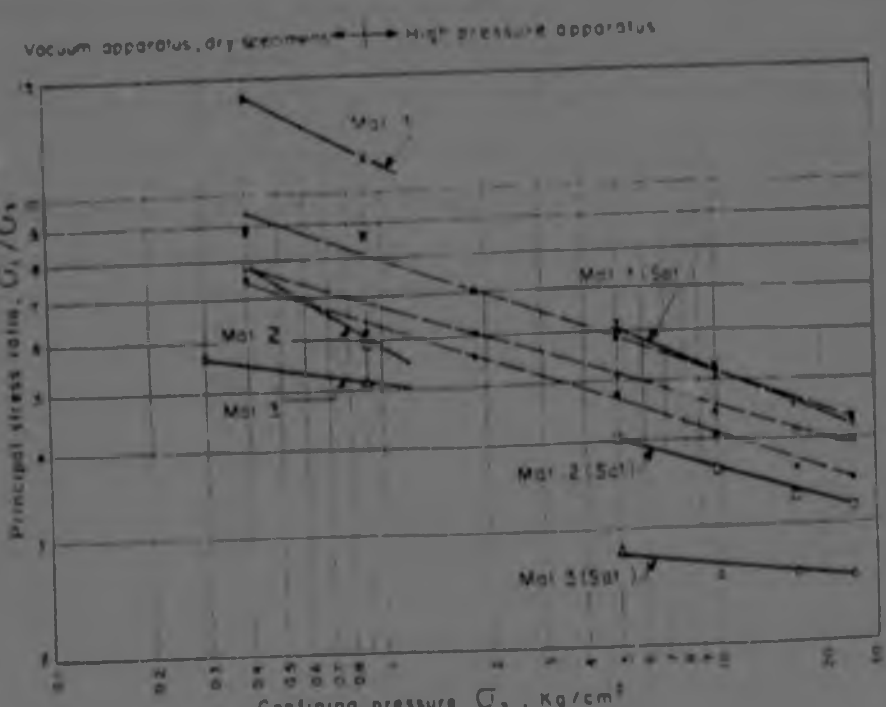

FIGURE 13 : Relationships between principal stress ratio at failure and confining pressure

TABLE 4 : FRICTION ANGLES FOR ROCKFILL SPECIMENS SUBJECTED TO TRIAXIAL TESTING [9]

Material	Testing conditions	Lateral confining pressures kg/cm^2				
		3	5	10	15	20
Tonalite	Dry (a)	45°	43°	42°	41°	40°
	Saturated (b) submerged	43°30'	42°	41°	40°	39°
Serpentine	Dry (a)	48°	47°	45°30'	43°30'	42°30'
	Saturated (b) submerged	47°	45°30'	44°	42°	41°

2.5.7 Intermediate Stress

The dilatancy is dependant on the intermediate stress acting in the shear plane perpendicular to the shear direction.

Intermediate stress prevents sideways movement of the particles during shear and hence an increased intermediate stress results in an increased angle of friction. Larsson[3] states that the influence of intermediate stress seems to be largest for coarse materials and decreases with decreasing particle size. Figure 14 shows the variation of measured friction angles versus intermediate stress level.

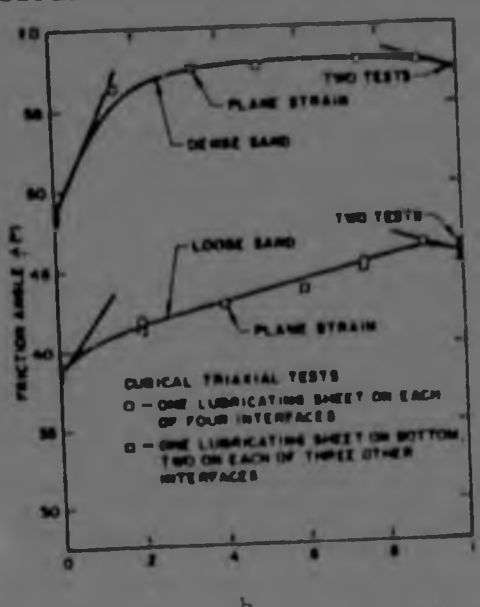

$$b = \frac{\sigma_2 - \sigma_3}{\sigma_1 - \sigma_3}$$

FIGURE 14 : Variation of measured friction angles versus intermediate stress level. From Lade and Duncan 1973[3].
*Explanation of b in the Appendix A1.

In direct shear or triaxial tests it is assumed that $\sigma_2 = \sigma_3$ or σ_1. Holtz[8] states that in order to investigate the influence of the intermediate principal stress, tests such as the plane strain or cuboidal shear tests must be used. Research summarised by Ladd, et al (1977)[8], indicates that ϕ in plane strain is larger than ϕ in triaxial shear by 4° to 9° in dense sands and 2° to 4° for loose sands. A conservative estimate of the plane strain angle of friction ϕ_{ps} may be found from triaxial results ϕ_{tx}, using the following equations [8].

$$\phi_{ps} = 1.5\,\phi_{tx} - 17^\circ \quad (\phi_{tx} > 34^\circ) \quad \ldots\ldots\ldots\ldots\ldots\ldots \quad (6)$$

$$\phi_{ps} = \phi_{tx} \quad (\phi_{tx} < 34^\circ) \quad \ldots\ldots\ldots\ldots\ldots\ldots \quad (7)$$

2.6 The Prediction of Rockfill Material Behaviour by Model Materials

Testing of triaxial specimens of prototype rockfill materials is often not possible due to the size of individual particles. Techniques have thus been developed to evaluate the properties of full scale rockfill materials on the basis of information from laboratory triaxial specimens containing the small fraction of the field material. Techniques include scalping and the use of laboratory specimens with similar grading curves to the field material.

Marachi[6] performed a number of triaxial tests on material with specimen grain-size distribution curves which were made parallel to the field gradation curve of the parent rockfill material. Three specimen sizes of 914 mm, 305 mm and 71 mm were used. The object of these tests was to determine the effects of modeling of the gradation curves on the strength, deformation characteristics and the prediction of the angle of internal friction of the actual rockfill material.

From the results of these tests Marachi was able to reach the following conclusions:

1. The modeling of rockfill materials did not materially affect the isotropic consolidation characteristics of specimens.

2. The angle of internal friction decreases with increasing size of the particles in the test specimen.

3. Volume changes were least compressive for the small specimens but the tendency was not pronounced. Marachi also noted that volume changes were influenced by particle shape to a greater extent than by mineralogy.

4. There is an increase in axial strain at failure as the particle size increases but again this tendency is not pronounced. Particle shape has greater influence than mineralogy.

5. The strength and deformation characteristics of the rockfill materials were affected by the confining pressures used.

6. The modeling technique seems to provide a useful method for predicting the strength and deformation characteristics of field rockfill materials.

2.7 Conclusion

In conclusion it can be stated that a large number of factors influence the strength of cohesionless soils. Traditionally the shear strength has been estimated by the linear relationship

$$\tau = (\sigma - u) \tan \phi \quad \ldots\ldots\ldots\ldots\ldots\ldots\ldots\ldots \quad (1)$$

however considerable evidence exists that the shear/normal relationship is not linear.

De Mello[12] has recommended the functions shown in Figure 8 to accomodate for the curvature in the strength envelope.

Banks[11], et al, has recommended the use of the equation

$$\phi_o = \phi_{ref} - P \log (\sigma_o/\sigma_{ref}). \quad \ldots\ldots\ldots\ldots \quad (5)$$

The factors affecting the strength of cohesionless soil and their effects are listed in Table 6 below:

TABLE 6 : SUMMARY OF FACTORS AFFECTING ϕ

FACTOR	EFFECT
Relative Density R	R ↑ ϕ ↑
Composition	Well graded ϕ > Uniform ϕ
Particle Size P	P ↑ ϕ ↓
Particle Breakage B	B ↑ ϕ ↓
Interparticle Friction F	F ↑ ϕ ↓
Water W	W ↑ ϕ ↓
Intermediate Principal Stress	$\phi_{plane\ strain}$ > $\phi_{triaxial}$

Marachi[6] has shown that the prediction of rockfill material behaviour by modeled materials gives reasonable results.

Holtz[8] has recommended Figure 15 for estimating the frictional characteristics of granular materials.

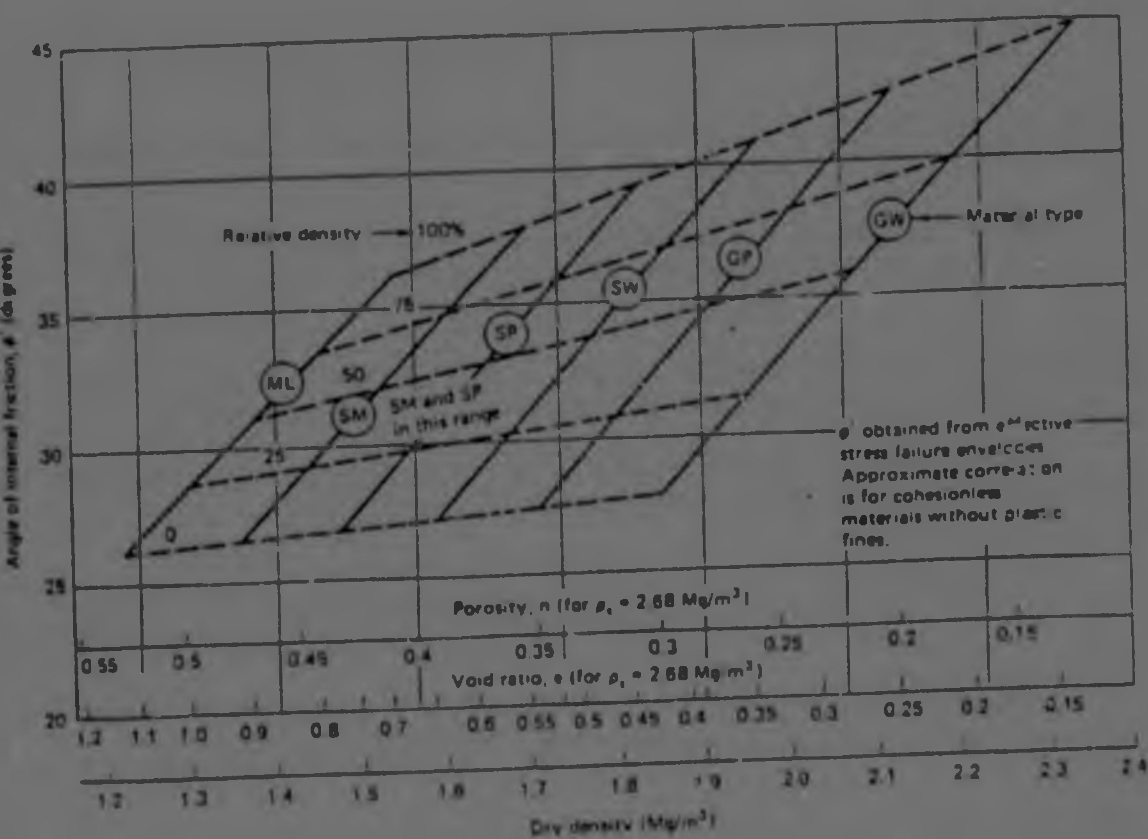

FIGURE 15 : Correlations between the effective friction angle in triaxial compression and the dry density, relative density, and soil classification (after U.S. Navy, 1971).

2.8 References

1. Call, R., "Evaluation of Material Properties", Design of Non-impounding Mine Waste Dumps Workshop, Society of Mining Engineers, A.I.M.E., Denver, 1981.

2. MARSAL, R. J., "Large Scale Testing of Rockfill Materials", Journal of the Soil Mechanics and Foundations Division, A.S.C.E. March, 1967.

3. LARSSON, R., "Shear Strength of Soils", Proceedings of the Interdisciplinary Conference, University of Luleå, Swden, September, 1978.

4. LAMBE, T.W. and WHITMAN, R., Soil Mechanics, John Wiley and Sons, New York, 1979.

5. VESIC, A.S., "Behaviour of Granular Materials Under High Stress", Journal of the Soil Mechanics and Foundations Division, A.S.C.E. May, 1968.

6. MARACHI, N.D., "Evaluation of Properties of Rockfill Materials", Proceedings of A.S.C.E. Vol. 98, January, 1972.

7. LEPS, T.M., "Review of Shearing Strength of Rockfill, Journal of the Soil Mechanics and Foundations Division, A.S.C.E., July, 1970.

8. HOLTZ, R.D. and KOVAS, W.D., "Shear Strength of Sands and Clays", An Introduction to Geotechnical Engineering, Prentice Hall

9. BERTACCHI, P and BELLOTTI, R., "Experimental Research On Materials for Rockfill Dams", 10th ICOLD Congress, Montreal 1970, pp. 511.

10. BELL, F.G., "Engineering Properties of Soils and Rocks, Butterworths Publications, 1981.

11. BANKS, D, MacIVER, B., and SOWERS, G., "Review of Shearing Strength of Rockfill", Discussion, A.S.C.E., Vol. 97, SM5, May, 1971.

12. DE MELLO, V.F.B., "Reflections on design decisions of practical significance to embankment dams", Geotechnique 27, No. 3, pp. 279-355, 1977.

CHAPTER 3 : FACTORS AFFECTING THE STABILITY OF COARSE MINE WASTE DUMPS

3.1 Introduction

The type of instability and the most appropriate stability analysis for a waste dump depends upon the following factors;

- the method and rate of dump construction
- the dump site and climatic conditions
- the dump site topography
- the dump site foundation conditions
- the physical characteristics of the dump material
- the water table or pore pressure that develops in the dump and the dump foundation.

3.2 Dump Construction Methods

The various ways in which dumps may be formed are illustrated in Figure 16. These can be classified under two headings;

- topography of dump site, and
- method of dump construction.

Figure 17 illustrates common dump construction methods. End dumped slopes (Figure 17a) are formed by a process of controlled failure. Dumps placed in lifts (Figure 17b) are constructed from the bottom up and control over the slope angle is easily affected. Heaped embankments (Figure 17c) are normally found in strip mine operations.

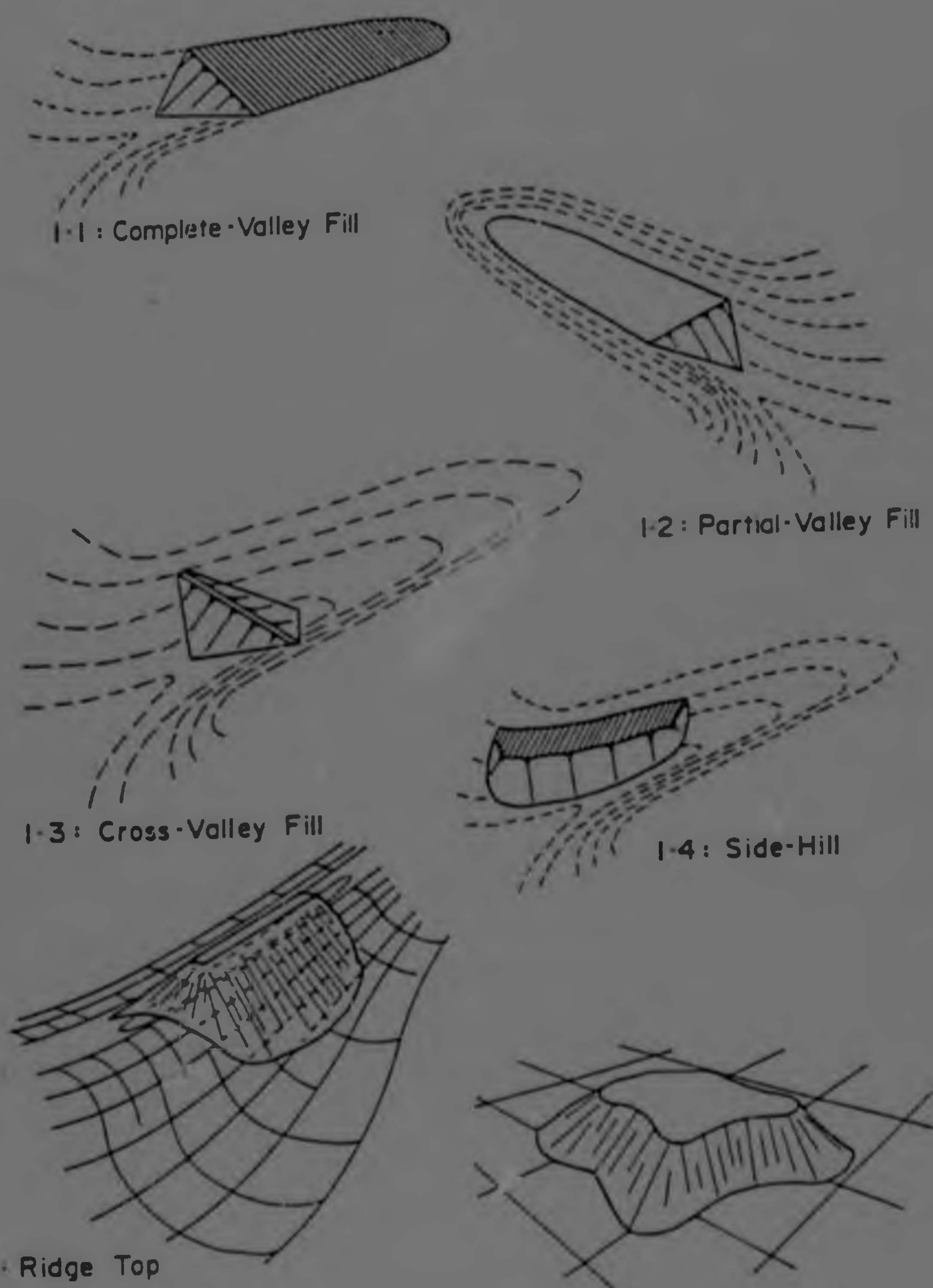

FIGURE 16 : Typical locations[4]

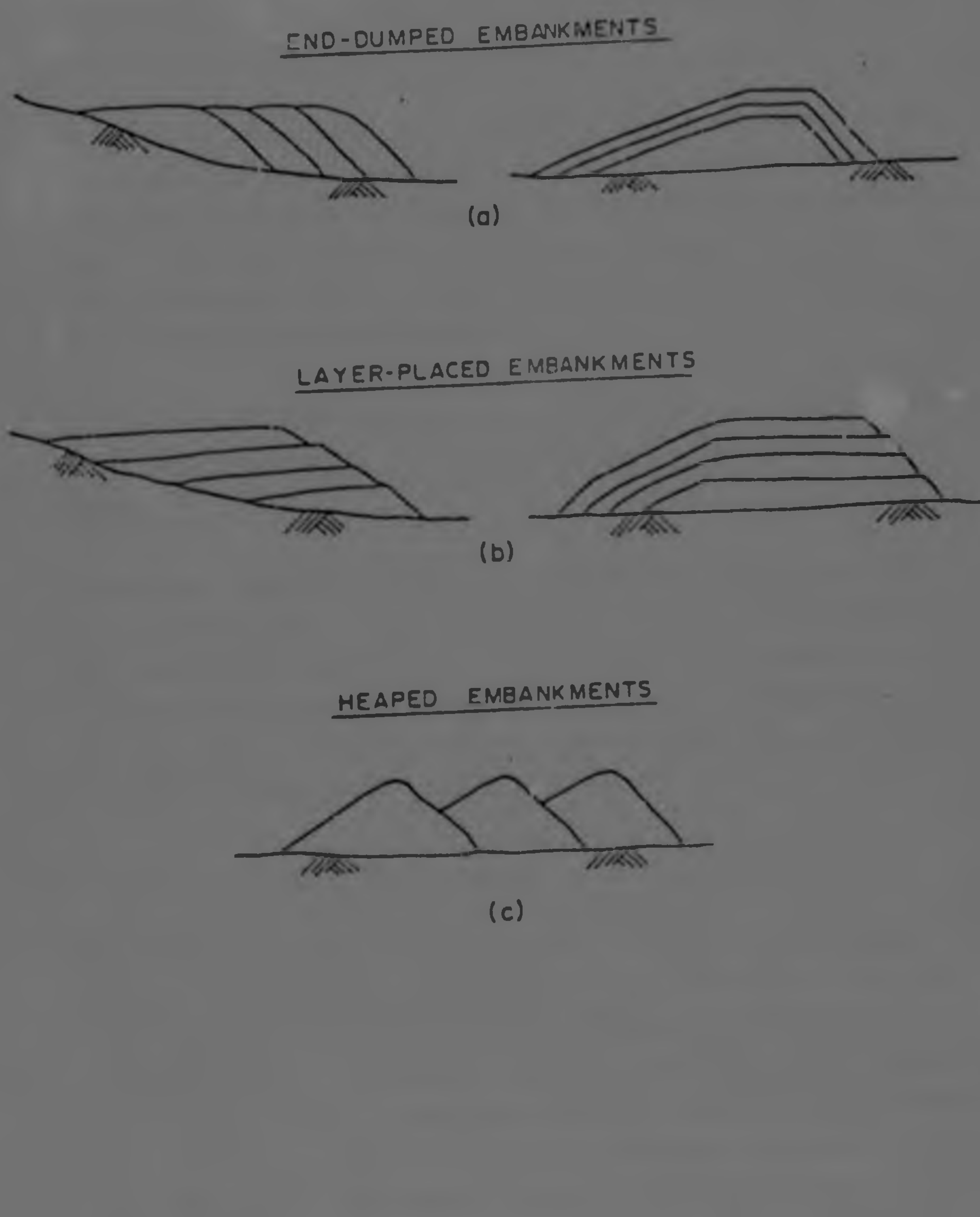

FIGURE 17 : Mine Waste Embankment Placement Methods

3.3 Modes of Failure

The various failure modes that can occur in mine waste embankments, according to Caldwell[4] are shown in Figure 18. The factors affecting and consequences of each of these failure modes again from Caldwell are listed in Table 7.

Analysis of coarse mine waste dumps by circular arc methods has shown that for the lowest factor of safety against failure, the failure arc approaches a shape coinciding with the surface of the dump. Thus the circular arc failure mode shown in Figure 18 will probably be similar to the surface or edge slides failure mode shown in the same diagram.

As toe spreading often represents the onset of base failure, refer to Figure 18 and Table 7, the modes of failure are probably the same.

It has been found by Blight[1] that the failure surface in a rock dump is plane and thus the shape of the failure surface through the dump in the foundation circular failure mode, Figure 18, is unlikely to be circular and is probably closer to that of a straight line. Blight's investigations of rock dumps will be discussed further later in this section.

3.3.1 Surface or Edge Slides

This mode of failure is most likely to occur in end-dumped embankments with a layer of fines below the slope surface and is best evaluated by the equations describing the stability of an infinite slope. Edge slides can result from the oversteepening of the upper portion of the slope which is caused by an accumulation of fines and temporary cohesion associated with negative pore water pressures. Bulging of the face of the waste pile, combined with short localised segments of steeper-than-average topographic slopes beneath the lower portion of the frontal slope pile can

TABLE 7 : CAUSE AND CONSEQUENCE OF DUMP FAILURE[1]

FAILURE MODE	INITIATING CAUSES	CONSEQUENCES
Surface or Edge Slide	-oversteepening caused by accumulation of fines or temporary cohesion	-Run-out area dependent upon foundation inclination and embankment area.
	-buried snow or ice lenses	-Generally of nuisance value only disrupting efficient dumping operations.
Shallow Flow Slide	-infiltration of rain or snowmelt	-failure can cover large distances rapidly.
		-Can cause substantial damage. Temporary suspension of dumping operations.
Block Translation	-melting snow or groundwater	-Dependent on natural ground slope.
	-decay of organic matter	-Can result in suspension of dumping operations
	-earthquakes	
Circular Arc Failure	-excessive height (cohesive material)	-Disturbance initially limited to immediate vicinity of slope.
	-reduction in toe support	-Partial loss of dump.
Base Failure	-excessive pore pressure	-Disturbance initially limited to immediate vicinity of slope.
	-excessive height	
	-decay of organic matter	-Progressive movement if dumping continued.
	-earthquakes	-Intermittent suspension of dumping operations
Foundation Circular Arc	-weak foundation materials	-Major disturbance.
	-excessive pore pressure	-Loss of dump.
Toe Spreading	-weak foundation materials	-Often signals on-set of base failure or block translation.
	-excess pore pressure in foundation.	

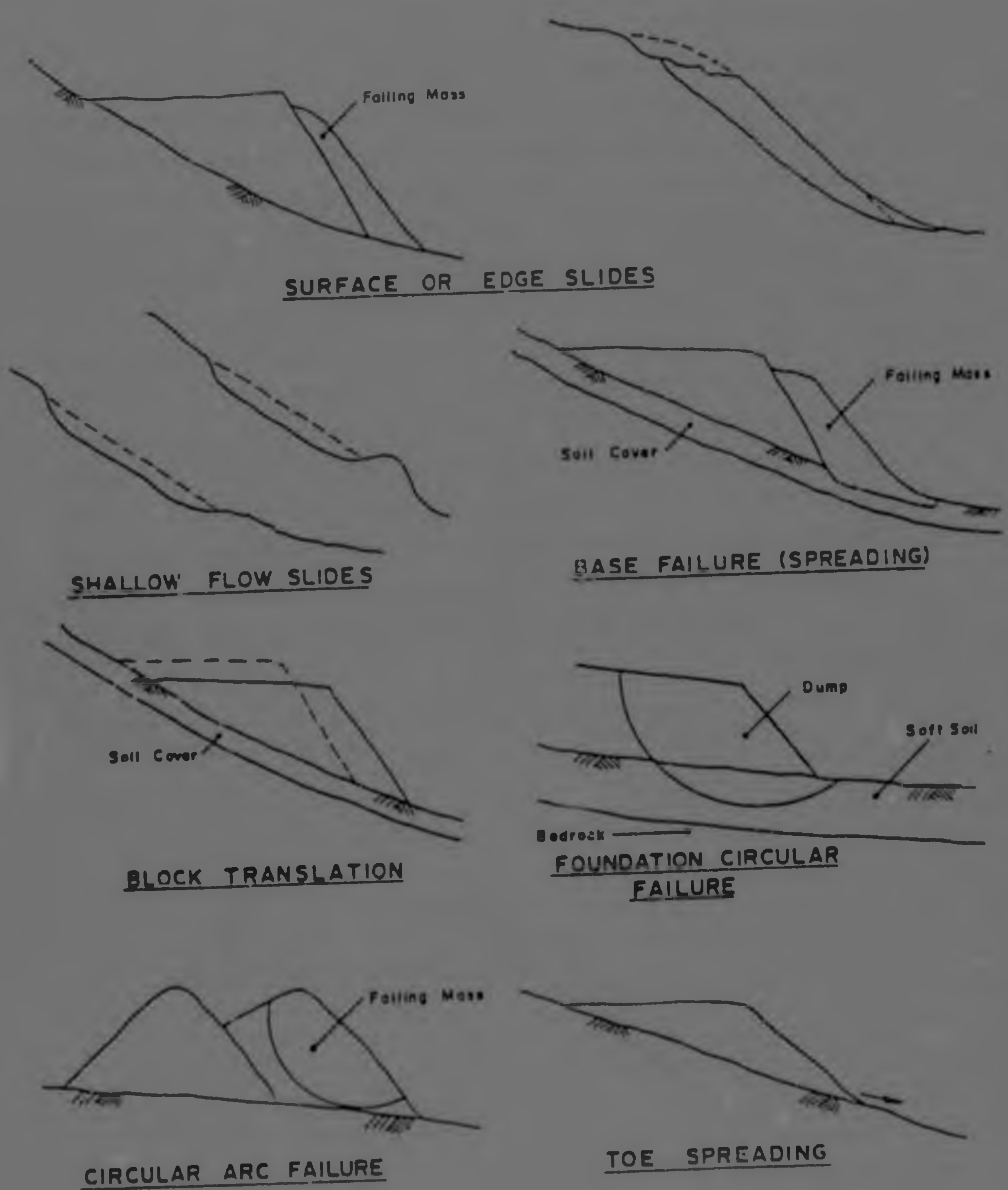

FIGURE 18 : Mine waste embankments possible failure modes[4]

result in failures on the face of a dump[5]. Such failures pose a potential hazard to men and equipment engaged in dumping operations at the crest of the pile. However, failure does not occur without warning and is preceded by a period of several days during which displacements at the crest of the pile increase at a progressively faster rate. A crude but effective measuring device has been used by Campbell and Shaw[5] to measure crest movements. The device is illustrated in Figure 19. The device consists of a pin driven into the face of the slope at a point slightly below the crest of the waste pile. As displacements occur on the face of the pile, the end of the wire attached to the pin is pulled downslope, raising the weight attached at the other end of the wire. A record of the rate of movement is obtained by taking periodic measurements of the vertical distance between the suspended weight and a reference point on the base of the stand. Hence forewarning of possible slides may be obtained.

FIGURE 19 : Sketch illustrating devise used to monitor movements at the crest of Clode waste pile.

In some instances, when mass sliding develops on the face of the waste pile, the material involved in the slide attains a high degree of mobility, and the slide debris has been recorded[5] extending to surprisingly large distances beyond the toe of the pile. Some of these failures have developed on the face of the rock waste dumps under dry conditions. In nature this type of rockfall is referred to as a sturzstrom and identification of a sturzstrom on the moons surface, has led to the conclusion that neither air nor water play a part in the sturzstrom mechanism.

3.3.2 Shallow Flow Slide

If sufficient water enters the slope and flows parallel to the face associated with a fines layer below the surface, a shallow flow slide may occur. Slides are frequently initiated by rain, snowmelt or broken water pipes. Infiltrating water can saturate surface soils provided an adequate supply of water is available to fill the air voids and the runoff or rainfall intensity exceeds the infiltration rate. Flow slides occur because of the shear failure of the slope material or the collapse of the soil structure. Pernichele and Kahle[6] have observed shallow flow sides travelling a distance of more than 400 m beyond the toe of the dump and at a rate of approximately 6 m per minute. Consideration of the likelihood of saturation of the rock mass and the equations for an infinite slope parallel to the face can be used to analyse such a failure.

3.3.3 Base/Foundation Failure

Dumps placed on flat ground of competent soil are least likely to fail. However, if the flat ground is covered by a thin layer of weak material, base failure may occur and if the ground is inclined base failure is more likely to occur. This mode may occur in both the end-dumped and layer placed embankments.

In some instances, when mass sliding develops on the face of the waste pile, the material involved in the slide attains a high degree of mobility, and the slide debris has been recorded[5] extending to surprisingly large distances beyond the toe of the pile. Some of these failures have developed on the face of the rock waste dumps under dry conditions. In nature this type of rockfall is referred to as a sturzstrom and identification of a sturzstrom on the moons surface, has led to the conclusion that neither air nor water play a part in the sturzstrom mechanism.

3.3.2 Shallow Flow Slide

If sufficient water enters the slope and flows parallel to the face associated with a fines layer below the surface, a shallow flow slide may occur. Slides are frequently initiated by rain, snowmelt or broken water pipes. Infiltrating water can saturate surface soils provided an adequate supply of water is available to fill the air voids and the runoff or rainfall intensity exceeds the infiltration rate. Flow slides occur because of the shear failure of the slope material or the collapse of the soil structure. Pernichele and Kahle[6] have observed shallow flow sides travelling a distance of more than 400 m beyond the toe of the dump and at a rate of approximately 5 m per minute. Consideration of the likelihood of saturation of the rock mass and the equations for an infinite slope parallel to the face can be used to analyse such a failure.

3.3.3 Base/Foundation Failure

Dumps placed on flat ground of competent soil are least likely to fail. However, if the flat ground is covered by a thin layer of weak material, base failure may occur and if the ground is inclined base failure is more likely to occur. This mode may occur in both the end-dumped and layer placed embankments.

Blight[1] investigated the foundation failures of four rockfill slopes. The failures were all short term failures of composite slopes, each slope consisting of a rockfill dump supported on a thin, relatively weak, strata of stiff fissured clay. All of the failures took place by undrained shearing through the clay foundation strata. Vertical displacement at the top of the dump as well as a scarp of soil pushed up at the toe of the dump, are typical characteristics of this failure. The emergence of the failure surface at the toe and crest of the dump could be observed directly, while the profile of the dump before failure could be inferred by comparison with unfailed sections adjacent to the failure. The failure surfaces within the dump were located by hand-augering from the surface and the depth of the failure surface in the clay at the toe of the dump, was located by drilling through the plateau of soil pushed up by the slide. A typical section through a "first-time" failed slope is shown in Figure 20a. The failure consists of plane slide through the rockfill and the foundation stratum with the failure surface in the rockfill intersecting the upper edge of the tipping face. Subsequent failures cut more deeply into the body of the rockfill behind the face as shown in Figure 20b.

Blight[3] further investigated the failure mode using laboratory models. The results show that "first-time" failure occurs by the formation of an active wedge bounded by the tip face and two shear surfaces inclined at steep angles to the horizontal, refer to Figure 21a. The active wedge displaces a passive wedge ahead of it, the displacement of the passive wedge taking place by shearing through the foundation. The angles indicated by Figure 21a are typical measured angles. Blight also simulated the condition of repeated failure in rock dumps using models and the results are diagrammatically represented in Figure 21b.

Blight concluded from the experiments that the models appear to faithfully reproduce the visible features of the prototype failures and hence that it was reasonable to assume that the models also

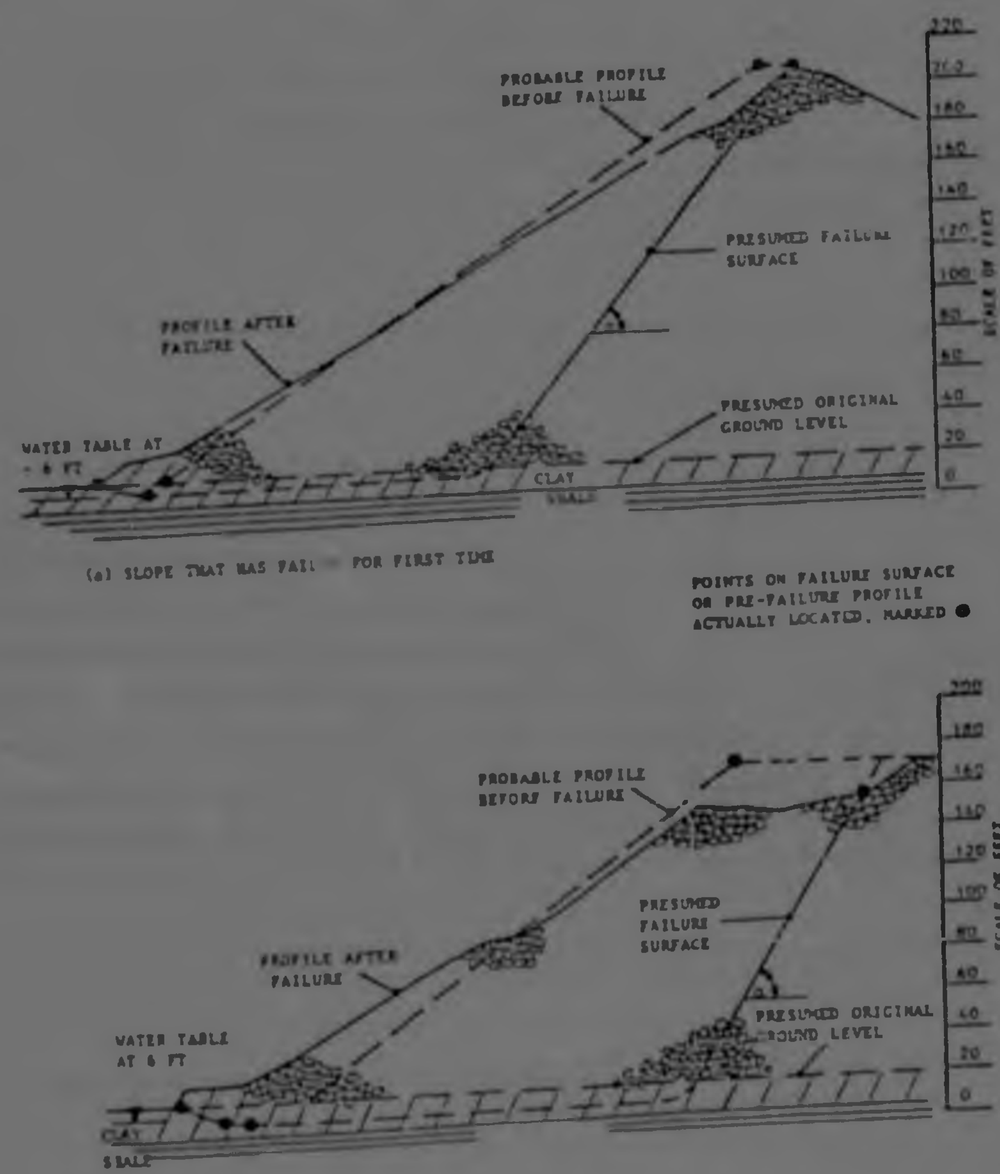

FIGURE 20 : Section through two typical failed rock dumps on thin horizontal clay foundations[7]

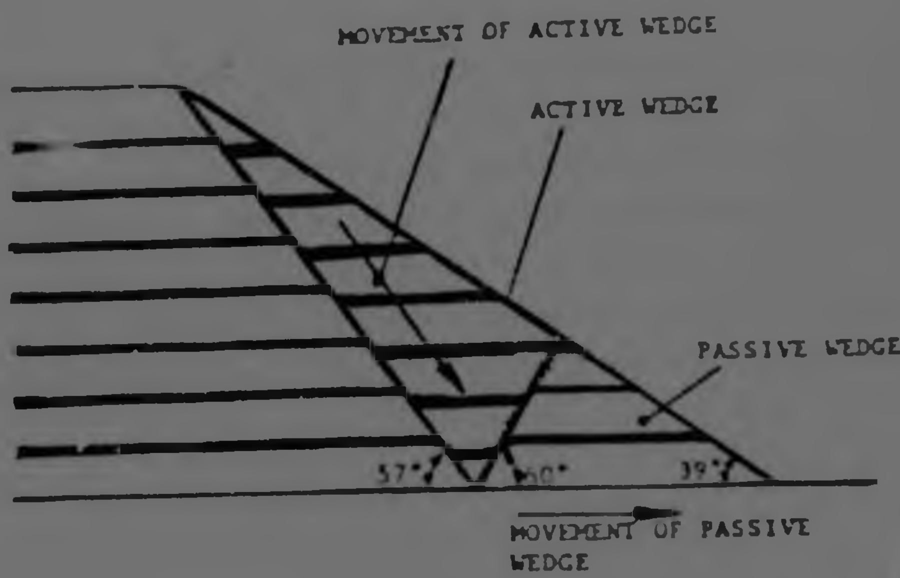

(a) Active and passive wedges in first-time failure

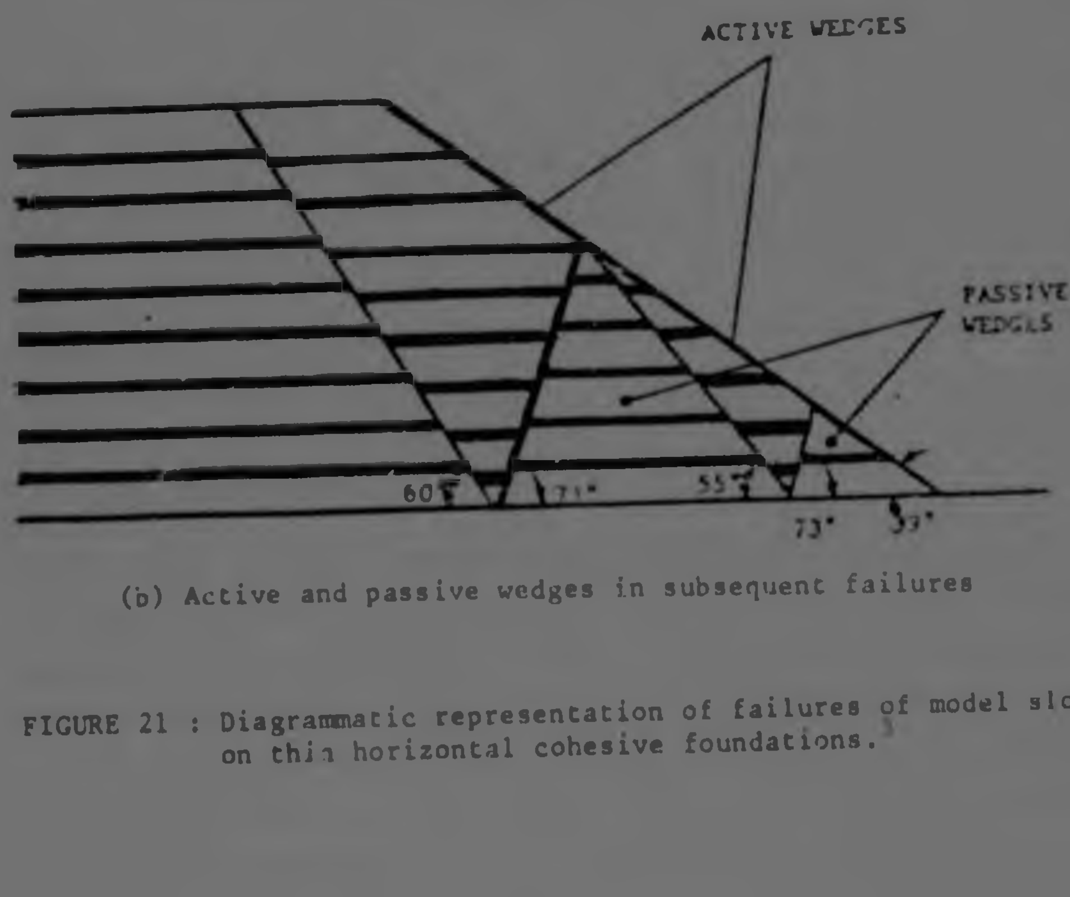

(b) Active and passive wedges in subsequent failures

FIGURE 21 : Diagrammatic representation of failures of model slopes on thin horizontal cohesive foundations.[3]

faithfully reproduce the internal failure surfaces in the rockfill.

Pernichele and Kahle[6] have also observed foundation failures of rockfill slopes. Their schematic drawing of a foundation failure, Figure 22, would appear to be similar to that of Blight, Figure 20a. Pernichele and Kahle found that failure movement was slow and was preceded by extensive development of tension cracks.

Figure 22 : Schematic drawing of foundation failure and one type of edge slump.[6]

3.3.4 Block Translation

If the shear strength parameters at the bottom of a dump on an inclined slope are lower than those within the dump, plane failure surfaces which coincide with or below the surface of the natural ground, below the dump, will be the critical mode of failure, refer to Figure 18. Where a dump is formed on inclined ground and the soil cover is thin and weak, block translation is likely to occur through the foundation. Waste dumps placed on steep slopes of competent material may translate along the contact between the embankment and the foundation. Initiation of block translation may be due to decay of organic matter beneath the dump, earthquakes, melting of buried snow, high water tables and other occurences of groundwater. The slope of the natural ground determines both the potential for and the consequences of block translation. As the slope of the foundation increases so does the potential for translation and the potential areas of impact. The likelihood of such a failure may be evaluated by analysing the block as a sliding rigid body.

3.3.5 Circular Arch Failure

Circular arc failure through the dump material is likely to occur where the dump is formed on a competent foundation and the dump material contains a significant percentage of fine grained soil, refer to Figure 18. The stability of a dump against such failure may be evaluated using any of a number of charts or circular arc failure methods.

Similarly, a circular arc failure surface may develop through a deep foundation soil deposit of fine grained soils, refer to Figure 18. Such failure may be analysed by circular arc methods or by bearing capacity analyses.

3.3.6 Toe Spreading

Toe spreading starts with local yielding of the foundation material at the outer edge of the dump. It often indicates the onset of major base failure or translation of the dump, refer to Figure 18.

3.3.7 Blowout

In contrast to the types of failures discussed, the blowout is catastrophic in nature and provides no warning prior to failure. Blowouts occur in old dumps and are usually caused by the intersection of a perched water zone with the dump slope. Eyewitness accounts[6] and studies of the distribution of debris in areas where blowouts have occurred, indicates that dump material is blown several hundred feet through the air at the start of failure. Large volumes of water invariably accompany failure.

Blowouts pose a serious threat to equipment and personnel because of the extremely rapid rate of movement and lack of observable surface changes prior to failure. It has been found[5] that control of the rate of water application to dumps where perched water zones are known to exist and the installation of drain holes to control saturation near the dump face has been effective in controlling blowout failures. A case study of such a failure has been reported by Pernichele and Kahle[8].

3.4 Foundation Shear Strength

It is evident that foundation shear strength is important in determining the mode and probability of dump failure. Table 8 lists recommendations by Zavodni[7] for dump site foundation field investigation.

It can be assumed that a clay foundation stratum is subjected to unconsolidated, undrained shear because of the low permeability of clay and the rapid rate of loading of the foundation due to dump advancement. Appropriate shear tests must therefore be of the unconsolidated undrained type. Blight[2] recommends the unconsolidated, undrained triaxial shear test and the quick shear box test as suitable laboratory tests. Recommended field tests are the cone penetrometer test and the vane shear test on remoulded soil. Blight also recommends that a minimum factor of safety of 1,5 be used for the design of dumps on stiff fissured clays because of the uncertainties involved in measuring the shear strength of these clays.

Obviously pore pressure plays an important part in the shear strength of clay foundations and hence dump stability. Zavodni[7] discusses an experiment where the foundation pore pressures were monitored and dumping rates adjusted to allow for maximum pore pressure dissipation. Such a monitoring system was found to be valuable in dump stability assessment with respect to foundation failure. For further details refer to Zavodni[7].

TABLE 8 : FIELD INVESTIGATION

INVESTIGATION	PROCEDURE	PURPOSE OF INVESTIGATION
Surface	Develop a geologic/topographic base map. A surface soils map should be developed employing the U.S.C.S.*	Information is required to enable assessment of dump stability, dump failure mode, dump failure runout distance, dump volume, dump surface configuration and dump boulder spray.
Subsurface	Test pits should be excavated and then logged employing the U.S.C.S.	Undisturbed and disturbed samples can be obtained for laboratory testing. Infiltration tests can be performed. Data can be obtained for the development of the geologic, soil and soil isopach maps.
	Seismic refraction surveys	Used for determining depths to bedrock, ground water and for broadly identifying bedrock quality. Also provides basic input for the soil isopach map.
	Boreholes	Used in areas too deep to be surveyed with pits. Soils should be logged according to the U.S.C.S. Bedrock lithology, structure and strength need to be identified along with the depth to the water table.
	Borehole hydraulic conductivity tests	Used to establish seepage characteristics of subsurface soil and rock materials.
	Infiltration tests	Conducted to determine the one-dimensional vertical seepage rate through surface and near surface materials above the water table.

*U.S.C.S. = Unified Soil Classification System (Table 9)

TABLE [illegible]

UNIFIED SOIL CLASSIFICATION [illegible]

MAJOR DIVISIONS			LETTER SYMBOL	TYPICAL DESCRIPTIONS
COARSE GRAINED SOILS More than 50% of material is LARGER than no. 200 sieve size	GRAVEL AND GRAVELLY SOILS More than 50% of coarse fraction RETAINED on no. 4 sieve	CLEAN GRAVELS (Little or no fines)	GW	Well-graded gravels, gravel-sand mixtures, little or no fines
			GP	Poorly-graded gravels, gravel-sand mixtures, little or no fines
		GRAVELS WITH FINES (Appreciable amount of fines)	GM	Silty gravels, gravel-sand-silt mixtures
			GC	Clayey gravels, gravel-sand-silt mixtures
	SAND AND SANDY SOILS More than 50% of coarse fraction PASSING no. 4 sieve	CLEAN SAND (Little or no fines)	SW	Well-graded sands, gravelly sands, little or no fines
			SP	Poorly-graded sands, gravelly sands, little or no fines
		SANDS WITH FINES (Appreciable amount of fines)	SM	Silty sands, sand-silt mixtures
			SC	Clayey sands, sand-clay mixtures
FINE GRAINED SOILS More than 50% of material is SMALLER than no. 200 sieve size	SILTS AND CLAYS	Liquid Limit LESS than 50	ML	Inorganic silts and very fine sands, rock flour, silty or clayey fine sands or clayey silts with slight plasticity
			CL	Inorganic clays of low to medium plasticity, gravelly clays, sandy clays, silty clays, lean clays
			OL	Organic silts and organic silty clays of low plasticity
	SILTS AND CLAYS	Liquid Limit GREATER than 50	MH	Inorganic silts, micaceous or diatomaceous fine sand or silty soils
			CH	Inorganic clays of high plasticity, fat clays
			OH	Organic clays of medium to high plasticity, organic silts
HIGHLY ORGANIC SOILS			PT	Peat, humus, swamp soils with high organic contents

NOTE: Dual symbols are used to indicate borderline soil classifications.

Dumps founded on intact soils such as aeolian sands, pose fewer problems as the shear strength of intact soils can be measured with less uncertainty. Blight[2] states that the tests recommended for stiff fissured clays are also valid for intact soils.

References

1. BLIGHT, G.E., "Foundation Failures of Four Rockfill Slopes", ASCE, Soil Mechanics and Foundations Division, May, 1969.

2. BLIGHT, G.E., "Shear Stability of Dumps and Dams of Gold Mining Waste", The Civil Engineer in South Africa, March, 1969.

3. BLIGHT, G.E., "On the Failure Mode of Waste Rock Dumps", Design of Non-Impounding Mine Waste Dumps Workshop, Society of Mining Engineers, AIME, Denver, 1981.

4. CALDWELL, J.A., ALLAN, S.E., Steffen Robertson and Kirsten, and VANDRE, B.C., "The Simplified Analysis of Mine Waste Embankments", Design of Non-Impounding Mine Waste Dumps Workshop, Society of Mining Engineers, AIME, Denver, 1981.

5. CAMPBELL, D.B. and SHAW, W.H., "Performance of a Waste Rock Dump on Moderate to Steeply Sloping Foundations", Proceedings of the First International Symposium on Stability in Coal Mining, Vancouver, British Columbia, Canada, Chapter 27, 1978.

6. PERNICHELE, A.D. and KAHLE, M.B., "Stability of Waste Dumps at Kennecct's Bingham Canyon Mine", Transcedings of Society of Mining Engineering, AIME, Volume 250, Number 4, December 1971, page 363.

7. ZAVODNI, Z.M., TREXLER, B.D. and PILZ, J., "Waste Dump Foundations Investigations and Treatment", Design of Non-Impounding Mine Waste Dumps Workshop, Society of Mining Engineers, AIME, DENVER, 1981.

8. LYLE, K., "Report on Increasing the Height of the Tailings Dump", Anglo American Corporation of South Africa Limited, June, 1982.

CHAPTER 4 : METHODS OF SLOPE STABILITY ANALYSIS

The factor of safety of a dump may be estimated using simple equations or stability charts and tables. Simplified slope stability methods refer to the analysis of simplified conditions such as simple slope geometry, uniform physical properties, saturated or unsaturated slopes and specific sliding surfaces. When analysing mine waste embankments, limitations in the accuracy of the limiting equilibrium methods frequently become insignificant when compared to the inability to accurately define the parameters in the stability analysis. Thus the factor of safety presented this way is a first approximation of the stability of the dump. These simplified methods are valuable because of their ease of use and potential for pin-pointing likely failure. Table 10 adapted from Caldwell[1] lists the analytical methods that may be used to study the potential dump instability. Choosing a method to analyse the stability of a dump can be based upon the model assumptions or the range or parameters or values considered. This information is summarised in Table 10 for each method.

4.1 Edge Slides and Shallow Flow Slides

This mode of failure is best evaluated using the equations describing the stability of an infinite slope. However, the analysis is complicated by our inability to predict the input parameters. Cohesion varies with moisture content and is transient. The friction angle may vary with particle size because of the low confining pressures. If the safety factor (F) is defined as the ratio of available shear strength to the mobilised shear strength, the following equation can be used, (refer to figure 23).

TABLE 10 : SIMPLIFIED METHODS OF ANALYSIS OF WASTE DUMPS [1]

FAILURE MODE	SIMPLIFIED METHODS OF ANALYSIS	MODEL DESCRIPTION	PARAMETERS
1. Surface or Edge Slide	$F = \frac{C + \gamma D \cos\beta \tan\phi}{\gamma D \sin\beta}$	Infinite slope: sliding surface parallel to slope, only the stresses in the sliding surface together with the weight of the soil enter into the limiting equilibrium analysis.	Safety factor (F) is the ratio of available shear strength to the mobilized shear strength. Unit weight (γ). Cohesion (C). Angle of shearing resistance (ϕ). Slope angle (β). Depth to sliding surface (D).
2. Shall - Flow Slide	$F = \gamma'/\gamma \; \frac{\tan\phi'}{\tan\beta}$	Same as edge slide model except seepage added acting parallel to slope.	F, β, ϕ, same as edge slide. Submerged unit weight (γ'). Saturated unit weight (γ).
3. Block Translation	Wedge Stability Analysis. See Huang[12].	The dump is taken as a rigid body that may slide down an inclined plane. Use standard equations from statics.	Weight of rock, geometry, strength along failure plane.
4. Circular Arc Failure	Huang Charts[12]. Any circular arc failure method (e.g. Bishop) See also Hunter and Schuster[17]	The failure of zone is taken as a circular body that slides.	Material strengths, slope geometry.

TABLE 10 : SIMPLIFIED METHODS OF ANALYSIS OF WASTE DUMPS[1]

FAILURE MODE	SIMPLIFIED METHODS OF ANALYSIS	MODEL DESCRIPTION	PARAMETERS
5. Base Failure			
a. Foundation spreading	Chart: stability coefficient ($\tau/\gamma H$) vs slope of Foundation Blight, 1981	Equilibrium of a system of wedges beneath a slope, the shear stress equals the horizontal component of thrust from the active wedge divided by the length of the base of the passive wedge. Sliding surface for active wedge inclined relative to horizontal at $45^o + \phi/2$, sliding surface for passive wedge along foundation interface (passive resistance of foundation ignored), slope angle (β) equals embankment ϕ.	Unconsolidated-undrained shear strength (τ), unit weight (γ), slope of foundation ($0-15^o$), height of slope measured Embankment ϕ ranges between $30-40^o$. $\tau/\gamma H$ ranges between 0.04-0.10, safety factor is the ratio between available τ and the mobilised τ.
b. Base Translation (toe wedges)	Chart: required angle of shearing resistance of foundation (ϕ_f) vs slope of foundation (i), Blight, 1981.	Same as Blight's Foundation Spreading model.	ϕ_f ranges between $5-30^o$. i ranges between $0-15^o$. Embankment ϕ ranges between $30-40^o$.
6. Foundation Circular Arc	Bearing capacity charts. See also Figure 11.	The dump is assumed to act as a loading on a foundation soil. The subsoil may fail by the formation of a circular arc failure surface beneath the dump.	Dump geometry weight, strength of subsoil.
7. Toe Spreading	Table: Required Angle of Friction (ϕ_α) In Inclined Base of Slope of Cohesionless Soil, Brauns, 1980 See Fig. 21.	ϕ_f determined graphically using Mohr diagram for the state of Active Rankine equilibrium.	ϕ_f ranges between $5-44.3^o$ ranges between $5-40^o$. Embankment ϕ ranges between $5-45^o$. Slope angle ranges between $5-45^o$.

$$F = \frac{c + \gamma D\cos\beta \tan\phi}{\gamma D \sin\beta} \quad * \quad \ldots\ldots\ldots\ldots \quad (8)$$

where c = cohesion = $c'/\cos\beta$

γ = unit weight of soil

ϕ = angle of shearing resistance

β = slope angle

D = depth to sliding surface

If c is assumed to be zero for a cohesionless dump, then equation (1) reduces to;

$$F = \frac{\tan\phi}{\tan\beta} \quad \ldots\ldots\ldots\ldots \quad (9)$$

For the shallow flow slide with seepage acting parallel to the slope equation (1) becomes;

$$F = \frac{c}{\gamma D \sin i} + \frac{\gamma' \tan\phi}{\gamma \tan\beta} \quad \ldots\ldots\ldots \quad (10)$$

where $\gamma' = \gamma - \gamma_w$

γ_w = unit weight of water

For a cohesionless dump, equation (3) reduces to;

$$F = \frac{\gamma'}{\gamma} \cdot \frac{\tan\phi'}{\tan\beta} \quad \ldots\ldots\ldots\ldots \quad (11)$$

*Refer to Appendix B for derivation.

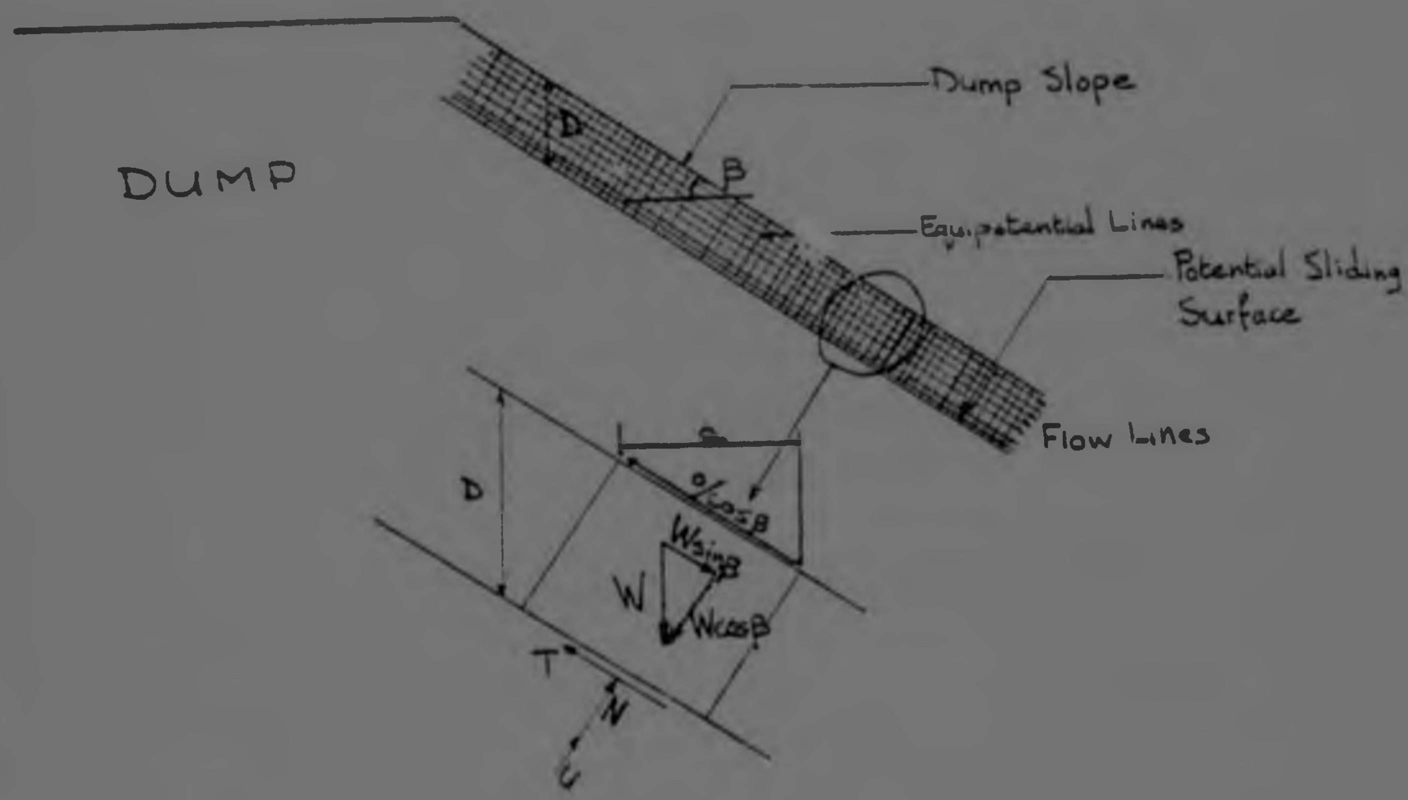

FIGURE 23 : Edge slidges and shallow flow slides[1]

4.2 Circular Arc Failure

Many circular arc methods exist for the analysis of dump slopes containing a significant percentage of cohesive material. Huang[2] has developed a number of charts based on the simplified Bishop method for determining the factor of safety of dump slopes. Wright[3] concluded after investigating limit equilibrium slope analysis procedures that the simplified Bishop method gave reasonable factors of safety for circular shear surfaces. The factor of safety, F, by Huang's method is given as follows:

$$F = F_1 \cdot C_f \quad \ldots\ldots\ldots\ldots\ldots\ldots\ldots\ldots \quad (12)$$

where F_1 = preliminary safety factor

$$= N \left| \frac{c'}{\gamma H} + \frac{(1 - r_u) \tan\phi'}{N_f} \right| \quad \ldots\ldots\ldots\ldots \quad (13)$$

N_s is the stability number, refer to Figure 24

N_f is the friction number, refer to Figure 24

r_u is the pore pressure ration

$$= \frac{\text{cross-sectional area of bench under water}}{2 \times \text{total cross-sectional area of bench}}$$

c' and ϕ' are the effective cohesion and friction angle of the embankment

γ is the mass unit weight

H is the height of the dump (reference Figure 24)

C_f is the correction factor dependant on ϕ', w and α (refer to Figure 25)

To illustrate the use of the charts the following example is giver: Assumed material parameters for fill; $c' = 9,6$ kN/m^2, $\phi' = 30^0$, $r_u = 0,05$ and $\gamma = 19,6$ kN/m^3.

Spoil dump parameters; $H = 9{,}2$ m, $w = 36^{\circ}$ and $\alpha = 20^{\circ}$

Solution: From Figure 24 ($w = 36^{\circ}$ and $\alpha = 20^{\circ}$), $N_s = 10{,}1$ and $N_f = 4{,}9$. From equation (13), $F_1 = 1{,}535$. From Figure 25, $P_c = 26{,}3\%$ and hence $C_f = 0{,}90$. Therefore $\underline{F = C_f . F_1 = 0{,}9 \times 1{,}535 = 1{,}38}$

Alternative circular arc methods do exist. Discussion and charts of the Bishop and Morgenstern method, Spencer method and the Hunter and Schuster method may be found in reference (4).

4.3 Foundation Circular Arc Failure

Caldwell[1] suggests that in order to evaluate the stability of a dump against rotational failure on a deep, soft foundation soil, the dump may be treated as a foundation applying a non-uniform load. This involves assuming that the dump has zero strength. Caldwell states that this assumption is not true, but deformation of the subsoil and the prescence of the resulting tension cracks mean that the dump itself may contribute little to the resisting forces along the potential failure plane. Blight[5] found from his studies on the failure of four rockfill slopes that the dump resisting forces along the failure plane contribute significantly to the total forces resisting failure. However, Caldwell has found that

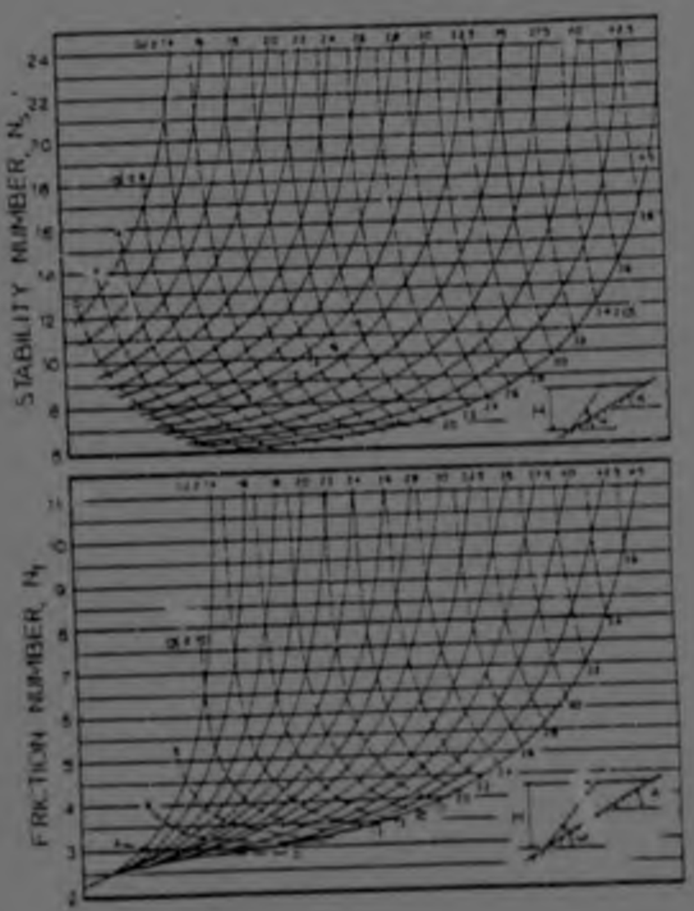

FIGURE 24 : Stability chart[2]

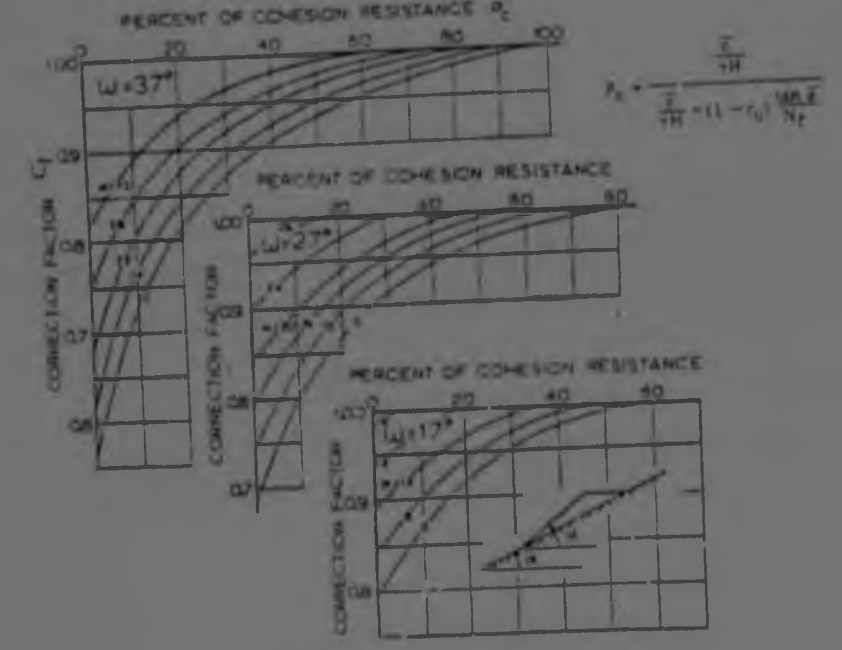

Figure 25 : Correction factor[2]

the assumption of zero dump strength yields reasonable results. Various bearing capacity charts may be used for stability analysis and Caldwell has recommended the equations, figures and charts shown in Figure 26. Figure 26 is the result of extensive theoretical and experimental studies by Suklje (1954)'. Suklje developed solutions for the bearing capacity problem of a layer of soft clay resting on a firm base in undrained conditions. Suklje verified his solutions by small-scale model experiments.

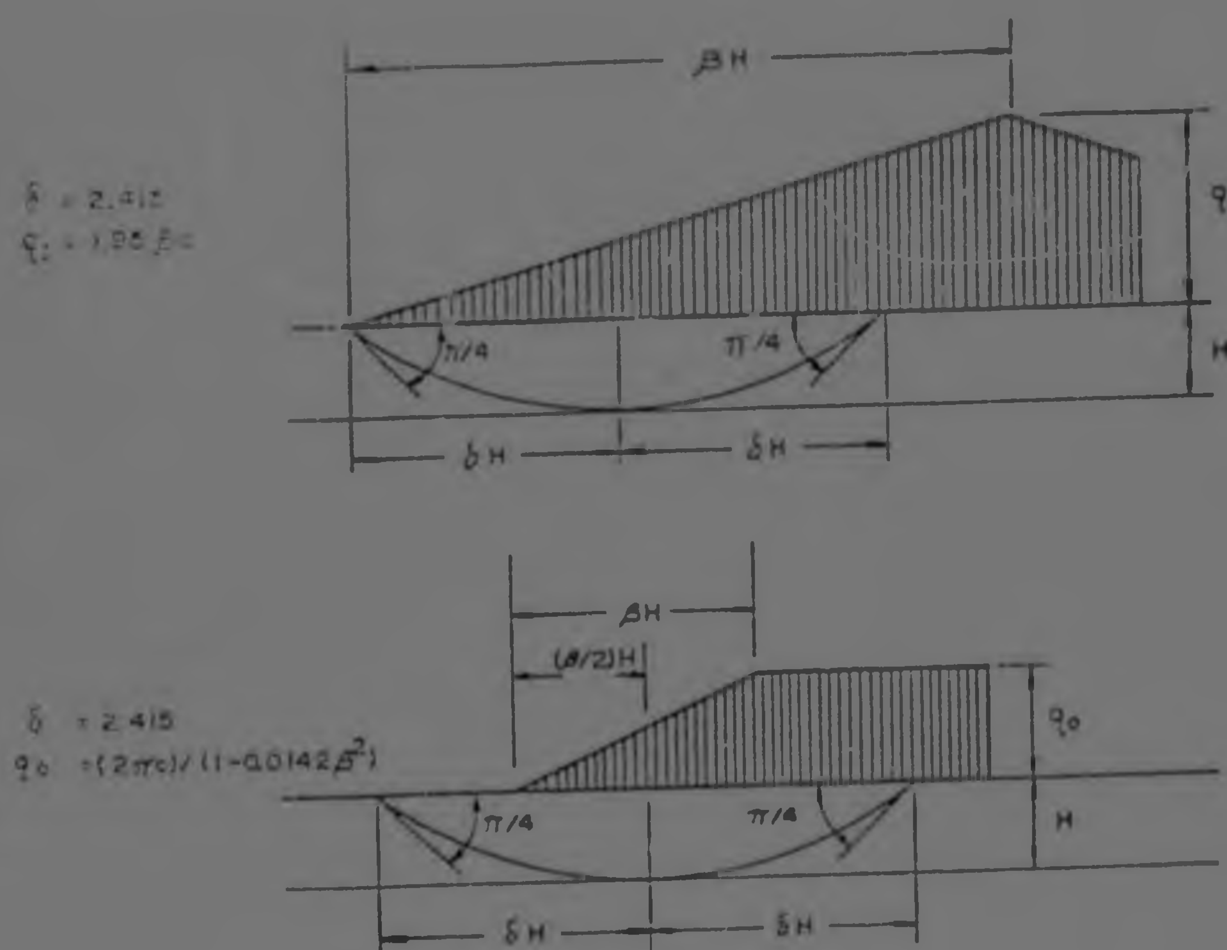

FIGURE 26 : Evaluation of foundation failure'

4.4 Block Translation

The following method of analysis for block translation has been proposed by Huang[2]. Figure 27 shows the forces considered by Huang in his calculations.

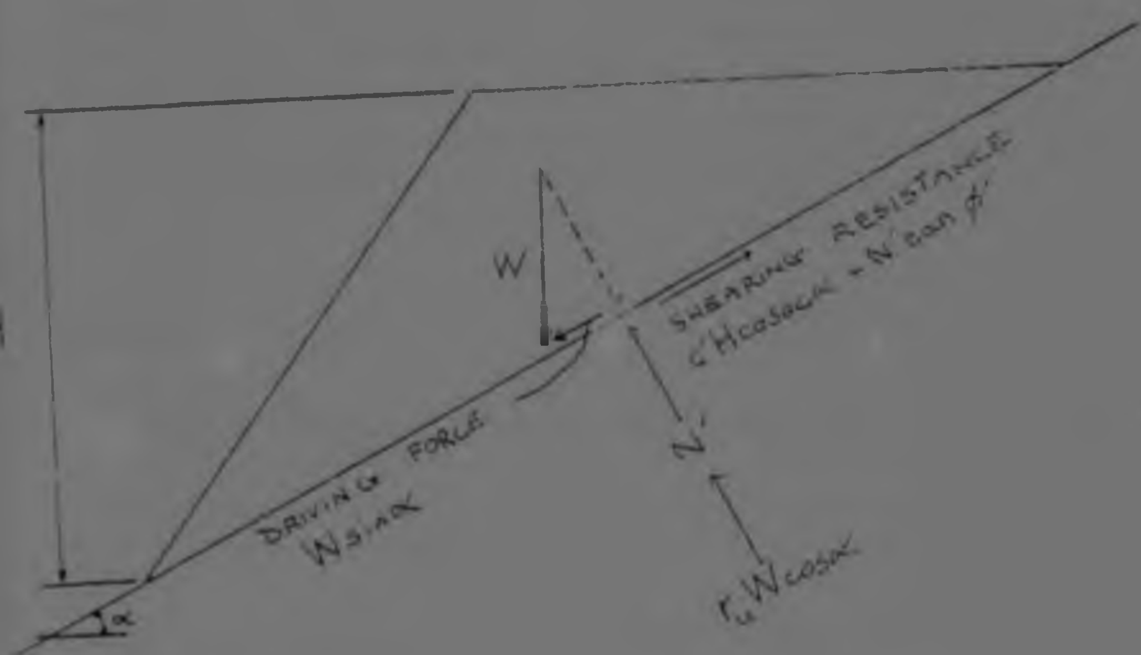

FIGURE 27 : Forces on spoil bank[2]

The factor of safety is defined as the ratio between the resisting force due to the shear strength of the soil along the failure surface to the driving force due to the weight of the fill. The resisting force is composed of two parts: one due to cohesion and equal to (c' H cosec α), where H cosec α is the length of the failure plane, and the other due to friction and equal to (N' tan ϕ'). Huang has defined N' the effective force normal to the failure plane, (see Appendix B) as follows;

$$N' = (1 - r_u)\ W \cos\alpha \ \ldots\ldots\ldots\ldots \qquad (14)$$

Where r_u is the pore pressure ratio as defined previously. Therefore the factor of safety, the ratio between shear resistance and the driving force, can be written as;

$$F = \left[\frac{c'H \operatorname{cosec}\alpha + (1-r_u)\ W \cos\alpha \tan\phi'}{W \sin\alpha}\right] \ \ldots\ldots \qquad (15)$$

in which

$$W = \left[\tfrac{1}{2}\ \gamma\ H^2 \operatorname{cosec}\omega \operatorname{cosec}\alpha\ \sin(\omega-\alpha)\right] \ \ldots\ldots\ldots \qquad (16)$$

and γ = mass unit weight of fill.

Substituting equation (16) into equation (15)

$$F = 2 \sin\omega \operatorname{cosec}\alpha \operatorname{cosec}(\omega\ \alpha)\left(\frac{c'}{\alpha H}\right)+(1-r_u).\tan\phi' \cot\alpha \ \ldots \qquad (17)$$

4.5 Foundation Failures

In South Africa, dump foundations generally consist of a relatively shallow stratum of weak material overlying hard material. As a result dump failures appear to consist of a plane slide through the dump combined with a plane slide through the foundation stratum. A study[5] of slides in rock dumps on foundations of thin clay strata overlying harder material and a study of slides in model rock dumps have confirmed that the failure surfaces are of this form.

Blight[6] considered the system of wedges that form within the dump during failure to make an approximate analysis of the stability of rock dumps. The possibility of first-time failure as illustrated in Figure 20a is considered here. The geometry of the sliding wedge analysis used by Blight is shown in Figure 28. The assumption of a vertical interface between the wedges will be discussed later in this section.

For a rock dump on a thin clay foundation stratum, $\phi=0$, Blight proposed that the average shear strength required for a state of limiting equilibrium to develop is given by (see Appendix B).

$$\frac{\tau}{\gamma H} = A\,(B + C) \quad \ldots\ldots\ldots\ldots\ldots\ldots\ldots\ldots \quad (18)$$

where H = maximum height of rock dump

τ = slope angle of ground on which dump is built.

$$A = \frac{\sin(\alpha - i)\sin\beta}{\sin(\alpha-\beta)\cos i} \quad \ldots\ldots\ldots\ldots\ldots\ldots\ldots \quad (19)$$

$$B = \left[\frac{\cos^2\alpha}{2}\,(1-\cot\alpha\tan\beta)(1-\cot\alpha\tan\phi)\left(1-\frac{\tan i}{A}\right)^2\right] \quad \ldots (20)$$

$$C = \left[\frac{\cos^2 i}{2}\cdot\frac{\sin i}{\sin\beta}\cdot\frac{\sin^2(\alpha-\beta)}{\sin^2(\alpha-i)}\left(\frac{\cos i}{\cos\beta}-\frac{\sin i}{\sin\beta}\right)\right] \quad \ldots\ldots (21)$$

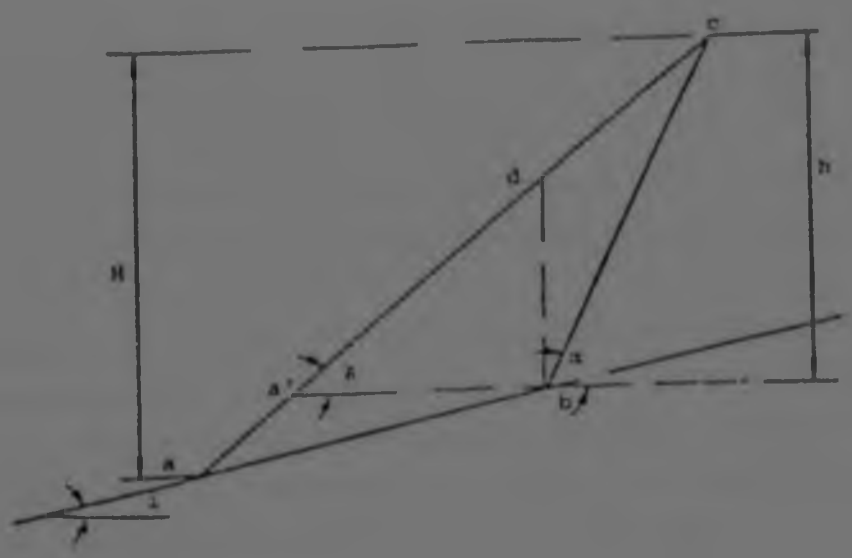

FIGURE 28a : Geometry of sliding wedge analysis[8]

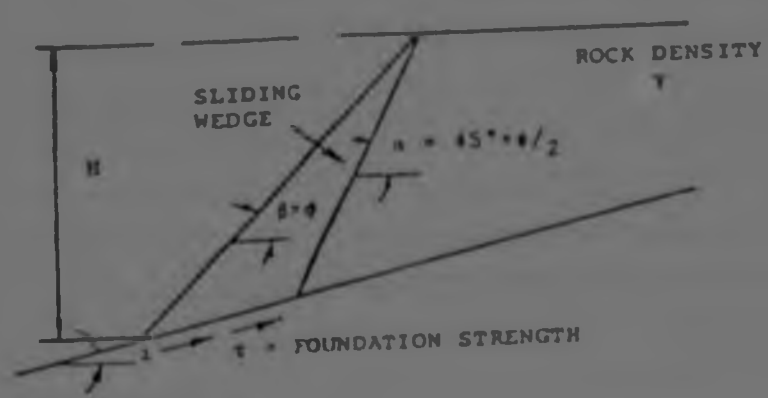

FIGURE 28b : Foundation strength corresponding to failure of dump on shallow cohesive foundation according to sliding wedge analysis[8].

α = inclination of failure surface within rockfill

β = inclination of tipping face of rock dump

γ = bulk density of rockfill

ϕ = angle of shearing resistance of rockfill

τ = average ϕ=0 shear strength of foundation clay stratum.

Blight[6] states that for the purposes of preliminary design, the approximations, $\phi=\beta$ and $\alpha=45^{o} + \phi/2$ are probably satisfactory. Using the assumptions, $\phi>\beta$ and $\alpha = 45^{o}+\phi/2$, a chart, refer to Figure 29, has been drawn up to show the required foundation average shear strength for varying conditions.

Blight[5] compared the range of measured foundation strengths of four first-time failures of rock dumps with values predicted from equation (18) as shown in Figure 30. The comparison shows that there is reasonable agreement between measurement and theoretical prediction and also illustrates the large range of measured shear strengths that can be expected to occur in a natural clay foundation stratum. For the same four dumps, Blight compared values for the stability of the rock dumps investigated by three different methods. These methods being the sliding wedge analysis, Rendulic analysis and the Janbu analysis. The results are tabulated in Table 11. The angle for the failure plane through the rockfill, α, requiring the largest shear stress, τ, to maintain equilibrium for each slope was accepted as critical. Blight concluded from this comparison that although there were appreciable differences in the shear strengths calculated by the three methods, the variation was not significant when compared with the natural variation in the shear strength.

According to Marais[7] the theories of Sokolovski, Booth, Nadai and Trollope for predicting the stress across the base of an embankment of cohesionless granular material are substantially in agreement both in magnitude and distribution to that of Rendulic. This is illustrated in Figure 31. Marais compared the method

BASE ANGLE I, IN DEGREES	SLOPE ANGLE B, IN DEGREES	ANGLE OF INTERNAL FRICTION OF SLOPE MATERIAL, φ, IN DEGREES						
		15	20	25	30	35	40	45
0	15	39	33	27	22	18	15	11
	20		45	37	30	25	20	16
	25			47	39	32	25	20
	30				45	39	31	25
	35					47	38	30
	40						46	36
	45							43
5	15	44	41	39	37	35	34	32
	20		54	49	46	43	40	38
	25			59	54	50	46	43
	30				62	56	52	48
	35					63	57	56
	40						63	56
	45							61
10	15	32	31	31	30	30	30	29
	20		51	49	48	47	46	45
	25			63	60	58	56	55
	30				70	67	64	62
	35					74	70	67
	40						76	72
	45							76
15	20		34	34	33	33	33	33
	25			55	54	53	53	52
	30				69	68	66	65
	35					78	76	74
	40						83	81
	45							86
20	25			35	35	35	35	35
	30				58	58	57	57
	35					74	73	73
	40						84	83
	45							91
25	30				36	36	36	36
	35					61	60	60
	40						79	78
	45							89
30	35					37	37	37
	40						62	63
	45							81
35	40						37	37
	45							64
40	45							37

FIGURE 29 : Required shear strength in thin strata of clay material (F.S.=1) $\tau/_{\gamma H}$ (10[illegible])

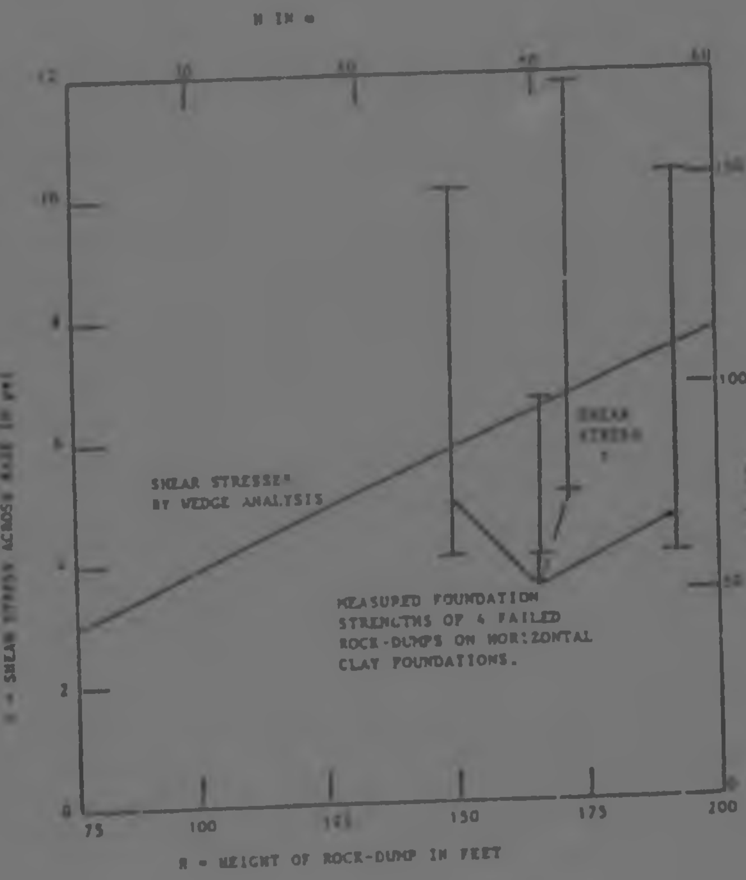

FIGURE 30 : Comparison of measured foundation strengths with strengths required for stability according to wedge analysis (Figure 13)[6]

TABLE 11 : SHEAR STRENGTHS CALCULATED FROM ROCK DUMP FAILURES BY THREE METHODS[5]

ROCK DUMP	SHEAR STRENGTH (τ) FOR FACTOR OF SAFETY OF 1							
	SLIDING WEDGE ANALYSIS			RENDULI ANALYSIS		JANBU ANALYSIS		
	Critical α	τ in kPa		Critical α	τ in kPa	Critical α	τ in kPa	
		$\phi = 39^o$ $\gamma = 17,5$ kN/m³	$\phi = 41^o$ $\gamma = 16,7$ kN/m³		$\phi = 41^o$ $\gamma = 17,5$ kN/m³		$\phi = 39^o$ $\gamma = 17,5$ kN/m³	$\phi = 41^o$ $\gamma = 16,7$ kN/m³
lakfontein (1)	55^o	63,6	55,3	62^o	57,4	60^o	93,3	81,6
(2)	55^o	49,8	43,5	62^o	51,1	62^o	74,0	62,9
arievale	55^o	43,5	38,0	59^o	46,3	62^o	69,1	60,8
ogelstruisbult	55^o	58,1	52,5	62^o	58,1	62^o	85,0	73,9
A Lands	55^o	39,4	33,9	62^o	43,5	62^o	58,7	50,5

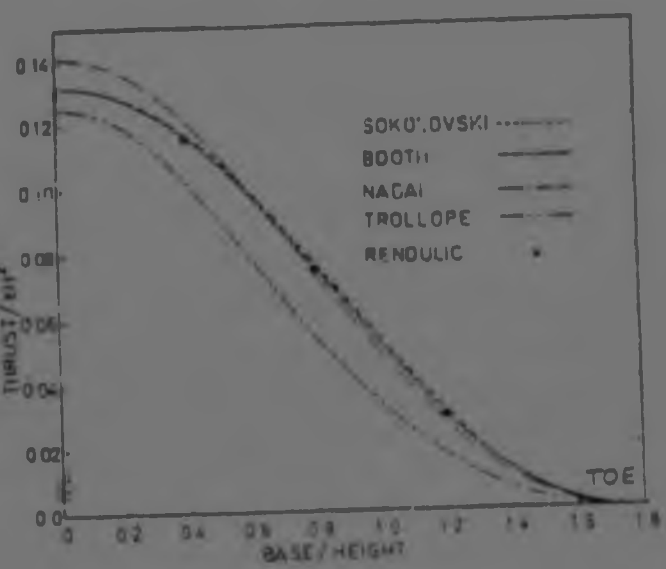

FIGURE 31 : Active horizontal thrusts in a symmetrical wedge composed of cohesionless materials according to various theories[7]

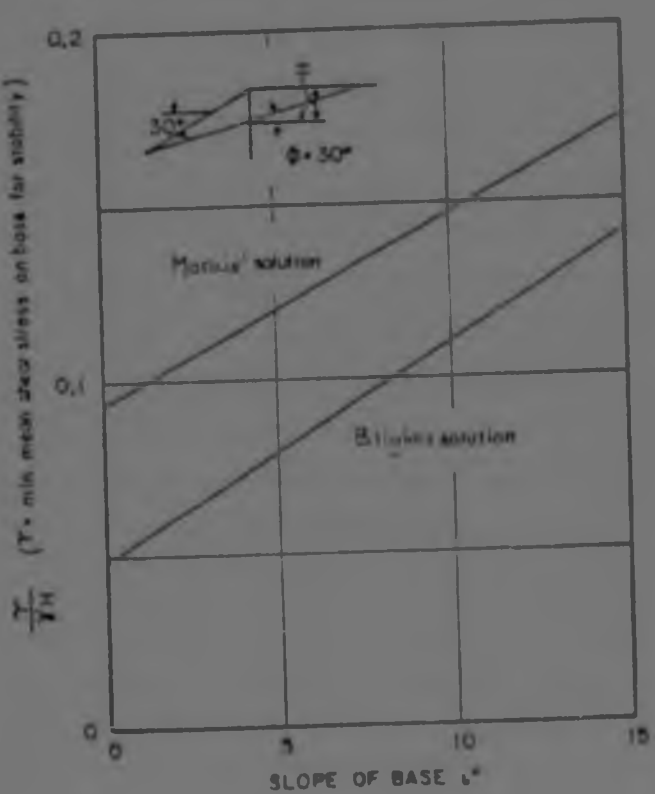

FIGURE 32 : Minimum mean shear resistance stress in base to prevent active failure of dump for various base slopes[7]

of Blight to that of Rendulic and concluded that Blight's method was too conservative and thus unsafe, refer to Figure 32. However Blight has found that the evidence from the earlier study of rock dump failures[5] indicates that actual shear stresses across the base of a rock dump tend to be even less than predicted on the basis of the simplified wedge analysis. Therefore this simplified analysis should be adequate to give a useful first estimate for the state of stability of a dump.

Using small-scale models Sultan and Seed[8] investigated slope stability calculations for sloping core earth dams consisting of embankments of gravel or rockfill. They concluded from their investigations that the assumption of a vertical interface between the active upper wedge and the lower passive wedge leads to an overestimate of the factor of safety. However they also found that the use of a triaxial test angle of friction leads to an underestimate of the factor of safety and hence incorporating both of these features in a stability analysis, leads to a factor of safety which, as a result of compensating errors, is close to that obtained by a correct analysis. The correct analysis being one using an inclined interface between the wedges and a plane strain angle of friction. Sultan and Seed investigated the above by failing model embankments and then comparing the computed predictions versus the actual conditions. The results of one of these tests and the model embankment cross-section are shown in Table 12 and Figure 33 respectively.

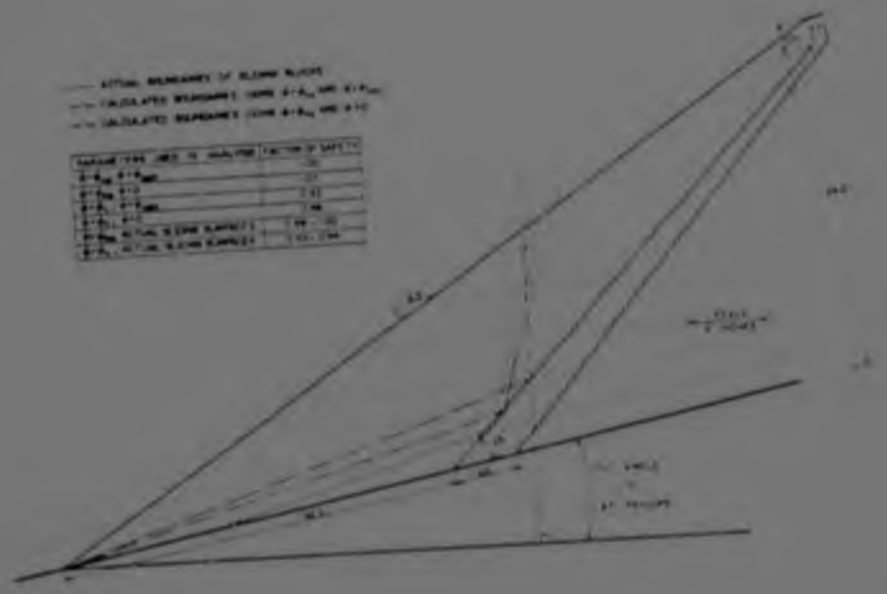

FIGURE 33 : Comparison of computed and actual sliding surfaces-embankment No. 1[5]

TABLE 12 : COMPUTED FACTORS OF SAFETY FOR TEST EMBANKMENT NO. 1[5]

Shear Strength of core, s, in pounds per square foot	Angle of Friction of shell material, ϕ, in degrees	Inclination of Boundary between blocks to vertical, ψ, in degrees	Factor of safety
2,5	$\phi = \phi_{ps} = 38$	$\psi = \psi_{crit} = 17$	1,0
2,5	$\phi = \phi_{ps} = 38$	$\psi = 0$	1,07
2,5	$\phi = \phi_{t} = 35,5$	$\psi = \psi_{crit} = 17$	0,92
2,5	$\phi = \phi_{ps} = 38$	actual failure surface	1,0
2,5	$\phi = \phi_{t} = 35,5$	actual failure surface	0,94

ps - plain strain $\psi = 0$ - vertical

t - triaxial

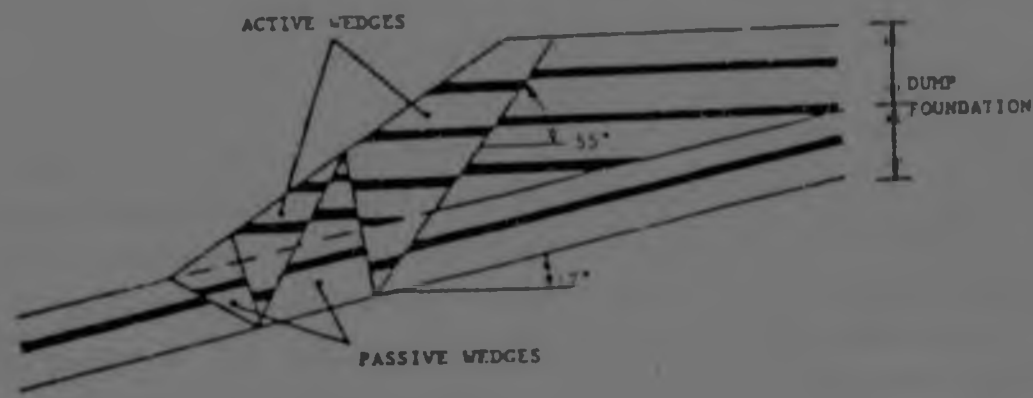

FIGURE 34 : Active and passive wedges developed in failure of a model of rock-dump on inclined frictional foundation[6]

Blight[6] has conducted a preliminary investigation into the stability of rock dumps on non-cohesive foundations. Blight found that failure was also developed by a system of active wedges displacing passive wedges see Figure 34. Blight concluded that for the limiting case of a shallow frictional foundation, a similar analysis to that described for dumps on shallow cohesive foundations may be developed. The result of this analysis indicates that the average angle of shearing resistance required for a state of limiting equilibrium to develop in the rockfill is given by (see Appendix B).

$$\tan \phi_f = \left[\frac{B}{D \cos^2 i} + \tan i \right] \quad \ldots\ldots\ldots\ldots\ldots\ldots \quad (22)$$

where

$$D = \frac{1}{2}\left[\frac{\sin^2 (\alpha-\beta)}{\sin^2 (\alpha-i)} \cdot \frac{\cos i}{\sin\beta} \left[\frac{\cos i}{\cos \beta} - \frac{\sin i}{\sin\beta} \right]\right] \quad \ldots\ldots\ldots\ldots \quad (23)$$

ϕ_f = average angle of shearing resistance of frictional foundation stratum i, B, α and β have the same values as before. It is interesting to note here that the result is independant of both the height of the dump and the density of the rockfill. A chart of the required ϕ_f for varying dump conditions is shown in Figure 35.

Brauns[9] investigated the problem of local slip in the interface between embankment and cohesionless foundation material. Braun's chart, Figure 36, showing required foundation friction angles for varying dump conditions, is based upon the theories of Rendulic and Brendlin. A comparison between Figure 35 and Figure 36 would suggest that Blight's results are too low. However, Braun's results are based on the theory of Rendulic which appeared to give high required average foundation shear strengths for the case of dumps on thin cohesive foundations. Thus Blight's results may in fact be closer to the conditions experienced in actual dumps. This would require further investigation.

Uriel[10] has presented two graphs, see Figure 37, for determining the required slope angle for slope stability under varying frictional strength values of the dump and foundation material. These results are only valid for horizontal foundations. Figure 37(a) shows the results when the ratio of the bulk density of the dump material, [illegible] and the foundation material, γ_1, is equal to unity. Figure 37([illegible]) shows the results when the ratio γ_1 to γ_2 is equal to 0,5. Unfortunately reference as to how Uriel obtained these figures is not available.

4.6 Sturzstrom-Type Slides

Data from four sturzstrom-type slides originating from the faces of waste rock dumps in eastern British Columbia indicate an empirical correlation between the vertical height of a waste rock dump and the fahrboschung, or vertical angle below the horizontal from the crest of the dump, before failure to the distall portion of the slide debris. The data is plotted in Figure 38 in

BASE ANGLE IN DEGREES (i)	SLOPE ANGLE IN DEGREES (β)	ANGLE OF INTERNAL FRICTION OF SLOPE MATERIAL, ϕ, IN DEGREES						
		15	20	25	30	35	40	45
0	15	5,7	4,6	3,8	3,0	2,4	1,9	1,5
	20		6,8	5,5	4,4	3,5	2,7	2,1
	25			7,7	6,1	4,8	3,7	2,8
	30				8,2	6,4	4,9	3,7
	35					8,5	6,4	4,8
	40						8,5	6,3
	45							8,3
5	15	8,8	8,1	7,5	7,0	6,6	6,3	6,0
	20		10,2	9,2	8,3	7,6	7,1	6,6
	25			11,2	9,9	8,9	8,0	7,3
	30				11,9	10,4	9,1	8,1
	35					12,4	10,6	9,2
	40						12,6	10,6
	45							12,5
10	15	11,9	11,6	11,3	11,0	10,8	10,7	10,5
	20		13,5	12,8	12,3	11,8	11,4	11,1
	25			14,7	13,7	12,9	12,3	11,8
	30				15,6	14,4	13,4	12,6
	35					16,3	14,8	13,6
	40						16,6	14,9
	45							16,7
15	20		16,8	16,4	16,2	15,9	15,7	15,5
	25			18,2	17,6	17,8	16,6	16,2
	30				19,3	18,4	17,6	17,0
	35					20,1	18,9	17,9
	40						20,7	19,2
	45							20,9
20	25			21,7	21,3	21,0	20,8	20,6
	30				23,0	22,3	21,8	21,4
	35					24,0	23,0	22,3
	40						24,7	23,5
	45							25,1
25	30				26,6	26,2	25,9	25,7
	35					27,8	27,1	26,6
	40						28,7	27,7
	45							29,3
30	35					31,5	31,1	30,8
	40						32,6	31,9
	45							33,4
35	40						36,4	36,0
	45							37,4
40	45							41,3

FIGURE 35 : Required angle of friction in foundation of cohesionless soil in degrees (F.S. = 1), from Blight equation (22).

BASE ANGLE, IN DEGREES	SLOPE ANGLE, IN DEGREES	ANGLE OF INTERNAL FRICTION OF SLOPE MATERIAL, ϕ, IN DEGREES						
		15	20	25	30	35	40	45
(1)	(2)	(3)	(4)	(5)	(6)	(7)	(8)	(9)
0	5	3,0	2,5	2,0	1,7	1,4	1,1	0,9
	10	6,4	5,2	4,2	3,4	2,8	2,2	1,7
	15	13,2	8,5	6,7	5,4	4,3	3,4	2,7
	20		16,1	9,9	7,7	6,0	4,7	3,7
	25			18,0	10,8	8,2	6,3	4,8
	30				19,1	11,1	8,2	6,2
	35					19,5	11,0	7,9
	40						19,2	10,5
	45							18,4
5	5	5	5	5	5	5	5	5
	10	8,3	7,6	7,1	6,7	6,4	6,1	5,9
	15	14,2	10,8	9,6	8,7	7,9	7,3	6,8
	20		17,6	12,7	10,9	9,6	8,6	7,8
	25			20,2	13,9	11,7	10,2	9,0
	30				21,9	14,6	12,1	10,3
	35					22,7	14,8	12,0
	40						22,8	14,6
	45							22,4
10	10	10	10	10	10	10	10	10
	15	14,8	13,0	12,4	11,9	11,5	11,2	10,9
	20		18,9	15,3	14,1	13,2	12,5	11,9
	25			22,1	17,0	15,2	14,0	13,1
	30				24,4	18,0	15,9	14,4
	35					25,8	18,5	16,1
	40						26,3	18,6
	45							26,3
15	15	15	15	15	15	15	15	15
	20		19,7	17,8	17,1	16,6	16,3	16,0
	25			23,6	19,9	18,6	17,8	17,1
	30				26,6	21,3	19,6	18,4
	35					28,6	22,2	20,1
	40						29,7	22,5
	45							30,0
20	20		20	20	20	20	20	20
	25			24,6	22,6	21,9	21,4	21,1
	30				28,3	24,5	23,2	22,4
	35					31,0	25,7	24,0
	40						32,7	26,4
	45							33,6
25	25			25	25	25	25	25
	30				29,5	27,4	26,7	26,3
	35					33,1	29,1	27,9
	40						35,5	30,1
	45							36,9
30	30				30	30	30	30
	35					34,5	32,2	31,5
	40						37,8	33,7
	45							40,0
35	35					35	35	35
	40						39,4	37,0
	45							42,4
40	40						40	40
	45							44,3

Note: Factor of safety against local slip in dam base, F = 1,0

FIGURE 36 : Brauns' charts[9]

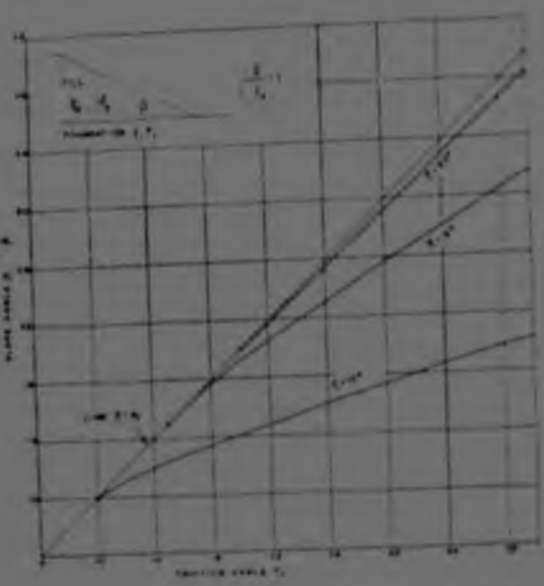

FIGURE 37(a) : Required slope angle for γ_1/γ_2 = 1,0 (after Uriel[10])

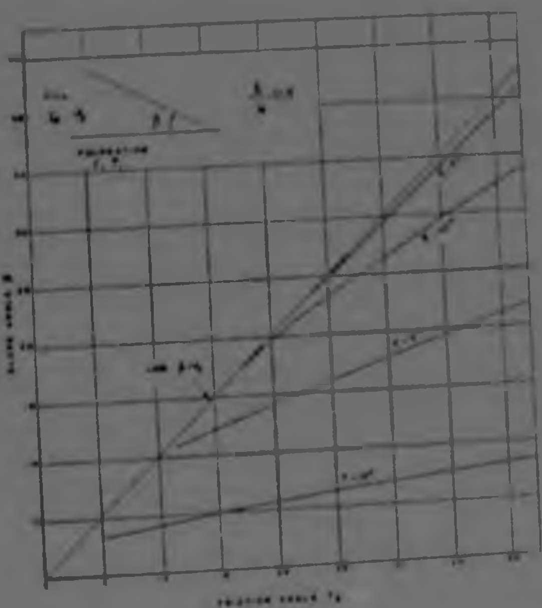

FIGURE 37(b) : Required slope angle for γ_1/γ_2 = 0,5 (after Uriel[10]) the form of the vertical height of the waste dump versus the contangent of the fahrboschung. Thus an estimate of the potential travel distance in the event f a sturzstrum-like slide may be made.

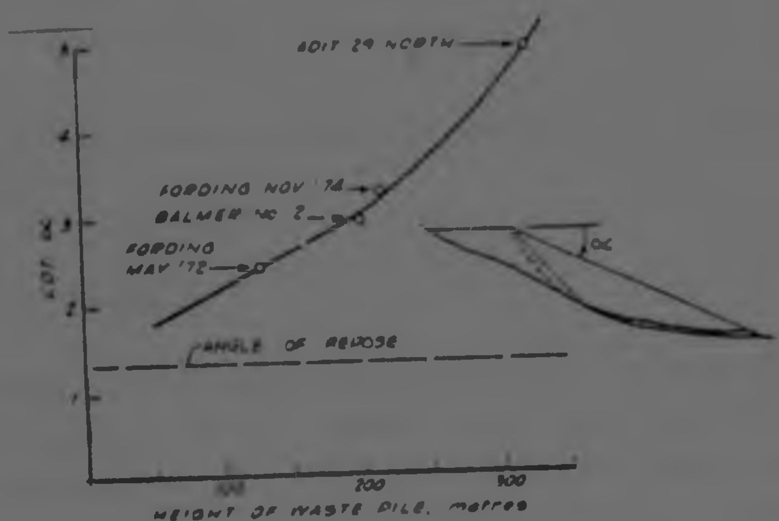

FIGURE 38 : Correlation between height of waste rock dump and cotangent of run-out angle[11]

4.7 Water Movement in Coarse Mine Waste Dumps

This section is based on the paper presented by Nelson and McWhorter[12] at the 1981 Society of Mining Engineers of AIME Fall meeting and exhibit.

Water movement in waste dumps is of interest primarily as it influences dump stability and as the rates of seepage impact the environment. Water is introduced to dumps by precipitation or during loading and a major concern is the ability of saturated zones to develop within the dump.

Nelson and McWhorter have developed equations for use in the prediction of the development of a phreatic surface within a waste dump. These equations are presented inthe following text.

Seepage into a waste dump may be considered as taking place in 3 stages.

4.7.1 Stage 1

A wetting front advances downward through the dump due to precipitation on the surface. Above this wetting front the soil may or may not be saturated. If the infiltration rate is less than the hydraulic conductivity of the soil, then the soil above the wetting front will be unsaturated. The volumetric water content, defined as the volume of water per unit volume of soil, above the wetting front is given by equation (24). If the infiltration rate is greater than the soil hydraulic conductivity then the soil above the wetting front will be saturated.

$$\theta_f = (n - \theta_r) \left(\frac{q}{K}\right)^{\lambda/(2+3\lambda)} + \theta_r \qquad (24)$$

where θf is the final volumetric water content

n is the porosity

q is the infiltration rate

K is the soil hydraulic conductivity

λ is the pore size distribution index

θ_r is the residual water content defined as the volumetric water content below which drainage alone will not cause a further decrease in water content.

4.7.2 Stage 2

When the wetting front contacts an impermeable stratum such as an impermeable foundation or an impermeable lens of waste dump material, a groundwater mound will develop and rise towards the surface of the dump. If the soil above the wetting front is unsaturated equation (25) may be used to estimate the time taken for the wetting front to travel the height of the dump. If the soil is saturated behind the wetting front equation (26) may be used to estimate the time taken for the wetting front to travel the dump.

$$T = \frac{D_f}{q}\left[(n-\theta_r)\left(\frac{q}{K}\right)^{\lambda/(2+3\lambda)} + (\theta_r-\theta_i)\right] \ldots\ldots\ldots\ldots \quad (25)$$

$$T = \left(\frac{n-\theta_i}{K}\right)\left[D_f-(H-h_d)\ell n\left[\frac{D_f-H-h_d}{H-h_d}\right]\right] \ldots\ldots\ldots\ldots \quad (26)$$

where T is the time required for the wetting front to travel through the dump and contact the foundation.

D_f is the height of the dump above the impermeable foundation.

θ_i is the initial dump soil vulumetric water content.

h_d is the displacement pressure head explained below.

The capillary pressure head of the soil is defined as being equal to the difference between the soil pore air pressure and the soil pore water pressure.

$$h = (u_a - u_w) \qquad (27)$$

where h is the capillary pressure head
u_a is the pore air pressure
u_w is the pore water pressure

Typical variation of hydraulic conductivity with capillary pressure head is shown in Figure 39 for two sands. From the diagram it can be seen that the displacement pressure head (h_d) is defined as being the minimum value of h for which the hydraulic conductivity (K) will be nearly constant and equal to its maximum value.

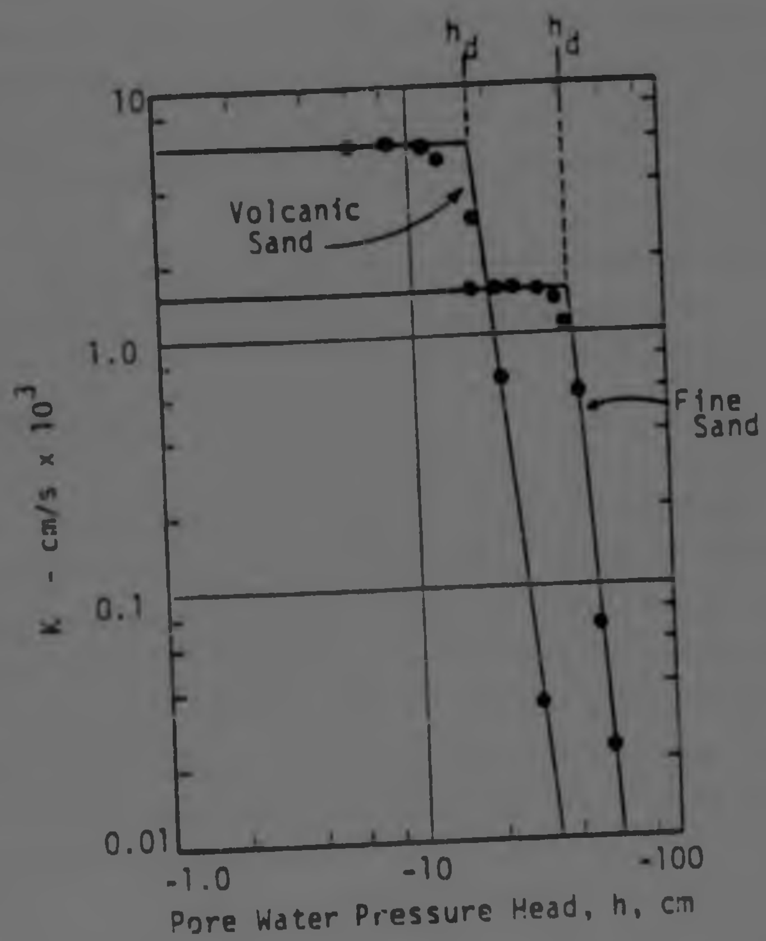

FIGURE 39 : Typical relationship between hydraulic conductivity (K) and pore-water pressure head[12].

If the soil is not saturated behind the wetting front, the time required for the phreatic surface to rise a specified distance once the wetting front has contacted the foundation, may be obtained by using equation (28).

$$t = \frac{(n-\theta_f)}{q} \cdot Y + T \quad \text{.......................} \quad (28)$$

where t is the time for the phreatic surface to rise a distance Y.

θ_f is the final volumetric content

All other symbols are the same as previously defined.

4.7.3 Stage 3

The groundwater mound establishes contact with the dump surface and if infiltration occurs over the entire dump area, the dump will be saturated and all surface water will runoff. Thus Stage 3 is not of concern and will not be considered.

The use of the equations presented in the preceding discussion is best depicted by the solution of example problems.

4.7.4 Example 1

Consider a 100 m high waste dump of large lateral extent. The general properties of the material are as shown in Figure 40. Water will be provided to the surface by precipitation during a prolonged period of rain at the rate of 3×10^{-6} meters per second. It is desired to compute the time required for the wetting front to contact the foundation and how long would be required for the phreatic surface to a) rise 50 m in the dump, and b) rise to the top surface.

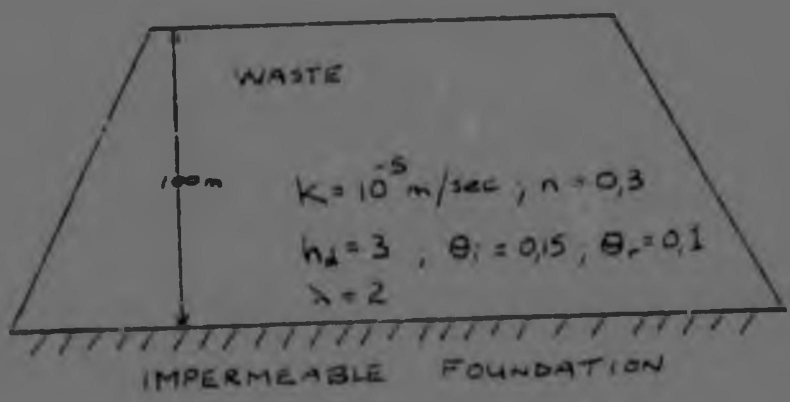

FIGURE 40 : Waste dump for example computations solution.

Solution

Because q < K, the soil above the wetting front will be unsaturated. The water content above the wetting front can be computed from Equation (24) as;

$$\theta f = (0,3-0,1)\left[\frac{3\times10^{-6}}{10^{-5}}\right]^{\frac{2}{2+6}} + 0,1 \quad \ldots\ldots\ldots \quad (29)$$

$$= \underline{0,25}$$

The time for the wetting front to traverse 100 m is computed from Equation (25);

$$T = \frac{100}{3\times10^{-6}}\left[(0,3-0,1)\right]\left[\frac{3\times10^{-6}}{10^{-5}}\right]^{0,25} + (0,1-0,15) \quad (30)$$

$$= 38 \text{ days}$$

The time for the phreatic surface to rise 50 m is computed from Equation (28);

$$t = \frac{(0,3-0,25)}{3 \times 10^{-6}} \times 50 + 38 \text{ days}$$

$$= 48 \text{ days} \qquad \ldots\ldots\ldots\ldots\ldots\ldots\ldots \qquad (31)$$

The time for the phreatic surface to rise 100 m is computed from Equation 28.

$$t = \frac{(0,3 - 0,25)}{3 \times 10^{-6}} \times 100 + 38 \text{ days}$$

$$= 57 \text{ days} \qquad \ldots\ldots\ldots\ldots\ldots\ldots\ldots \qquad (32)$$

4.7.5 Example 2

For the waste dump used in Example 1, if surface water is ponded to a depth of 0,3 metres compute the quantities requested in Example 1.

The time required for the wetting front to traverse the depth of the waste dump can be computed from Equation (26).

$$T = \frac{0,3-0,15}{10^{-5}} \left[100-(0,3+3,0) \ln \left[\frac{100+0,3+3,0}{0,3+3,0} \right] \right]$$

$$= 15,4 \text{ days} \qquad \ldots\ldots\ldots\ldots\ldots\ldots\ldots \qquad (33)$$

Because the soil above the wetting front is saturated, the rate of rise of the phreatic surface would be virtually instantaneous (within a matter of hours or less).

4.7.6 Discussion

The example computations presented in the previous section provide indications of general rates of rise that may be expected to occur within an impoundment. It must be recognized that some uncertainty will exist with regard to the material properties. Furthermore, the waste dump will not be uniform and some zones of less permeable material will exist throughout. Consequently, the results arrived at in the computations must be used as a general guide on which to base decisions rather than to consider the results as absolute quantities.

The following points should be noted with regard to the results of the examples:

1. The foundation material was considered to be impermeable in the computations. Some seepage will occur through the foundation. Although the permeability of the foundation stratum would not affect the time required for the wetting front to reach that surface, it may have a pronounced effect on the time required for the phreatic surface to rise within the waste dump. This could be taken into account by adjusting Equation (28) to reflect that the inflow term would be the surface infiltration less foundation losses.

2. The above analysis has assumed that all seepage occurs in a vertical direction with no lateral seepage losses out of the sides of the impoundment. Because some lateral seepage may occur out of the face of the embankment, particularly as the phreatic surface is rising within the waste dump, some inaccuracies are espected to exist particularly around the edges of the dump. For a waste dump of large lateral extent the development of a large mound within the impoundment with seepage losses out of the face would be tantamount to a steady-state condition until the mound has dissipated.

3. The presence of lenses of low permeable material will cause ground water mounds to be perched within the impoundment as shown in Figure 41. These perched mounds will result in positive pore water pressures being developed within the zones immediately beneath the mounds. If the critical failure surface for slope stability analyses intersects the perched mounds, porewater pressure could seriously affect the stability of the impoundment. The development of these mounds and the distribution of the impermeable lenses throughout the waste dump are difficult to predict.

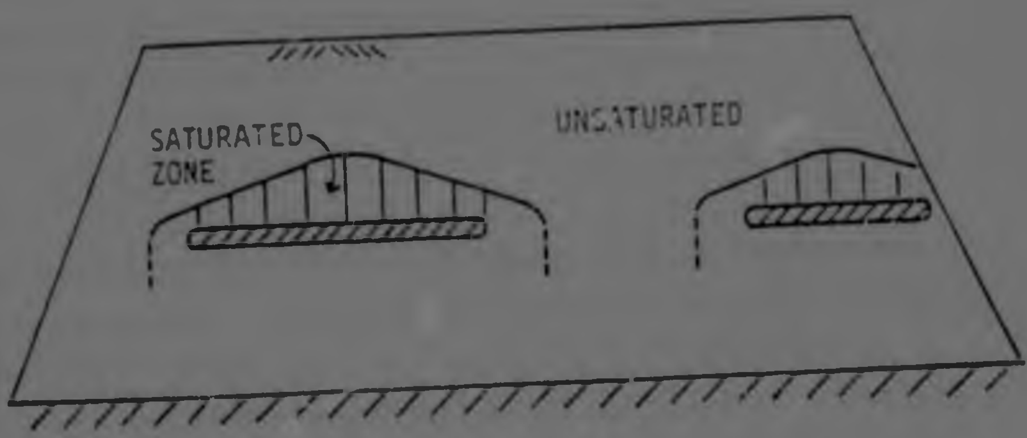

FIGURE 41 : Development of perched mounds over impermeable lenses

4. The example computations assumed that the inflow of water on the surface of the waste dump would occur continuously for the period of time under consideration. It is unlikely that rain would continue for periods of time required for the wetting front to progress through the bottom of the waste dump. Thus, if the source of water on the surface of the dump stops after a certain period time, a slug of water would move downward throughout the dump. Some distribution of this water would take place over a period of time. If precipitation events occur as short time intervals, analyses could proceed along

lines similar to those presented in the examples if the effect of previous precipitation events is taken into account as influencing the initial volumetric water content for subsequent computations.

The above methods of analysis have been presented to provide a means of computing general rates of movement of water through unsaturated, non-impounding waste dumps. The methods of analysis presented herein are intended to serve as a guide for decision making and to provide a means of estimating general times required for zones of saturation to be developed within a non-impounding waste dump.

4.8 The v=o Method

One may evaluate the stability of dumps using the methods previously discussed. Alternatively the y=o method may be used and a simplified approach[1] to this method is discussed here. Robertson[13] describes the derivation of the rigorous y=o method. The advantages of using this method is that it is simple, quick to use and can be used with any failure surface shape.

The principle of the method may be illustrated by the analogy of blocks sliding on an inclined plane to slope failure[13], refer to Figure 42(a). If the disturbing forces D.F. and the resisting forces, R.F. are as shown in the diagram, then the factors of safety are 1,33, 1,11 and 0,75 respectively. Placing the three blocks with their sides touching, Figure 42(b) then the combined factor of safety is 0,97 and thus just unstable. However the factor of safety of blocks 1 and 3 is only 0,91 and hence these two blocks slide down leaving block 2, factor of safety of 1,11 to "hang up". In an actual slope a possible failure surface is defined and the portion of the slope above the failure surface is divided into a number of slices. The blocks thus represent the slices and the same principles that were applied to the blocks can be applied to the slices.

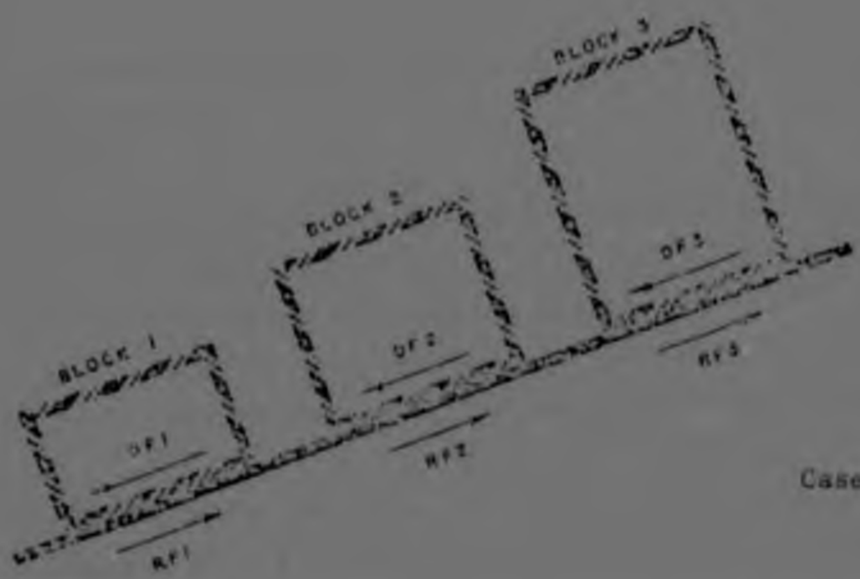

Case (a)

$DF_1 = 1\frac{1}{2}$ units $DF_2 = 2\frac{1}{4}$ units $DF_3 = 4$ units

$RF_1 = 2$ units $RF_2 = 2\frac{1}{2}$ units $RF_3 = 3$ units

$F_1 = \frac{2}{1.5} = 1.33$ $F_2 = \frac{2\frac{1}{2}}{2\frac{1}{4}} = 1.11$ $F_3 = \frac{3}{4} = .75$

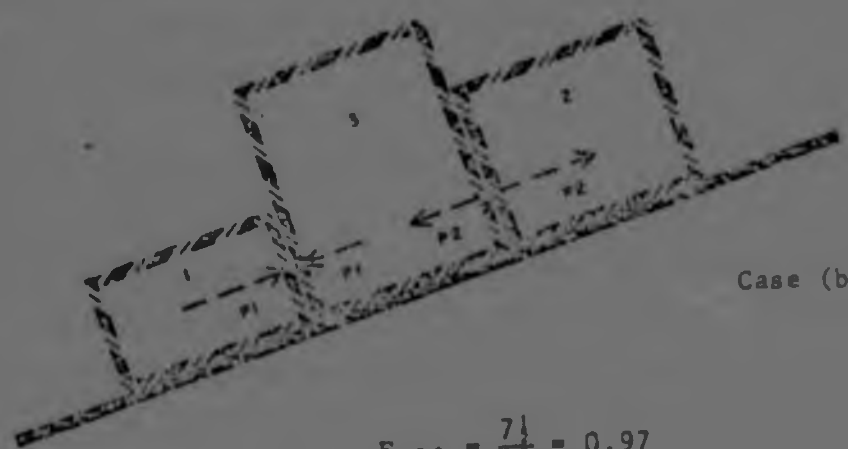

Case (b)

$$F_{123} = \frac{7\frac{1}{2}}{7\frac{3}{4}} = 0.97$$

$$F_{13} = \frac{5}{5\frac{1}{2}} = 0.91$$

FIGURE 42 : Blocks sliding along an inclined plane[11]

A number of assumptions must be made about the slope material and these are:

- the slope material is incapable of withstanding tensile stress
- the crack will form vertically
- a crack will form when the forces across any vertical section above the failure surface is zero or tensile.

Now consider the slope and the potential failure surface shown in Figure 43. If a crack were to form at any vertical section such as CD, then the factor of safety of the failing segment BCD is defined as;

$$F = \frac{\Sigma(RF)max}{\Sigma DF} \quad \dots\dots\dots\dots\dots\dots\dots\dots \quad (34)$$

where $\Sigma(RF)max$ is the maximum resistance to sliding that can be developed along the sliding surface and ΣDF is the force tending to produce sliding. A force P is defined as follows:

$$P = \Sigma(RF)max - \Sigma DF \quad \dots\dots\dots\dots\dots\dots\dots\dots \quad (35)$$

P may be thought of as the force that acts across a vertical section such as CD. If P is positive, there is an excess of potential sliding resistance, the segment will not slide and the factor of safety will be greater than one. If P is negative the segment will slide and the factor of safety will be less than one. Substituting equation (35) into equation (34) gives:

$$F = \frac{\Sigma DF + P}{\Sigma DF} = 1 + \frac{P}{\Sigma DF} \quad \dots\dots\dots\dots\dots\dots\dots\dots \quad (36)$$

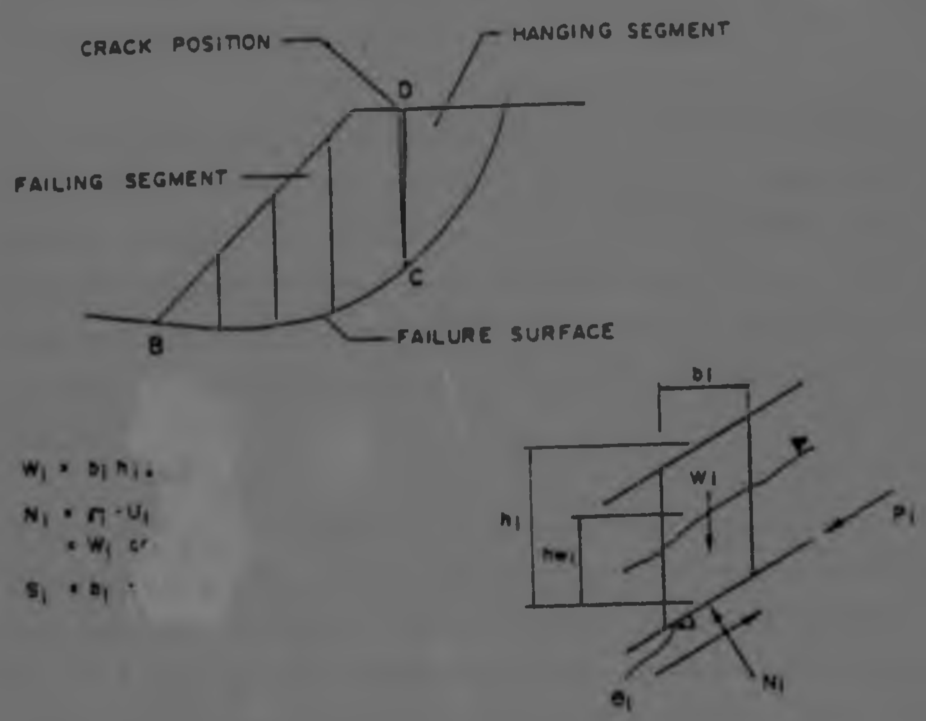

$DF_i = W_i \sin\theta + aW_i \cos\theta$

$RF_i = S_i + N_i \tan \phi$

$P_i = RF_i - DF_i + P_{i-1}$

c = cohesion on base

ø = soil friction

a = earthquake acceleration

U = water pressure

The factor of safety of the segment below the right hand side of slice is thus

$$F = 1 + \frac{P_i}{\sum_{1}^{i} (DF)}$$

FIGURE 43 : Solution of y = o method[1]

In order to calculate the value of P and hence F at any section, start with the first slice at the base of the failure zone, and then using the equations shown in Figure resisting and disturbing force for that slice. Hence P can be calculated. If an external force is applied it may be considered as an additional resisting or disturbing force depending in which direction it acts.

If P is positive it may be called upon to help stabilise the next slice in the event that the part of the slope above the first segment cannot hold itself up. Accordingly, when the P force from the second segment is calculated, the P force from the first segment contributes to the maximum potential sliding resistance in the second slice. This is shown in the equations given in Figure 23.

This procedure is repeated up the failure plane and as long as P is positive, compressional forces exist across vertical planes in the slope and cracking will not occur. However if the P forces become negative, the factor of safety of the slope becomes less than one and that part of the slope will fail. For the example shown in Figure 44, the factor of safety of the lower segments is greater than one, but soon after the P forces become negative, the factor of safety of the lower segment becomes less than one and that part of the slope will move out. A hanging wedge will probably remain beyond about point C.

Robertson[13] found that stability analyses by Bishop's Simplified, U.S.B.R. and y=o methods gave factors of safety that are close in agreement. The y=o simplified method will be used later in this thesis.

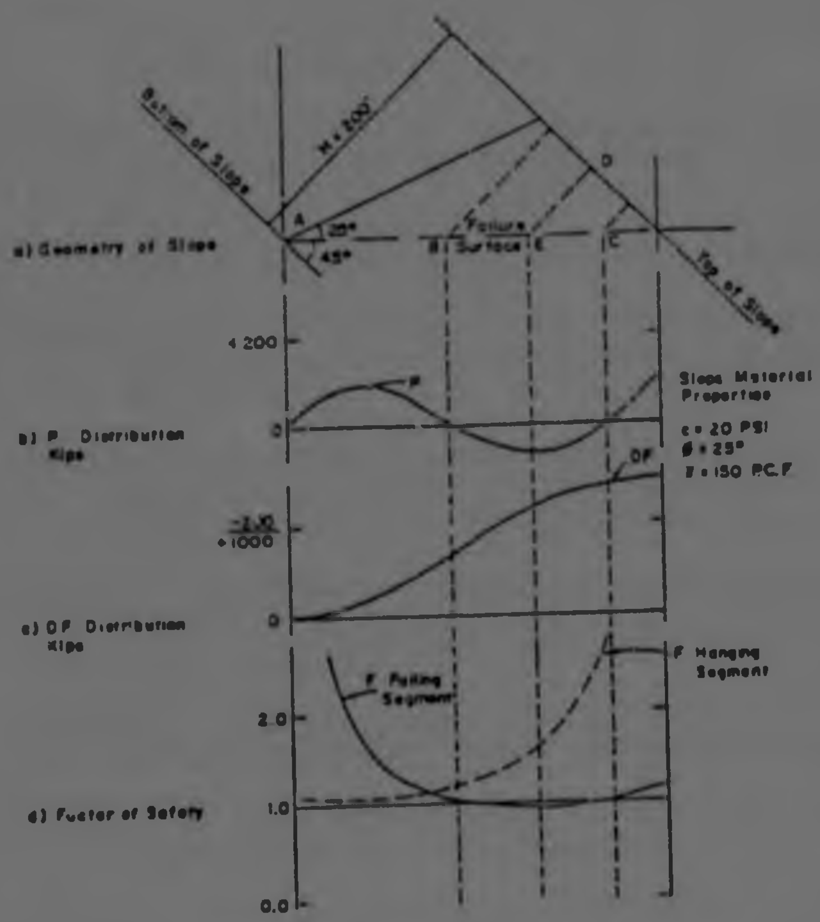

FIGURE 44 : Distribution of P, DF, F failing segment & F hanging segment along failure surface, from Robertson (1977)[13]

4.9 References

1. CALDWELL, J.A., ALLAN S.E., Steffen Robertson and Kirsten, and Vandre B.C., "The Simplified Analysis of Mine Waste Embankments", Design of Non-Impounding Mine Waste Dumps Workshop, Society of Mining Engineers, AIME, Denver, 1981.

2. HUANG, Y.H., "Stability of Mine Spoil Banks and Hollow Fills", Proceedings of the Conference on Geotechnical Practice for Disposal of Solid Waste Materials, ASCE, Michigan, June, 1977.

3. WRIGHT, S.G., "Limit Equilibrium Slope Analysis Procedures", Design of Non-Impounding Mine Waste Dumps Workshop, Society of Mining Engineers, AIME, Denver, 1981.

4. WINTERKORN, H and FANG, H, "Foundation Engineering Handbook", Van Nostrand Reinhold Company, U.S.A., 1975.

5. BLIGHT, G.E., "Foundation Failures of Four Rockfill Slopes", ASCE, Soil Mechanics and Foundations Division, May, 1969.

6. BLIGHT, G.E., "On the Failure Mode of Waste Rock Dumps", Design of Non-Impounding Mine Waste Dumps Workshop, Society of Mining Engineers, AIME, Denver, 1981.

7. MARAIS, G. Discussion on the paper "The Stability of Hillside Dumps of Anthracite", The Civil Engineer in South Africa, Number 5, Volume 14, May, 1972, Page 182.

8. SULTAN, H and SEED, H., "Stability of Sloping Core Earth Dams", Journal of the Soil Mechanics and Foundati ns Division, ASCE, Volume 93, Number SM4, July, 1967.

9. BRAUNS, J., "Safety Against Slip in Inclined Base of Slope Toes", ASCE, Geotechnical Journal, Volume 106, GT10, October, 1980.

10. URIEL, S., "Discussion to Question Number 37", Transactions, XI ICOLD, Volume VI, 1970, Page 526.

11. CAMPBELL, D.B. and SHAW, W.H., "Performance of a Waste Rock Dump on Moderate to Steeply Sloping Foundations", Proceedings of the First International Symposium on Stability in Coal Mining, Vancouver, British Columbia, Canada, Chapter 27, 1978.

12. NELSON, J.D. and McWHORTER, D.B., "Water Movement in Non-Impounding Waste Dumps", Society of Mining Engineers, AIME, Denver, 1981.

13. ROBERTSON, A.M., "The Determination of the Stability of Slopes in Jointed Rock", PhD Thesis, University of the Witwatersrand, Johannesburg.

4.9 References

1. CALDWELL, J.A., ALLAN S.E., Steffen Robertson and Kirsten, and Vandre B.C., "The Simplified Analysis of Mine Waste Embankments", Design of Non-Impounding Mine Waste Dumps Workshop, Society of Mining Engineers, AIME, Denver, 1981.

2. HUANG, Y.H., "Stability of Mine Spoil Banks and Hollow Fills", Proceedings of the Conference on Geotechnical Practice for Disposal of Solid Waste Materials, ASCE, Michigan, June, 1977.

3. WRIGHT, S.G., "Limit Equilibrium Slope Analysis Procedures", Design of Non-Impounding Mine Waste Dumps Workshop, Society of Mining Engineers, AIME, Denver, 1981.

4. WINTERKORN, H and FANG, H, "Foundation Engineering Handbook", Van Nostrand Reinhold Company, U.S.A., 1975.

5. BLIGHT, G.E., "Foundation Failures of Four Rockfill Slopes", ASCE, Soil Mechanics and Foundations Division, May, 1969.

6. BLIGHT, G.E., "On the Failure Mode of Waste Rock Dumps", Design of Non-Impounding Mine Waste Dumps Workshop, Society of Mining Engineers, AIME, Denver, 1981.

7. MARAIS, G, Discussion on the paper "The Stability of Hillside Dumps of Anthracite", The Civil Engineer in South Africa, Number 5, Volume 14, May, 1972, Page 182.

8. SULTAN, H and SEED, H., "Stability of Sloping Core Earth Dams". Journal of the Soil Mechanics and Foundations Division, ASCE, Volume 93, Number SM4, July, 1967.

9. BRAUNS, J., "Safety Against Slip in Inclined Base of Slope Toes", ASCE, Geotechnical Journal, Volume 106, GT10, October, 1980.

10. URIEL, S., "Discussion to Question Number 37", Transactions, XI ICOLD, Volume VI, 1970, Page 526.

11. CAMPBELL, D.B. and SHAW, W.H., "Performance of a Waste Rock Dump on Moderate to Steeply Sloping Foundations", Proceedings of the First International Symposium on Stability in Coal Mining, Vancouver, British Columbia, Canada, Chapter 27, 1978.

12. NELSON, J.D. and McWHORTER, D.B., "Water Movement in Non-Impounding Waste Dumps", Society of Mining Engineers, AIME, Denver, 1981.

13. ROBERTSON, A.M., "The Determination of the Stability of Slopes in Jointed Rock". PhD Thesis, University of the Witwatersrand, Johannesburg.

CHAPTER 5 : LABORATORY TESTING

The objective of the laboratory testing programme was to investigate the shear strength behaviour of coarse mine waste material subjected to high stresses. Material shear strength was determined by standard consolidated, drained triaxial tests.

5.1 Material Description

Physical descriptions of the samples are contained in Table 13. Photographs and grading curves of the samples are contained in Appendix C. The samples were all non-plastic with clay contents not exceeding 5% except for the Kleinsee 2 sample which had a clay content of 12%. The samples were all predominantly sand or gravel.

5.2 Triaxial Testing

As stated previously, the samples were tested using standard consolidated, drained triaxial tests. Specimens were 152 mm long with a diameter of 76 mm. The Premier and Kleinsee 1 and 2 samples were tested at cell pressures ranging from 0 to 1000 kPa. The Jwaneng, Koingnaas, Tweepad and Kleinsee 3 samples were tested at cell pressures ranging from 0-2000 kPa.

Figures 45 and 46 show the strain controlled machine used for testing and the general arrangement of apparatus.

TABLE 13: SAMPLE DESCRIPTION

SAMPLE	CLASSIFICATION					PARTICLE DESCRIPTION		
	DISTRIBUTION (%)				USCS CLASSIFICATION	SHAPE	TEXTURE	MAXIMUM PARTICLE SIZE, x(mm)
	SILT	SAND	GRAVEL	$D_{60} \div D_{10}$				
PREMIER	0	12	88	5	GW	Flaky	Granular & Rough	x > 23
JWANENG	4	32	64	4,3	GP	Irregular	Rough	x > 23
KOINGNASS	3	60	37	10,5	SP	Rounded & Irregular	Smooth & Rough	13,2< x< 23
TWEE PAD	3	82	15	4,1	SP	Elongated Flaky & Irregular	Rough	13,2< x <23
KLEINSEE 1	4	71	25	4,3	SP	Flaky & Elongated	Rough & Granular	13,2< x< 23
KLEINSEE 2	12	38	50	58	SW	Angular & Flaky	Rough	13,2< x< 23
KLEINSEE 3	3	85	12	2,5	SP	Flaky & Elongated	Rough & Granular	13,2 x 23

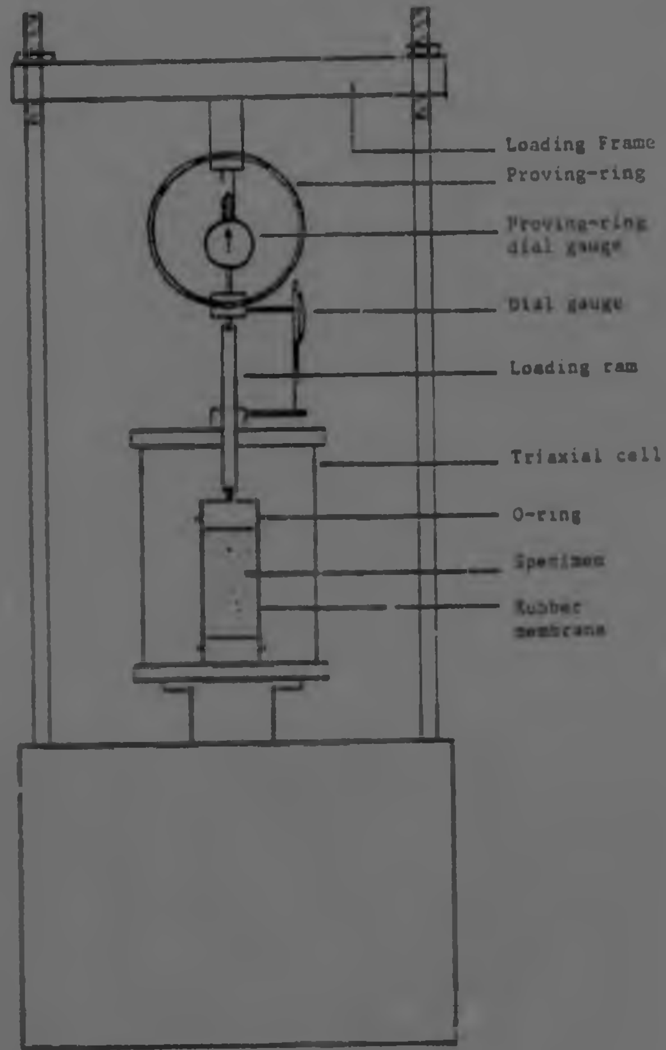

(a) Illustration

(b) Photograph

FIGURE 45 : Strain-controlled machine and triaxial cell set-up

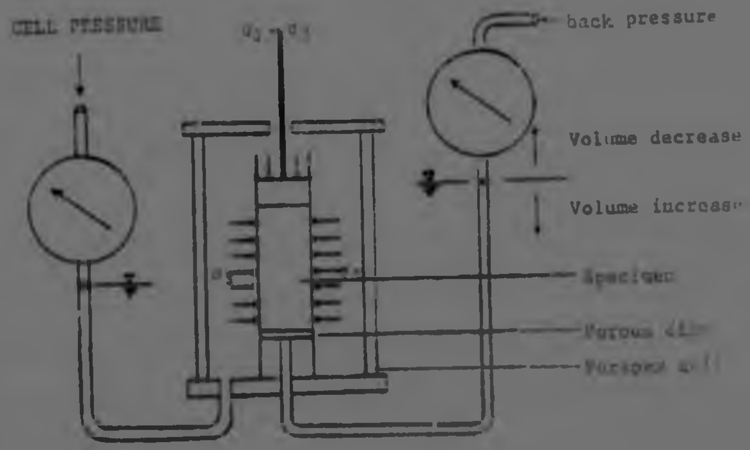

(a) Illustration

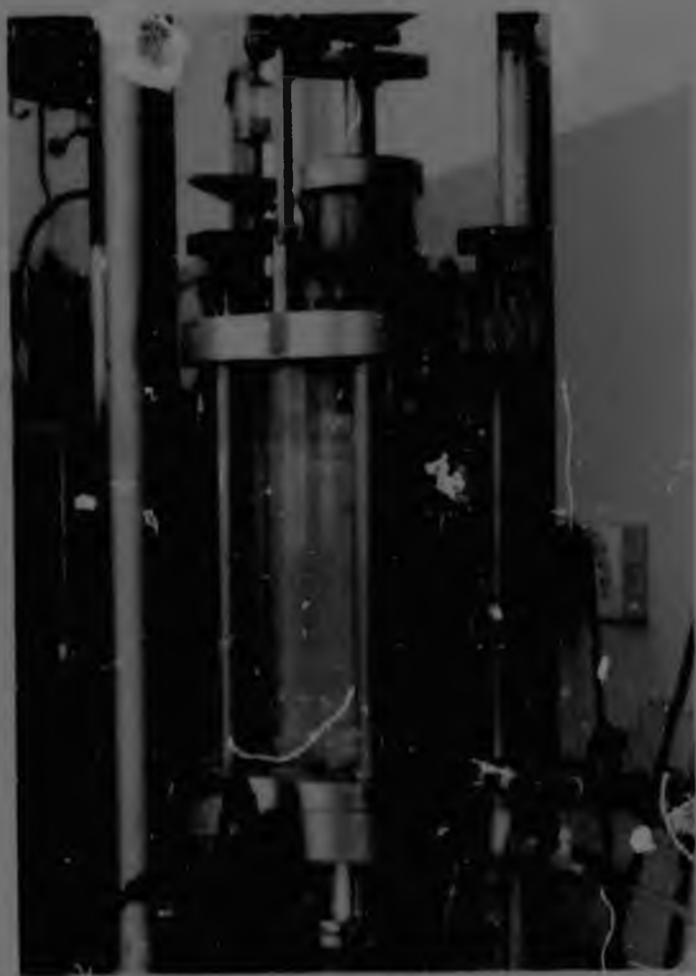

(b) Photograph

FIGURE 46 : Consolidated-drained triaxial test with volume change measurements

5.3 Test Results

A full tabulation of the test results is contained in Table C1 in Appendix C. If it is accepted that cohesionless material does not develop cohesive strength even if particle crushing occurs during loading, then the friction angle of the tests may be calculated as

$$\phi_s = \sin^{-1}\left[\frac{(\sigma_1 - \sigma_3)_{failure}}{(\sigma_1 - \sigma_3)_{failure}}\right] \quad \ldots\ldots\ldots\ldots\ldots\ldots \quad (2)$$

where ϕ_s is the secant friction angle and is the slope of the line tangent to the Mohr circle and passing through the origin. ϕ_s is tabulated in Table C1 in Appendic C. Inspection of the data shows that there is a trend for ϕ_s to decrease with increasing stress levels. This effect is most evident in the Kleinsee 3, Jwaneng and Twee Pad results.

The test results are summarized in Figure 47. Strength values for all materials coincided at low stresses, but diverged as stresses increased. It is evident from the plot that at high stresses the Kleinsee 3, Jwaneng and Twee Pad samples experience a significant decrease in strength. The relationship which gives the best fit to the test data is

$$\tau = 1{,}15 \;.\; \sigma_o^{\;0{,}932} \quad \ldots\ldots\ldots\ldots\ldots\ldots\ldots\ldots\ldots \quad (37)$$

where τ is the shear strength (kPa) and σ_o is the normal stress (kPa). The relationships which give the best fit for the data of the individual samples are listed in Table 14.

5.3 Test Results

A full tabulation of the test results is contained in Table C1 in Appendix C. If it is accepted that cohesionless material does not develop cohesive strength even if particle crushing occurs during loading, then the friction angle of the tests may be calculated as

$$\phi_s = \sin^{-1}\left[\frac{(\sigma_1 - \sigma_3)_{failure}}{(\sigma_1 - \sigma_3)_{failure}}\right] \quad \ldots\ldots\ldots\ldots\ldots\ldots \quad (2)$$

where ϕ_s is the secant friction angle and is the slope of the line tangent to the Mohr circle and passing through the origin. ϕ_s is tabulated in Table C1 in Appendic C. Inspection of the data shows that there is a trend for ϕ_s to decrease with increasing stress levels. This effect is most evident in the Kleinsee 3, Jwaneng and Twee Pad results.

The test results are summarized in Figure 47. Strength values for all materials coincided at low stresses, but diverged as stresses increased. It is evident from the plot that at high stresses the Kleinsee 3, Jwaneng and Twee Pad samples experience a significant decrease in strength. The relationship which gives the best fit to the test data is

$$\tau = 1{,}15 \,.\, \sigma_o^{\,0{,}932} \quad \ldots\ldots\ldots\ldots\ldots\ldots\ldots\ldots \quad (37)$$

where τ is the shear strength (kPa) and σ_o is the normal stress (kPa). The relationships which give the best fit for the data of the individual samples are listed in Table 14.

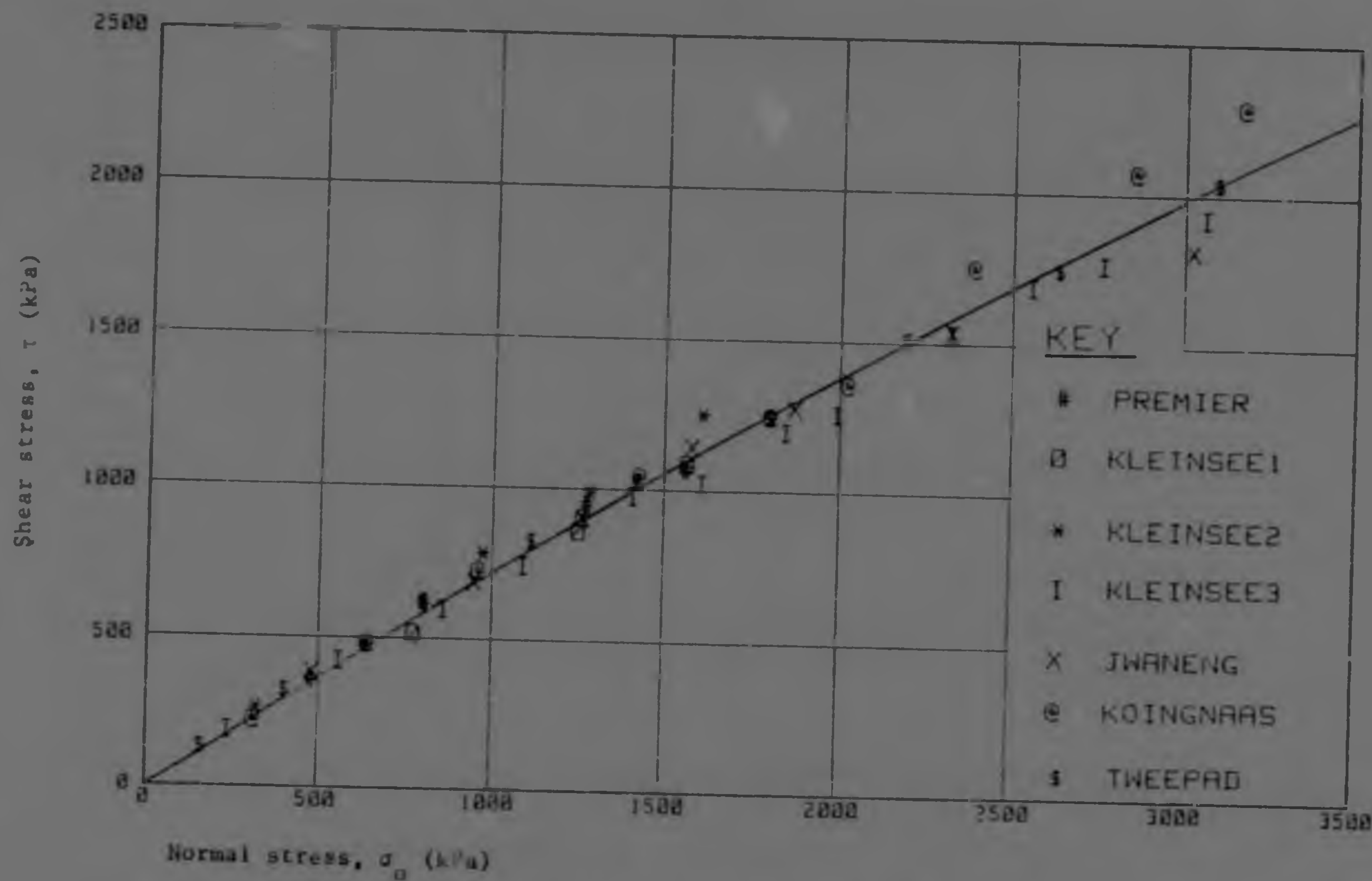

FIGURE 47 : Test results and plot of $\tau = 1{,}15.\sigma_o^{\,0{,}932}$

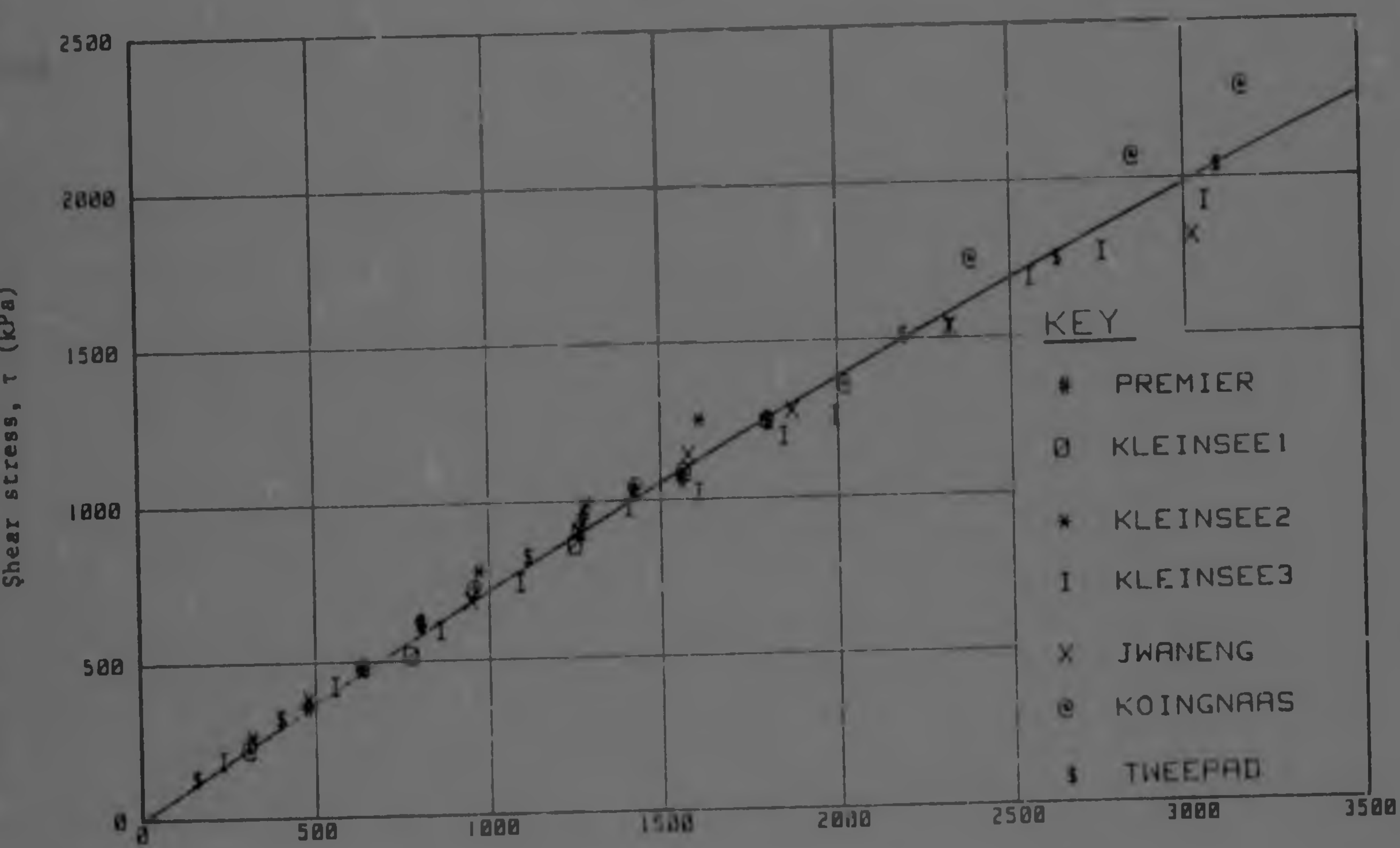

Normal stress, σ_o (kPa)

FIGURE 47 : Test results and plot of $\tau = 1{,}15.\sigma_o^{\;0{,}932}$

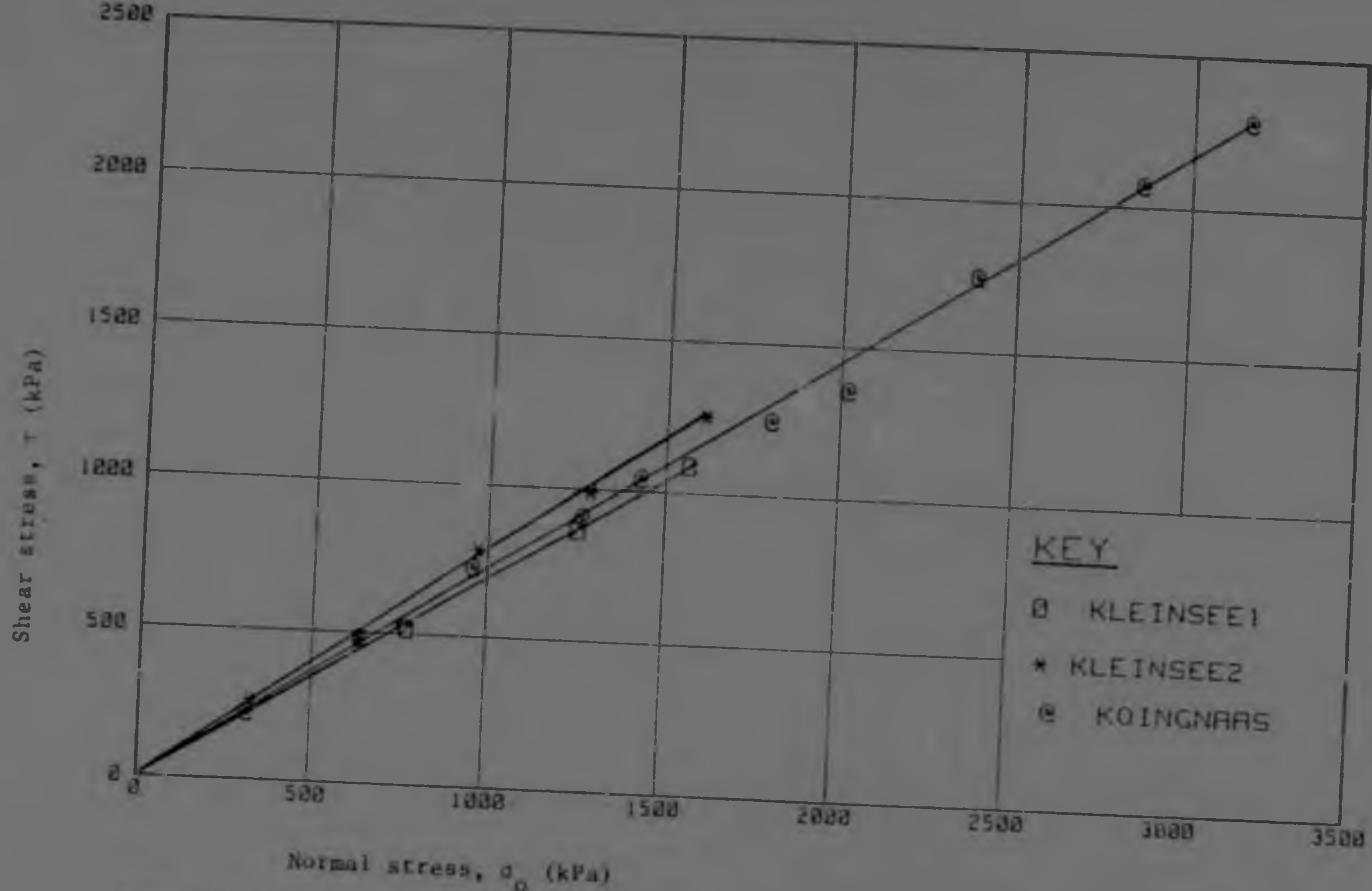

FIGURE 48 : Test results

TABLE 14 : $\tau - \sigma_o$ RELATIONSHIPS

SAMPLE	NORMAL STRESS (kPa)	BEST FIT RELATIONSHIP (kPa)	LINEAR REGRESSION
Premier	0-1600	$\tau = 1,00.\sigma_o^{0,953}$	37^o
Kleinsee 1	0-1600	$\tau = 0,69.\sigma_o^{1,00}$	35^o
Kleinsee 2	0-1600	$\tau = 0,83.\sigma_o^{0,99}$	38^o
Kleinsee 3	0-3100	$\tau = 1,20.\sigma_o^{0,920}$	32^o-34^o
Jwaneng	0-3100	$\tau = 1,78.\sigma_o^{0,871}$	27^o-35^o
Tweepad	0-3100	$\tau = 1,21.\sigma_o^{0,927}$	31^o-36^o
Koingnaas	0-3100	$\tau = 0,74.\sigma^{1,00}$	36^o

The exponent of 1 for Koingnaas and Kleinsee 1, and an exponent of 0,99 for Kleinsee 2 shows that a straight line fit is accurate for these samples. This is illustrated in Figure 48.

The typical failure shape of the triaxial specimens is shown in Figure 49. Time to failure was between 30-90 minutes which, because of the coefficient of consolidation of this material, is adequate for drained test conditions to exist. The axial and volumetric strains at failure were found to increase with an increase in confining pressure. Figure 50 shows the axial strain (ε_a) and volumetric strain (ε_v, positive ε_v is compression) at failure versus the confining pressure (σ_3) for the Koingnaas and Twee Pad samples.

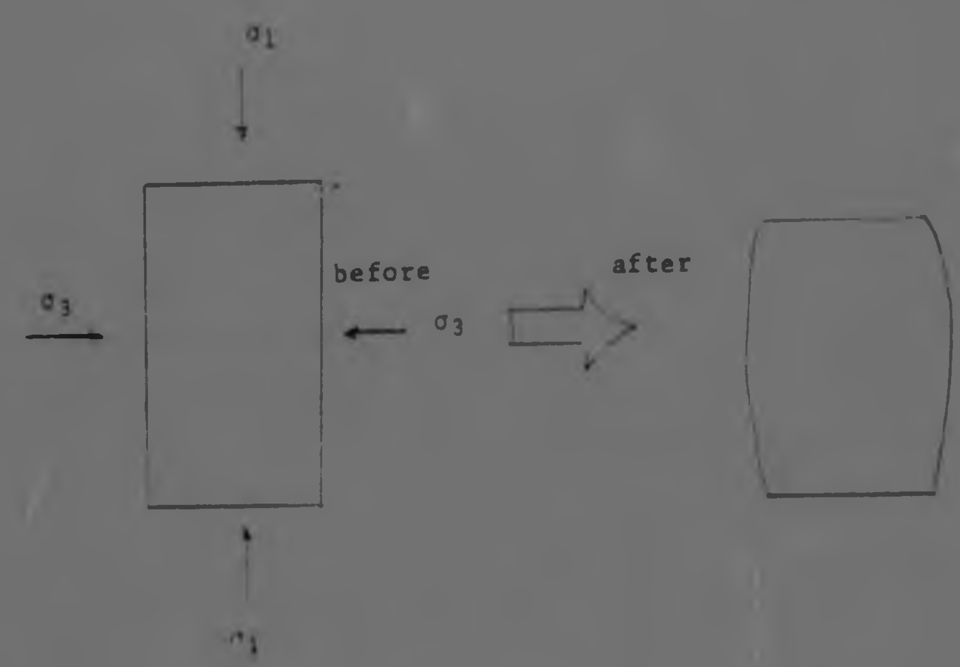

(a) Illustration

(b) Photograph

FIGURE 49 : Typical failure shape

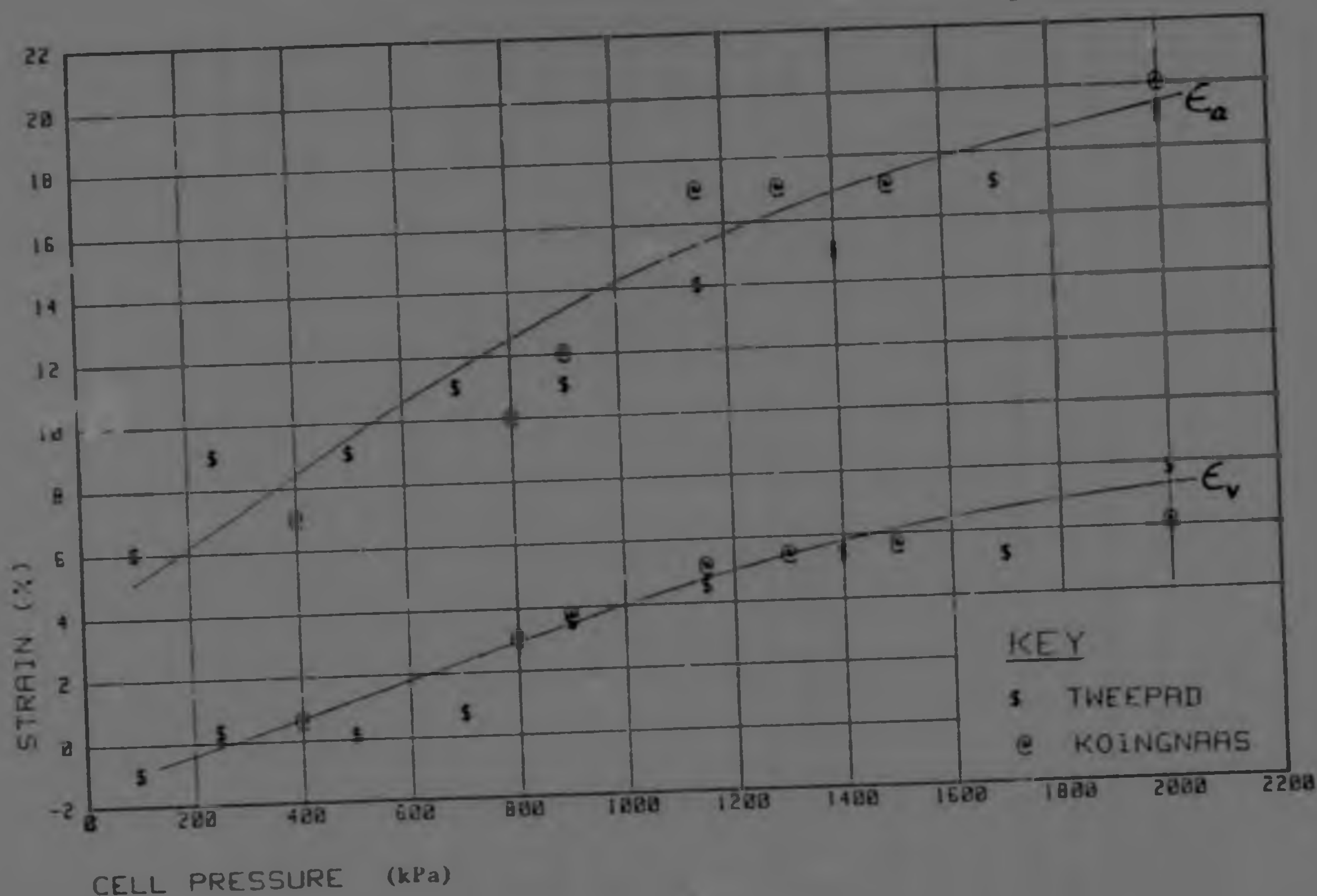

FIGURE 50 : Strain at failure versus cell pressure

5.4 Discussion

The Premier, Kleinsee 1 and 2 samples which were tested at cell pressures up to 1000 kPa (normal stress, σ_o, of approximately 1600 kPa) show little and no curvature of the strength envelope, (refer to Figure 47 and 48, and Table 14). In fact for all the samples tested, at σ_o equal to 1600 kPa there is little difference between the ϕ values from a linear regression analysis or the power relationships shown in Table 14. A comparison of friction angles obtained from the different methods is shown in Table 15.

TABLE 15: ϕ at σ_o = 1600 kPa

SAMPLE	$\tau = a.^{b}$	LINEAR REGRESSION
Premier	35,3°	36,8°
Kleinsee 1	34,6°	34,6°
Kleinsee 2	37,6°	37,9°
Kleinsee 3	33,6°	34,2°
Jwaneng	34,5°	35,3°
Twee Pad	35,2°	35,7°
Koingnaas	36,5°	35,8°

On the basis of the results shown in Table 15 it would seem reasonable to suggest that up to σ_o equals 1600 kPa, linear regression may be used to estimate the friction angle of sand-gravel soil.

The Kleinsee 3, Jwaneng, Twee Pad and Koingnaas samples were all tested at cell pressures of up to 2000 kPa (σ_o approximately 3100 kPa). With the exception of Koingnaas all the samples showed significant curvature of the strength envelope, (refer to Figure 47 and Table 14. Thus when σ_o is greater than 1600 kPa it is preferable to use the power relationships shown in Table 14 for predicting values of ϕ.

The Koingnaas results show no curvature of the strength envelope, refer to Figure 48. Particle shape and texture may be factors affecting the reason why no curvature of the envelope has occurred. Inspection of Table 13 shows that the Koingnaas particles are rounded and irregular in shape with a smooth surface texture. Thus particle contact forces during loading would be at a minimum and little or no particle breakage would occur. If no particle breakage occurs then no reduction in strength can be expected and a linear relationship between shear strength and normal stress will develop.

It will be of interest to compare the relationships for curved strength envelopes in granular materials predicted by De Mello (Chapter 2, Figure 8) to those shown in Table 14. De Mello's relationships are based on the results of Marsal's rockfill tests and it would appear that the exponents of these relationships are generally smaller than those of the sand-gravel relationships of Table 14. The exponent determines the rate of curvature of the strength envelope and this may have interesting implications with respect to particle breakage. The rockfill material has large particle sizes and would thus experience greater inter-particle contact forces than the sand-gravel mixtures. The greater contact forces would cause the rockfill particles to fracture at lower nominal stresses than the sand-gravel particles and hence this could account for the rockfill strength envelope curving more rapidly.

A grading curve of Kleinsee 3 material tested at a cell pressure of 2000 kPa (σ_o = 3100 kPa) has been compared to that of normal Kleinsee 3 material in Figure 51. It can be seen in Figure 51 that a significant but not a large amount of particle breakage has occurred.

In Chapter 2 it was stated that Banks[11] has suggested that ϕ_s has a linear relationship with the common logarithm of the normal stress. Banks expressed this relationship as

$$\phi_o = \phi_{ref} - P \log (\sigma_o/\sigma_{ref}) \quad \text{(5)}$$

where ϕ_o is the predicted value of ϕ_s and the other symbols are as previously defined.

The relationship which gives the best fit to the test data, $\tau = 1{,}15 . \sigma_o^{0{,}932}$ (refer to Figure 47), has been used to obtain values of ϕ_s which have been plotted against the common logarithim of σ_o. This plot is shown in figure 52 and also contains the straight line obtained by using equation (5).
the predicted values of ϕ_s as shown by the straight line are reasonably close and conservative with the agreement decreasing with the increasing stress level. Thus if only ϕ_{ref} or σ_{ref} (refer to Chapter 2) are available, equation (5) will be useful in predicting conservative values of ϕ.

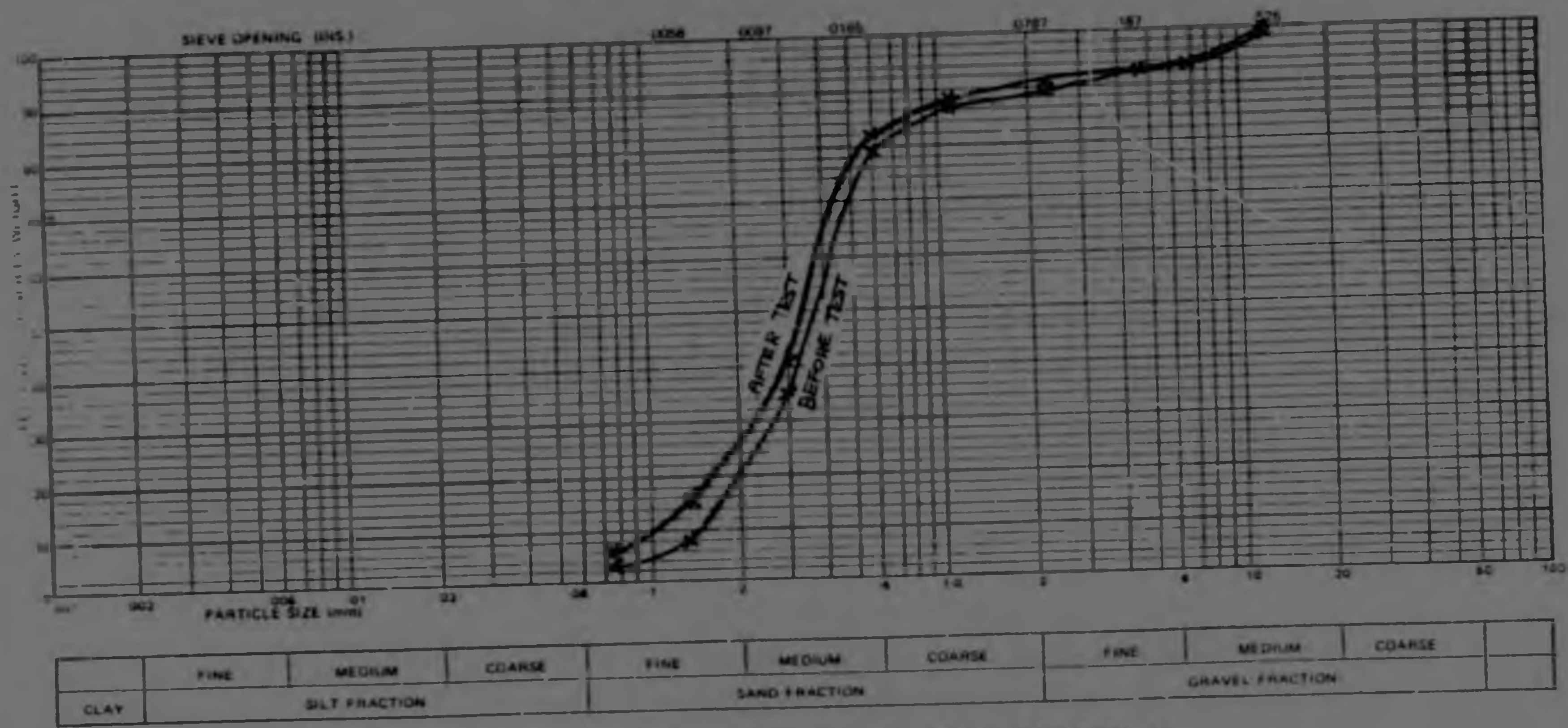

FIGURE 51 : Percent finer by weight, before and after testing, Kleinsee 3

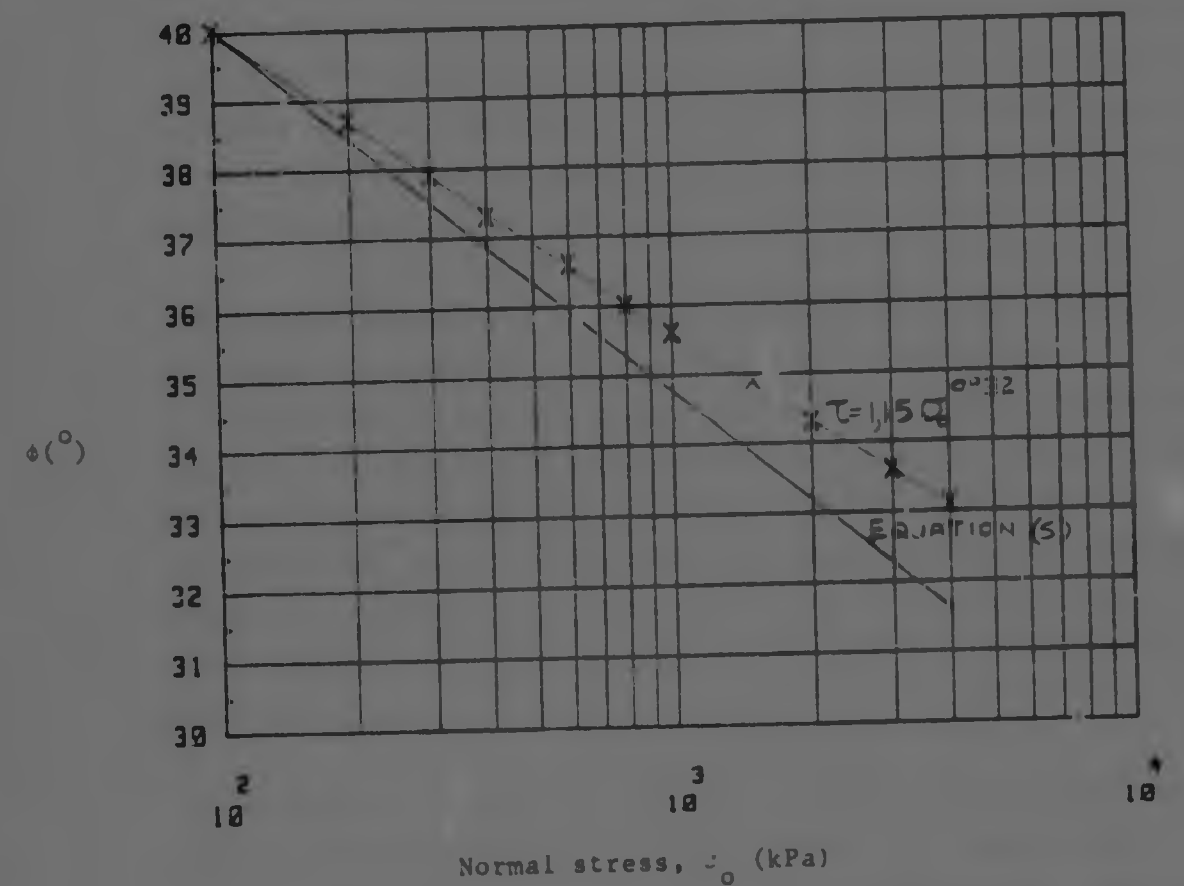

FIGURE 52 : ϕ versus σ_o

CHAPTER 6 : SAMPLE SLOPE STABILITY ANALYSES

In order to assess the effect of the curved strength envelope on slope stability analysis the following examples are presented. The failure shape is of the form predicted by Blight in Chapter 3. The method of slope stability analysis used is the simplified $y=o$ method presented in Chapter 4. The dump is assumed to have the same material properties as the Twee Pad sample and two angles of friction will be considered. The angles are a constant $\phi_1 = 36^\circ$ from linear regression analysis and a variable ϕ_2 obtained from the power relationship $\tau = 1,21.\sigma_o^{0,927}$, (refer to Table 14).

The assumed geometry of the sample dumps is shown in Figure 53. Two cases of foundation conditions are to be considered. In Case 1 the foundation is assumed to have frictional strength properties greater than that of the dump material. Thus the failure surface will be confined to within the dump. In Case 2 a thin foundation of clayey soil overlying bedrock is assumed. The soil strength parameters are $C=60$ kN/m and $\phi = 20^\circ$. The failure surface is shown in Figure 53. The results of the analyses are shown in Table 16.

The results of the analyses for Case 1 show that the factor of safety calculated using ϕ_1 is independent of the dump height. This is in agreement with Blight's conclusions (Chapter 4). The results of the analyses for ϕ_2 show that the factor of safety decreases with increasing dump height. This is due to the decrease of ϕ with increasing stress levels. However the differences between the factors of safety calculated for ϕ_1 and ϕ_2 are smaller.

CHAPTER 6 : SAMPLE SLOPE STABILITY ANALYSES

In order to assess the effect of the curved strength envelope on slope stability analysis the following examples are presented. The failure shape is of the form predicted by Blight in Chapter 3. The method of slope stability analysis used is the simplified y=o method presented in Chapter 4. The dump is assumed to have the same material properties as the Twee Pad sample and two angles of friction will be considered. The angles are a constant $\phi_1 = 36^o$ from linear regression analysis and a variable ϕ_2 obtained from the power relationship $\tau = 1,21.\sigma_e^{0,927}$, (refer to Table 14).

The assumed geometry of the sample dumps is shown in Figure 53. Two cases of foundation conditions are to be considered. In Case 1 the foundation is assumed to have frictional strength properties greater than that of the dump material. Thus the failure surface will be confined to within the dump. In Case 2 a thin foundation of clayey soil overlying bedrock is assumed. The soil strength parameters are C=60 kN/m and $\phi = 20^o$. The failure surface is shown in Figure 53. The results of the analyses are shown in Table 16.

The results of the analyses for Case 1 show that the factor of safety calculated using ϕ_1 is independent of the dump height. This is in agreement with Blight's conclusions (Chapter 4). The results of the analyses for ϕ_2 show that the factor of safety decreases with increasing dump height. This is due to the decrease of ϕ with increasing stress levels. However the differences between the factors of safety calculated for ϕ_1 and ϕ_2 are smaller.

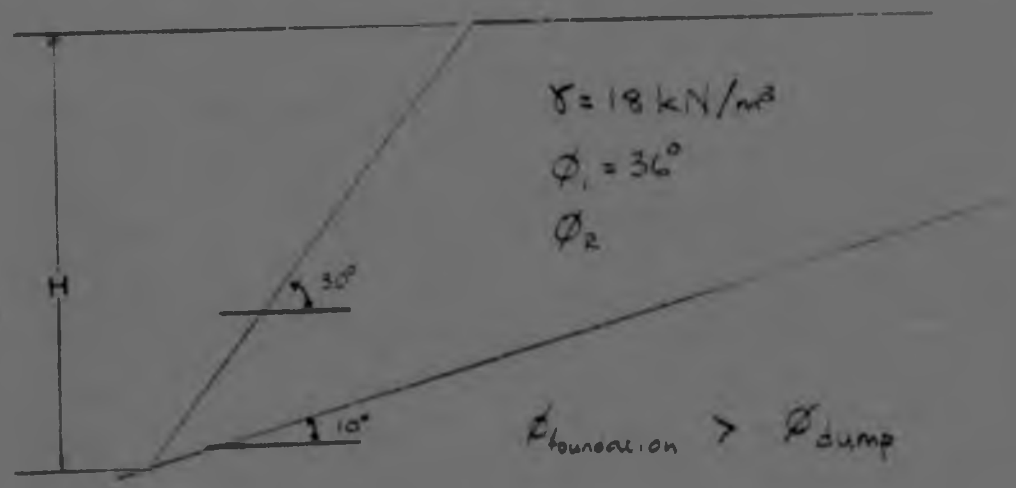

Case 1

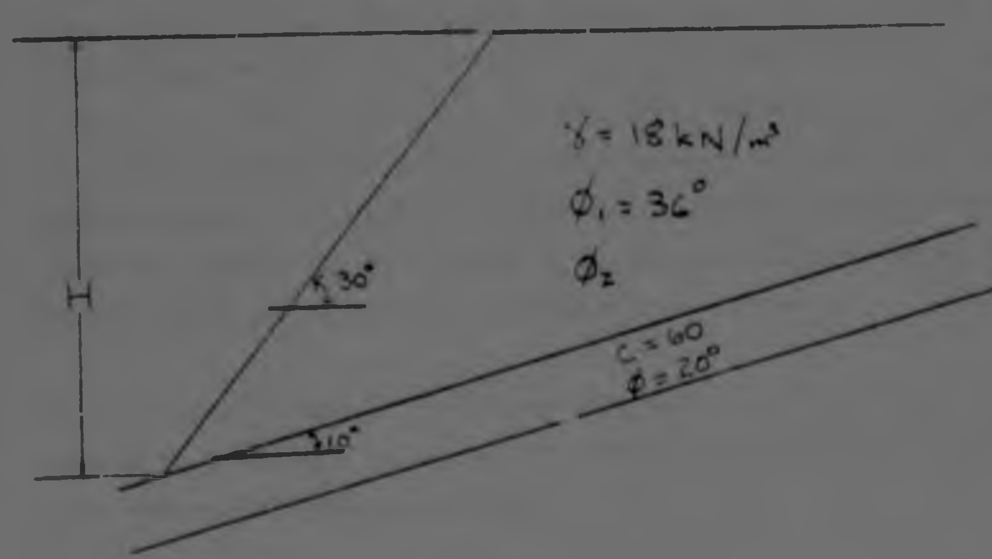

Case 2

FIGURE 53 : Example dump

TABLE 16 : RESULTS OF γ=o STABILITY ANALYSES

DUMP HEIGHT H (m)	FACTOR OF SAFETY			
	CASE 1		CASE 2	
	ϕ_1	ϕ_2	ϕ_1	ϕ_2
150	1,84	1,87	1,23	1,23
200	1,84	1,84	1,19	1,19
250	1,84	1,80	1,15	1,15
300	1,84	1,78	1,13	1,13

ϕ_1 - From linear regression = 36^o

ϕ_2 - From $\tau = 1{,}21.\sigma_o^{0{,}927}$

Note: $\phi_2 = \phi_1$ when σ_o = 1100 kPa

The results of the analyses for Case 2 show that there is no difference between the factors of safety obtained from using either ϕ_1 or ϕ_2. This is because the failure surface passes through the dump for only a short distance and because of the dump geometry, stress levels are high ($\phi_2 < \phi_1$) for an even shorter distance. Thus the effect of a decreasing ϕ_2 value with increasing stress levels does not influence the factor of safety.

Thus in conclusion it can be stated that for Case 1 the curved strength envelope has a small influence on the factor of safety but has no influence for Case 2.

CHAPTER 7 : SUMMARY AND GENERAL CONCLUSIONS

7.1 Literature Review

7.1.1 The Behaviour of Cohesionless Material

It is evident from the literature review that a large number of factors influence the behaviour of coarse mine waste (cohesionless material). Factors such as relative density, particle size, saturation or water content and soil composition all influence soil behaviour.

The assumption of a linear relationship between shear strength and normal stress is incorrect in general. The experimental results of various authors show that significant curvature of the Mohr strength envelope occurs with increasing normal stress.

7.1.2 Factors Affecting the Stability of Coarse Mine Waste Dumps

The literature review has shown that a variety of dump failure modes can occur. The type of failure depends on factors such as foundation conditions, dump material properties and climatic conditions.

Blight investigated the failure of four rock dumps and concluded that failure results in the formation of a system of wedges that develop beneath the dump slope. As failure occurs, an active wedge at the top of the slope displaces a passive wedge at the base of the slope, displacement taking place by shearing through the foundation.

Block translation occurs when the shear strength parameters at the bottom of a dump on an inclined slope are lower than those within the dump. Sliding occurs along plane failure surfaces which coincide with or just below the surface of the natural ground.

Surface or edge slides can occur if an accumulation of a layer of fines occurs below the dump slope surface.

The foundation shear strength is important in determining the mode and probability of failure. Blight has recommended the unconsolidated undrained triaxial shear test and the quick shear box tests as laboratory tests. The cone penetrometer and the vane shear test on remoulded soil are recommended field tests for assessing foundation shear strength.

7.1.3 Methods of Slope Stability Analysis

The factor of safety of a dump slope may be estimated using simple equations or stability charts and tables. Simple slope stability methods refer to the analysis of simplified conditions such as simple geometry, uniform physical properties, saturated and unsaturated slopes and specific sliding surfaces. The limitations in the accuracy of these methods become insignificant when compared to the inability to accurately define the parameters in the stability analysis. Thus simplified methods are valuable because of their ease of use and potential for pin-pointing likely failure. A number of methods are presented in this dissertation for analysing dump slope stability.

The simplified y=o method has been recommended because it is quick, easy to use and can be applied to any failure surface. The y=o method has been found to give results in close agreement with the simplified Bishop and U.S.B R. methods.

7.2 Laboratory Work

The results of consolidated, drained triaxial tests on typical mine waste materials show that slight curvature of the Mohr strength envelope occurs above a normal stress of 1600 kPa. The power equation which fits tha test data is

$$\tau = 1,15.\sigma_o^{0,932} \quad \ldots\ldots\ldots\ldots\ldots\ldots\ldots\ldots \quad (1)$$

Comparison of equation (1) with power equations for rockfill data shows that rockfill experiences greater curvature of the strength envelope. This can be attributed to greater particle breakage occurring in rockfill material during testing.

The use of equation (5)

$$\phi_o = \phi_{ref} - P \log (\sigma_o/\sigma_{ref}) \quad \ldots\ldots\ldots\ldots\ldots\ldots \quad (5)$$

for predicting values of the soil friction angle, has been found to produce conservative values with reasonable agreement to the test results.

7.3 Sample Slope Stability Analyses

Sample analyses have shown that there is little or no difference in the factor of safety obtained by using a constant friction angle from linear regression or a variable friction angle derived from the power equations which describe the curved strength envelope. Thus it can be concluded that the curvature of the strength envelope has little influence on the factor of safety of mine waste dumps.

APPENDIX A

CONTENTS

TABLE A1: FRICTION ANGLE OF ROCKFILL

Location (1)	Material (2)	Maximum particle, in inches (3)	Dry density, in pounds per cubic foot (4)	Normal pressure, in pounds per square inch (5)	Maximum friction angle, in degrees (6)
Isabella	Granite	4	97,0	7,5	47,0
		4	95,0	23,0	43,5
Cachuma	Gravel	0,75	126,0	6,3	54,7
		0,75	125,0	11,3	49,5
		0,75	123,0	21,5	44,5
		0,75	125,0	43,0	45,0
		0,75	124,0	84,0	41,0
		0,75	124,0	165,0	39,5
		0,75	125,0	162,0	38,5
Cachuma	Gravel	3	126,0	6,2	54,0
		3	124,0	11,8	49,5
		3	124,0	22,1	47,0
		3	127,0	45,0	46.5
		3	125,0	86,0	43,5
		3	127,0	167,0	41,5
Cachuma	Quartz Monz.	3	122,0	20,0	40,0
		3	123,0	65,0	39,5
		3	122,0	123,0	39,0
		3	129,0	22,0	44,0
		3	128,0	60,0	42,0
Cachuma	Quartz Monz.	3	130,0	125,0	41,0
		3	117,0	42,0	44,0
		3	117,0	59,0	41,0
		3	127,0	44,0	47,0
		3	127,0	63,0	46,0
Oroville	Tailings	1,5	144,0	490,0	40,0
		1,5	142,0	484,0	38,8
		1,5	148,0	424,0	43,0
		1,5	147,0	700,0	40,5
		1,5	148,0	1160,0	40,0
		3	143,0	208,0	42,0
		3	143,0	206,0	41,3
		3	150,0	213,0	45,0
Soledad	Gravel	3,5	1,02[a]	8,2	44,8
		3,5	0,88	16,6	42,8
		3,5	0,64	8,8	50,0
		3,5	0,69	16,9	47,2
Infiernillo	Diorite	7	0,82	8,3	44,0
		7	0,86	16,1	44,0
		7	0,69	9,1	49,5
		7	0,70	17,2	46,5
		7	0,65	8,7	49,0
		7	0,70	11,7	46,5
		7	0,60	16,0	46,5
Infiernillo	Diorite	8	0,45	9,8	50,0
		8	0,61	21,4	46,1
		8	0,62	44,5	44,4
		8	0,73	114,0	40,7
		8	0,55	230,0	38,0
		8	0,51	385,0	35,0
		8	0,50	567,0	34,7

Location	Material	Maximum particle, in inches	Dry density, in pounds per cubic foot	Normal pressure, in pounds per square inch	Maximum friction angle, in degrees
(1)	(2)	(3)	(4)	(5)	(6)
Infiernillo	Conglomerate	8	0,62[a]	16,1	46,1
		8	0,55	45,0	45,5
		8	0,55	113,0	41,0
		8	0,62	230,0	39,[illegible]
		8	0,51	390,0	37,[illegible]
		8	0,45	570,0	37,1
		8	0,51	44,8	45,6
		8	0,50	114,0	42,2
		8	0,40	232,0	39,5
		8	0,40	390,0	37,6
		8	0,46	570,0	36,3
Malpaso	Conglomerate	8	0,42	9,6	50,0
		8	0,35	21,9	49,2
		8	0,42	45,5	48,0
		8	0,32	116,0	45,2
		8	0,44	230,0	39,0
		8	0,38	390,0	39,0
		8	0,40	570,0	36,9
		8	0,43	570,0	37,2
		8	0,42	570,0	37,4
		8	0,33	570,0	38,9
		8	0,33	575,0	39,5
Pinzandaran	Gravel	8	0,33	10,2	53,1
		8	0,36	22,3	52,3
		8	0,32	45,6	48,5
		8	0,32	116,0	45,5
		8	0,32	233,0	42,5
		8	0,34	390,0	39,3
		8	0,35	573,0	38,9
Infiernillo	Basalt	7	0,30	10,4	60,0
		7	0,30	25,6	55,0
		7	0,30	122,0	45,7
		7	0,30	239,0	42,7
Infiernillo	Gneiss X	7	0,32	10,0	51,0
		7	0,32	23,0	45,0
Infiernillo	Gneiss Y	7	0,62	6,3	45,0
		7	0,62	20,4	41,3
Contreras	Gravel	7	0,68	8,0	41,6
		7	0,65	8,4	41,6
		7	0,68	17,3	41,0
		7	0,54	8,4	45,5
		7	0,53	17,0	45,5
Santa Fe	Andesite	7	1,06	8,0	42,7
		7	1,07	15,9	40,2
		7	0,92	8,7	48,0
		7	0,84	17,0	46,8
Port Peck	Sand	No. 20	0,70	27,8	37,9
		No. 20	0,70	55,5	37,1
		No. 20	0,70	83,0	36,3
		No. 20	0,70	111,0	35,3

Location	Material	Maximum particle, in inches	Dry density, in pounds per cubic foot	Normal pressure, in pounds per square inch	Maximum friction angle
(1)	(2)	(3)	(4)	(5)	(6)
Scituate	Sand	No. 8	0,57[a]	27,8	38,0
		No. 8	0,57	55,5	37,5
		No. 8	0,57	111,0	35,5
Ottawa Std.	Sand	No. 14	0,59	6,9	33,6
		No. 14	0,59	13,9	33,0
		No. 14	0,59	27,8	31,8
		No. 14	0,59	41,6	30,8
		No. 14	0,59	55,5	30,0

[a]All subsequent numbers in this column are void ratios.

INTERMEDIATE STRESS

Consider a standard shear box test as shown below;

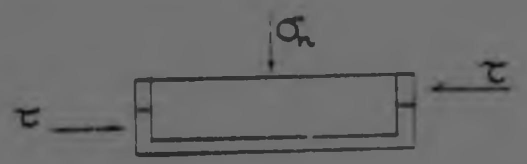

Maintaining the normal stress (σ_n) constant the following form of shear force/displacement diagram can be expected.

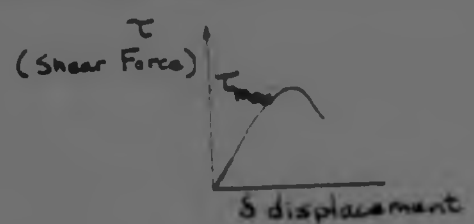

Repeating a number of tests with differing σ_n the Mohr-coulomb envelope can be plotted;

σ_n cannot be considered the major principle stress and considering the Mohr-coulomb envelope, the major and minor principle stresses as well as their orientation can be determined for a specific σ_n

Considering again the standard shear box test, it can be seen in the diagram below the σ_1 and σ_3 occupy two directions and the third direction can be considered as the intermediate stress (σ_2) direction.

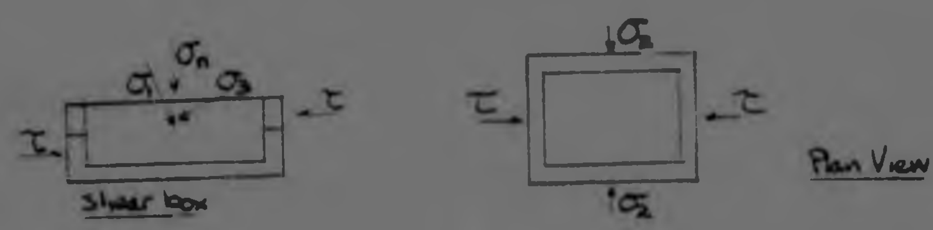

During shear failure, particles tend to climb up and over each other. This is associated with a volume increase. This increase is restricted in the vertical direction by σ_n and hence the specimen expands laterally. The function of the intermediate stress is to prevent this expansion and hence increase the shear strength and consequently the angle of internal friction. For shear failure to occur in the σ_3 direction, the intermediate stress must be greater than or equal to σ_3. Larssons ratio.

$$b = \frac{\sigma_2 - \sigma_3}{\sigma_1 - \sigma_3}$$

is based on the above concept. Larsson has defined the following two limits on his diagram; $\sigma_2 = \sigma_3$ the condition of virtual lateral non-constraint

$\sigma_2 = \sigma_1$ the condition of "complete" lateral constraint.

APPENDIX B

CONTENTS

....

EDGE SLIDES AND SHALLOW FLOW SLIDES

Infinite Slope in C and ϕ Material with Seepage Parallel to Slope

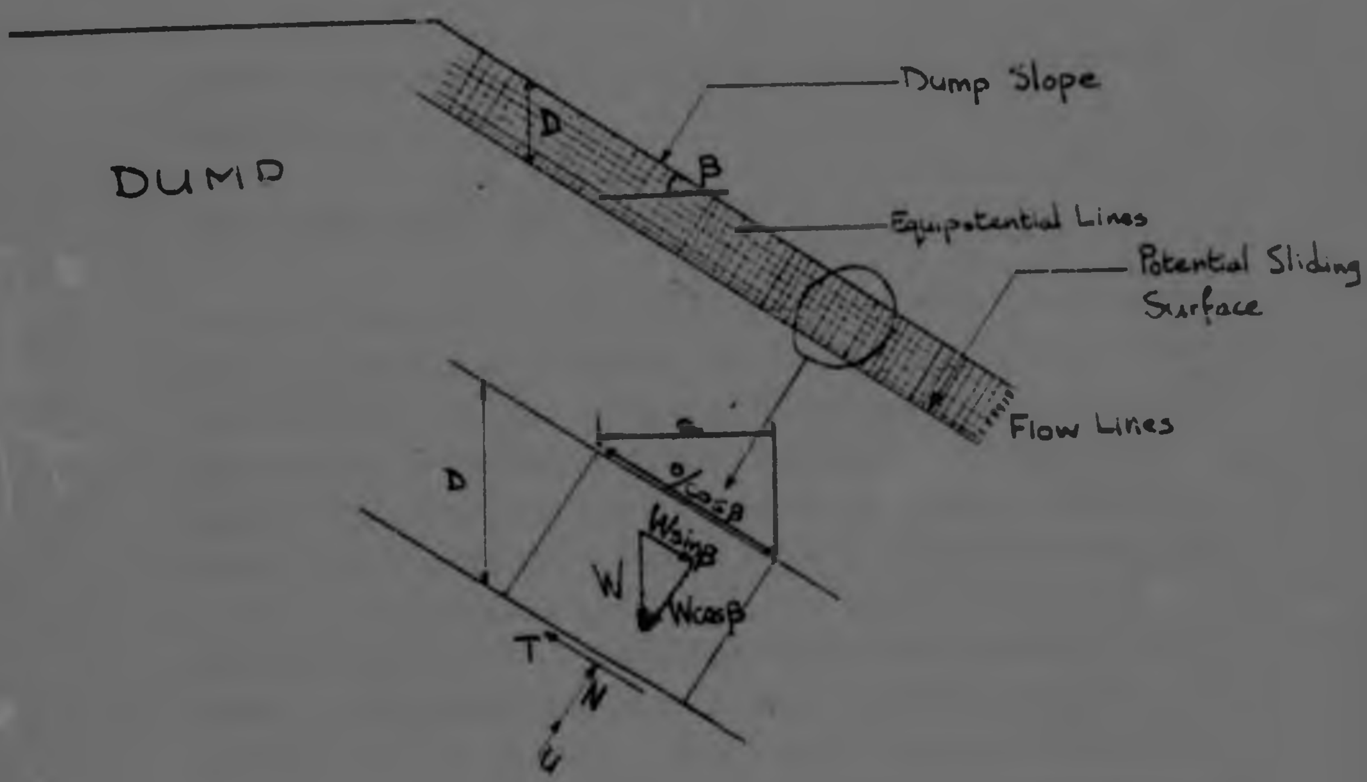

where W = weight of slice
N = normal force
U = pore water force
T = shear resistance

For limiting equilibrium:

$W \sin \beta = T$ where $W = aD\gamma$

$N = aD\gamma \cos\beta$

$U = \gamma_w D\cos^2\beta \cdot \frac{a}{\cos\beta}$

$= \gamma_w \, aD\cos\beta$

$T = \frac{c'a}{\cos\beta} + aD \left[\gamma\cos\beta \;\; \gamma_w \cos\beta\right] \tan\phi'$

$$\therefore \quad aD\gamma\sin\beta = \frac{c'a}{\cos\beta} + aD\cos\beta\left[\gamma-\gamma_w\right]\tan\phi'$$

$$F = \frac{c'}{\gamma D\sin\beta\cos\beta} + \frac{\gamma'}{\gamma}\frac{\tan\phi'}{\tan\beta} \qquad \ldots\ldots\ldots\ldots \quad (B1)$$

Making the relevant substitutions will result in equations (8) to (11).

BLOCK TRANSLATION[12] DERIVATION OF N'

Figure B1 shows the forces acting on a spoil bank. The factor of safety is defined as a ratio of the resisting force due to the shear strength of soils along the failure surface to the driving force due to the weight of fill. The resisting force is composed of two parts: one due to cohesion and equal to $\bar{c}H \csc \alpha$, where $\bar{c}$ is the effective cohesion of soil, H is the height, and $H \csc \alpha$ is the length of failure plane; and the other due to friction and equal to $\bar{N} \tan \bar{\phi}$, where N is the effective force normal to the failure plane and $\bar{\phi}$ is the effective angle of internal friction of soil. Both $\bar{c}$ and $\bar{\phi}$ can be determined from laboratory tests of soil samples. If there is no seepage, or no pore pressure along the failure plane. $\bar{N}=W\cos\alpha$, where W is the total weight of fill. If seepage exists within the slope, N can be determined by the concept of pore pressure ratio as described below.

FIGURE B1 : Forces acting on a spoil bank

The pore pressure ratio, r_u, is a ratio between the pore pressure along the failure plane and the overburden pressure. The average overburden pressure for the spoil bank is W/(H cotα), so the average pore pressure along the failure plane is $r_u W/(H \cot\alpha)$. The total neutral force perpendicular to the failure plane is H cscα $r_u W/(H \cot\alpha)$, which can be simplified to $r_u W \sec\alpha$. By equating to zero all the forces in a direction normal to the failure plane, the effective normal force, N, can be obtained by

$$N = W \cos\alpha - r_u W \sec\alpha \quad \ldots\ldots\ldots\ldots\ldots\ldots \quad (B2)$$

The pore pressure ratio depends on the location of the phreatic line. The unit weight of a typical spoil bank is about twice that of water. When water seeps throughout the entire bank, the phreatic line will lie on the top and along the outslope of the fill. If the phreatic line is considered as a static water table, the pore pressure ratio in this case is equal to o,5. When there is no seep..., or the phreatic line lies below the failure plane, the pore pressure ratio is zero. Depending on the percentage of area below the phreatic line, a pore pressure ratio ranging from 0 for zero percent area to 0,5 for 100 percent area can be assumed, or

$$r_u = \frac{\text{cross-sectional area of bench under water}}{2 \times \text{total cross-sectional area of bench}} \quad \ldots\ldots \quad (B3)$$

The use of $r_u W \sec\alpha$ as the neutral force is not reasonable because when $r_u = 0{,}5$ and $\alpha > 45^{\circ}$, the effective normal force $\bar{N}$ is negative, as can be seen from Eq. B2. To avoid this difficulty, engineers have long used the concept of submerged unit weight for determining the stress normal to the failure surface. The resultant force due to pore pressure is assumed to be vertical, so the effective normal force becomes

$$N = (1-r_u) W \cos\alpha \quad \ldots\ldots\ldots\ldots\ldots\ldots \quad (B4)$$

Another reaso- favouring the use of Eq. B4 is that the phreatic line is not static. It is well-known that for an infinite slope of inclination with seepage parallel to the slope, the pore pressure at a depth, h, below the phreatic line is $\gamma_w h \cos^2\alpha$ instead of $\gamma_w h$ for the static case, where γ_w is the unit weight of water. Consequently, the neutral force $r_u W \sec\alpha$ should be multiplied by $\cos^2\alpha$, or an expression of $r_u W \cos\alpha$ is obtained.

APPENDIX - DERIVATION OF WEDGE STABILITY ANALYSIS[3]

Figure 28 represents a section through a rock dump built on ground sloping at i to the horizontal. The density of the rockfill is γ and the dump is sliding along the surface abc. The disturbing force results from the downhill component of the weight of the sliding wedge abc and restoring forces are generated along the sliding surfaces ab (through the foundation soil) and bc (through the rockfill).

The weight W_1 of wedge bcd is given by .... (B5)

$$W_1 = \frac{\gamma h^2}{2} \cot\alpha(1-\cot\alpha\tan\beta)$$

The net horizontal driving force F_1 that results from this wedge is

$$F_1 = W_1 \cos\alpha\,(\sin\alpha - \cos\alpha\tan\phi) \qquad \text{.............. (B6)}$$

and is the difference of the wedging force exerted by W_1 and the horizontal component of the frictional resistance to sliding along bc.

$$F_1 = \frac{\gamma h^2}{2} \cos^2\alpha(1-\cot\alpha\tan\beta)(1-\cot\alpha\tan\phi') \qquad \text{........... (B7)}$$

and is the same regardless of the slope i. of the base of the dump.

F_1 = can be expressed in terms of H by means of the relationship

$$h = H\cdot\left[1 - \frac{\sin(\alpha-\beta)\sin i}{\sin\beta\sin(\alpha-i)}\right] \qquad \text{................ (8)}$$

i.e.

$$F_1 = \frac{\gamma H^2}{2}\cos^2\alpha(1-\cot\alpha\tan\beta)(1-\cot\alpha\tan\phi)\left[1-\frac{\sin(\alpha-\beta)\sin i}{\sin\beta\sin(\alpha-i)}\right] \qquad \text{(B9)}$$

The weight of W_2 of wedge abd is given by:

$$W_2 = \frac{\gamma H^2}{2} \cdot \frac{\sin^2(\alpha-\beta)}{\sin^2(\alpha-i)} \cdot \frac{\cos i}{\sin\beta} \cdot \left(\frac{\cos i \quad \sin i}{\cos\beta \;\; \sin\beta}\right) \qquad \text{(B10)}$$

The horizontal wedging force exerted by W_2 is

$$F_2 = W_2 \cdot \cos i \cdot \sin i$$

while the normal force across ab from W_2 is

$$N = W_2 \cdot \cos i$$

A DUMP ON A COHESIVE FOUNDATION

The restoring force along ab is given by

$$\tau . ab. = \tau . H. \frac{\sin(\alpha-\beta)}{\sin\beta . \sin(\alpha-i)} \qquad \text{(B11)}$$

Hence for horizontal equilibrium of the dump

$$F_1 + F_2 = \tau . H. \frac{\sin(\alpha-\beta)\cos i}{\sin(\alpha-i)\sin\beta}$$

Hence $\dfrac{\tau}{\gamma H} = \dfrac{\sin(\alpha-i)\sin\beta}{\sin(\alpha-\beta)\cos i}\left[\dfrac{F_1}{\gamma H^2} + \dfrac{F_2}{\gamma H^2}\right]$

or $\dfrac{\tau}{\gamma H} = A \cdot \left[B + C\right]$ (B12)

where

$$A = \frac{\sin(\alpha-i)\sin\beta}{\sin(\alpha-\beta)\cos i} \qquad \text{(B13)}$$

$$B = \frac{\cos^2\alpha}{2} \cdot (1-\cot\alpha\tan\beta) \cdot (1-\cot\alpha\tan\phi) \cdot \left[1 - \frac{\tan i}{A}\right]^2 \qquad \text{(B14)}$$

$$C = \frac{\cos^2 i}{2} \cdot \frac{\sin i}{\sin\beta} \cdot \frac{\sin^2(\alpha-\beta)}{\sin^2(\alpha-i)} \left(\frac{\cos i}{\cos\beta} - \frac{\sin i}{\sin\beta}\right) \qquad \text{(B15)}$$

If $i = 0$, $\dfrac{\tau}{\gamma H} = A \cdot B$

A DUMP ON A FRICTIONAL FOUNDATION

The restoring force along ab is given by

$$W_2 \cdot \cos i \cdot \tan\phi_f$$

Hence for horizontal equilibrium of the dump:

$$F_1 + F_2 = W_2 \cos^2 i \tan\phi_f = F_1 + W_2 \cos i \sin i$$

Hence $\tan\phi_f = \dfrac{F_1}{W_2 \cos^2 i} + \tan i$

or $\tan\phi_f = \dfrac{B}{D \cos^2 i} + \tan i$ (B16)

In which

$$D = \frac{1}{2} \cdot \frac{\sin^2(\alpha-\beta)}{\sin^2(\alpha-i)} \cdot \frac{\cos i}{\sin\beta} \cdot \left(\frac{\cos i}{\cos\beta} - \frac{\sin i}{\sin\beta}\right) \qquad \text{(B17)}$$

If $i = 0$

$$\tan\phi_f = \frac{B}{D}$$

APPENDIX C

CONTENTS

Page

TABLE C1 : TRIAXIAL TEST RESULTS

SPECIMEN	CELL PRESSURE σ_3, (kPa)	NORMAL STRESS σ_o, (kPa)	SECANT FRICTION ANGLE ϕ_s, (°)
PREMIER	300,0	479.3	36,7
	500,0	804,4	37,5
	800,0	1277,0	36,6
	1000,0	1563,5	34,3
JWANENG	300,0	485,1	38,1
	600,0	951,0	35,8
	800,0	1264,6	35,5
	1000,0	1583,4	35,7
	1200,0	1874,5	34,2
	1500,0	2325,7	33,4
	2000,0	3027,1	30,9
KLEINSEE 1	200,0	337,7	43,5
	500,0	775,2	33,4
	800,0	1252,0	34,4
	1000,0	1567,8	34,6
KLEINSEE 2	200,0	325,0	38,7
	400,0	636,8	36,3
	600,0	975,1	38,7
	800,0	1287,1	37,5
	1000,0	1612,9	37,8

TABLE C1 : TRIAXIAL TEST RESULTS continued

SPECIMEN	CELL PRESSURE σ_3,(kPa)	NORMAL STRESS σ_o,(kPa)	SECANT FRICTION ANGLE ϕ_s,(^{o})
KLEINSEE 3	150,0	241,1	37,4
	350,0	559,7	36,8
	550,0	861,5	34,5
	700,0	1092,4	34,1
	900,0	1411,1	34,6
	1050,0	1611,1	32,3
	1200,0	1850,0	32,8
	1300,0	1992,7	32,2
	1500,0	2323,5	33,3
	1650,0	2558,3	33,4
	1800,0	2767,1	32,5
	2000,0	3062,8	32,1
TWE PAD	100,0	162,5	38,7
	250,0	404,9	38,3
	500,0	804,4	37,5
	700,0	1115,4	36,4
	900,0	1425,2	35,7
	1150,0	1803,0	34,6
	1400,0	2193,0	34,5
	1700,0	2638,3	33,5
	2000,0	3098,5	33,3
KOINGNAAS	200,0	314,4	34,9
	400,0	639,6	36,8
	600,0	960,3	36,9
	800,0	1264,6	35,5
	900,0	1429	36,0

TABLE C1 : TRIAXIAL TEST RESULTS continued

SPECIMEN	CELL PRESSURE σ_3, (kPa)	NORMAL STRESS σ_o, (kPa)	SECANT FRICTION ANGLE ϕ_s, (^{o})
KOINGNAAS	1150,0	1803,0	34,6
	1300,0	2022,5	33,8
	1500,0	2385,9	36,2
	1800,0	2855,5	35,9
	2000,0	3169,9	35,8

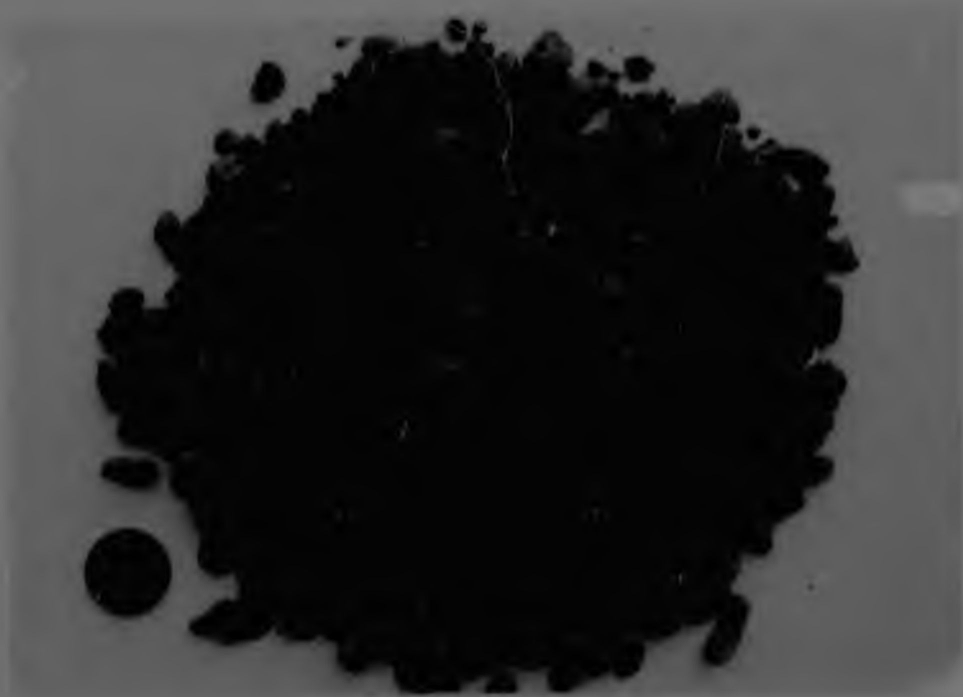

FIGURE C2(a): Premier

FIGURE C2(b) : Jwaneng

FIGURE C2(c) : Koingnaas

FIGURE C2(d) : Twee Pad

FIGURE C2(e) : Kleinsee 1

FIGURE C2(f) : Kleinsee 2

FIGURE C2(g) : Kleinsee 3

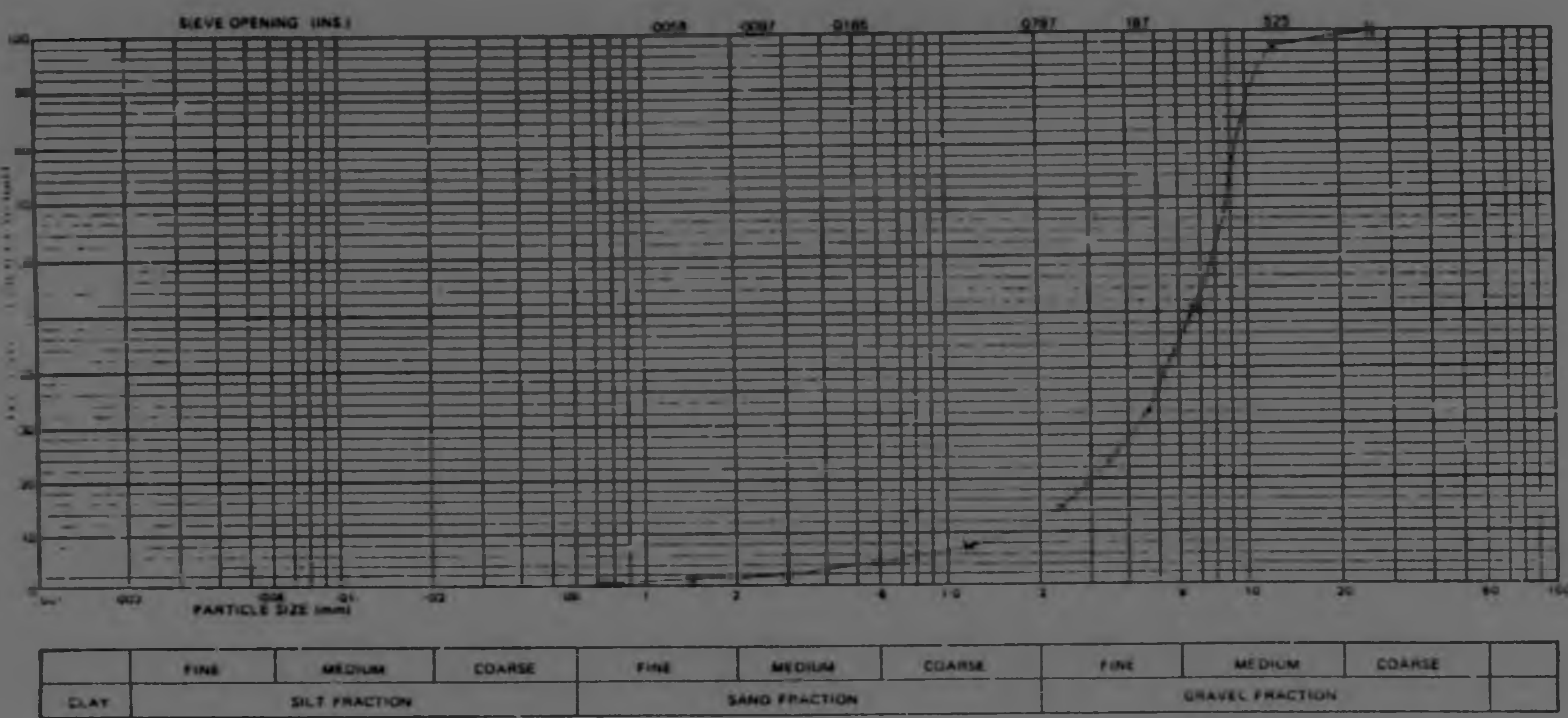

FIGURE C3(a) : Percent finer by weight, Premier

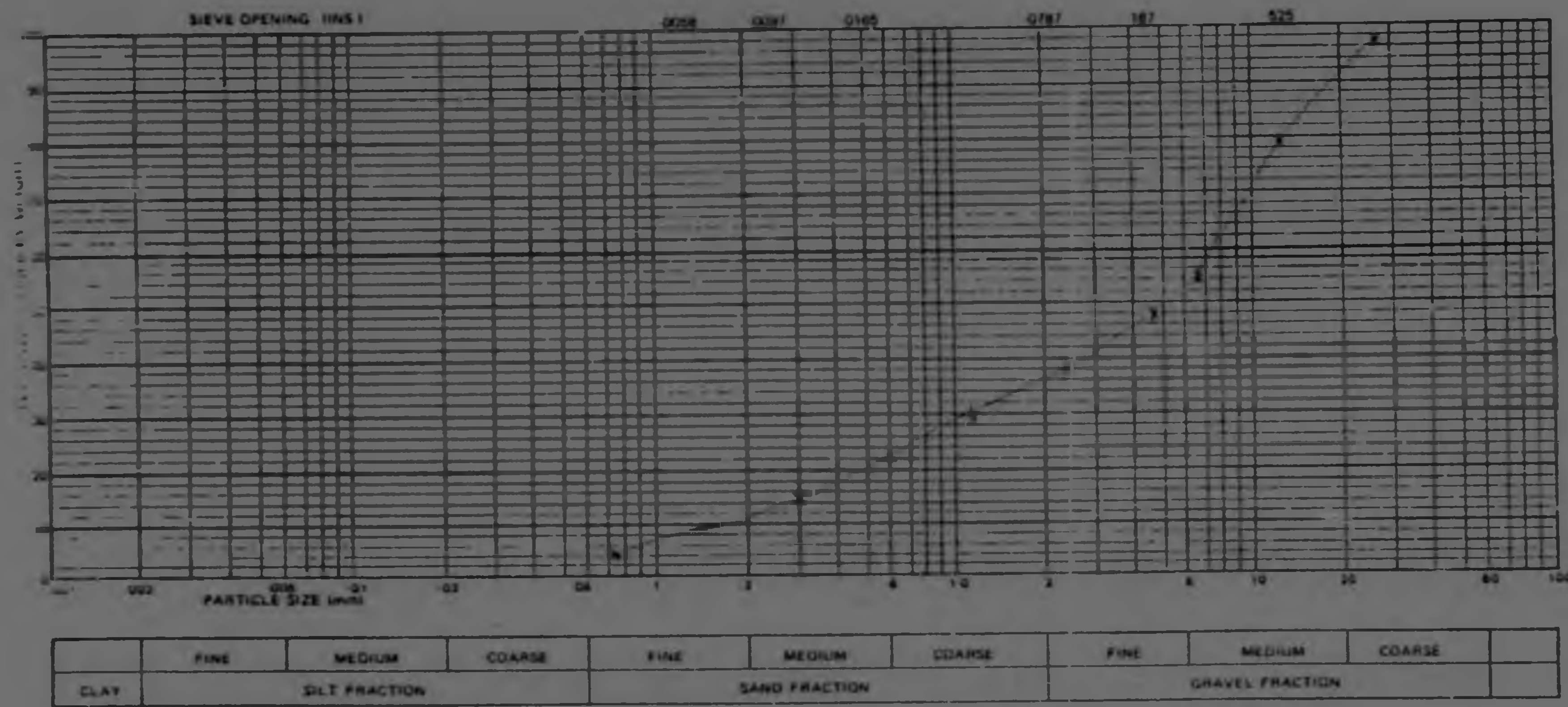

FIGURE C3(b) : Percent finer by weight, Jwaneng

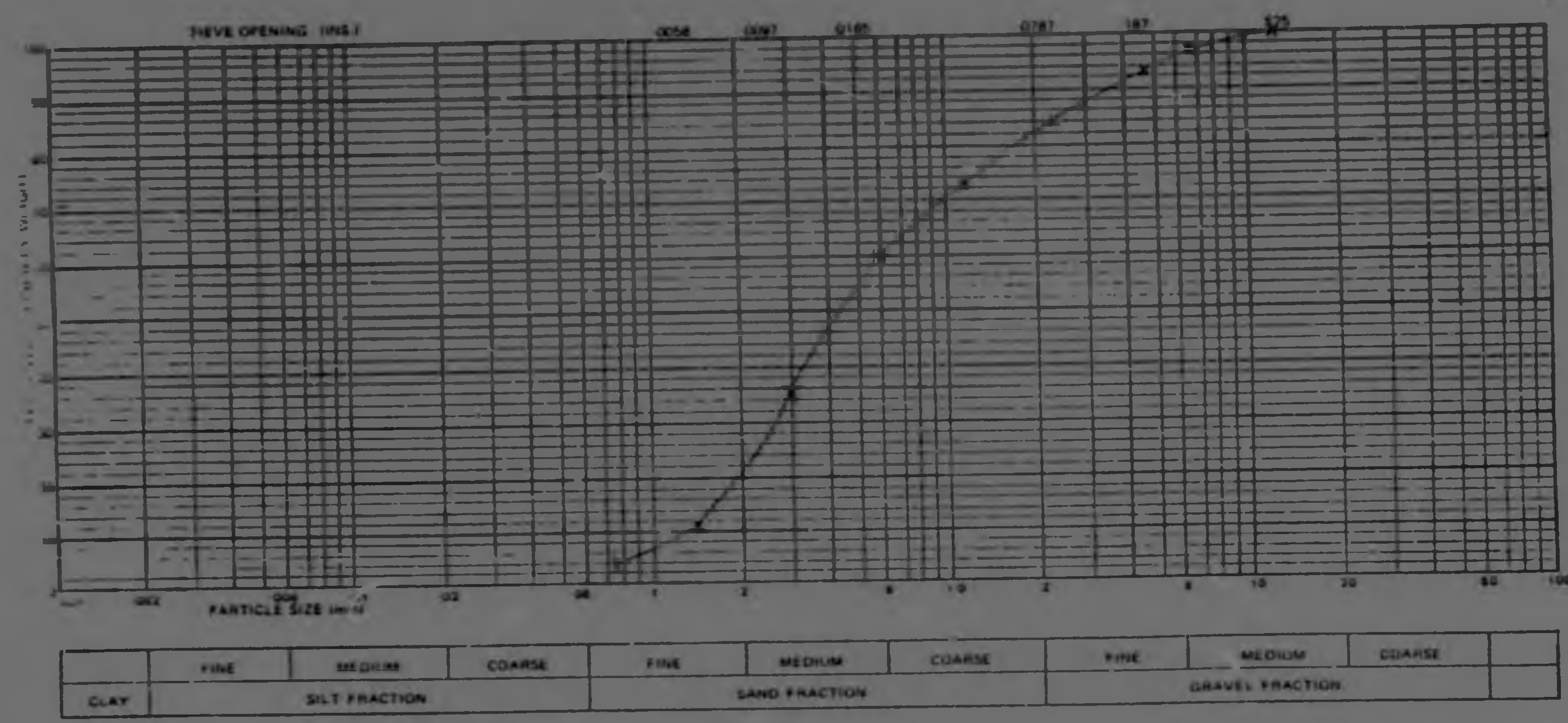

FIGURE C3(c) : Percent finer by weight, Kleinsee 1

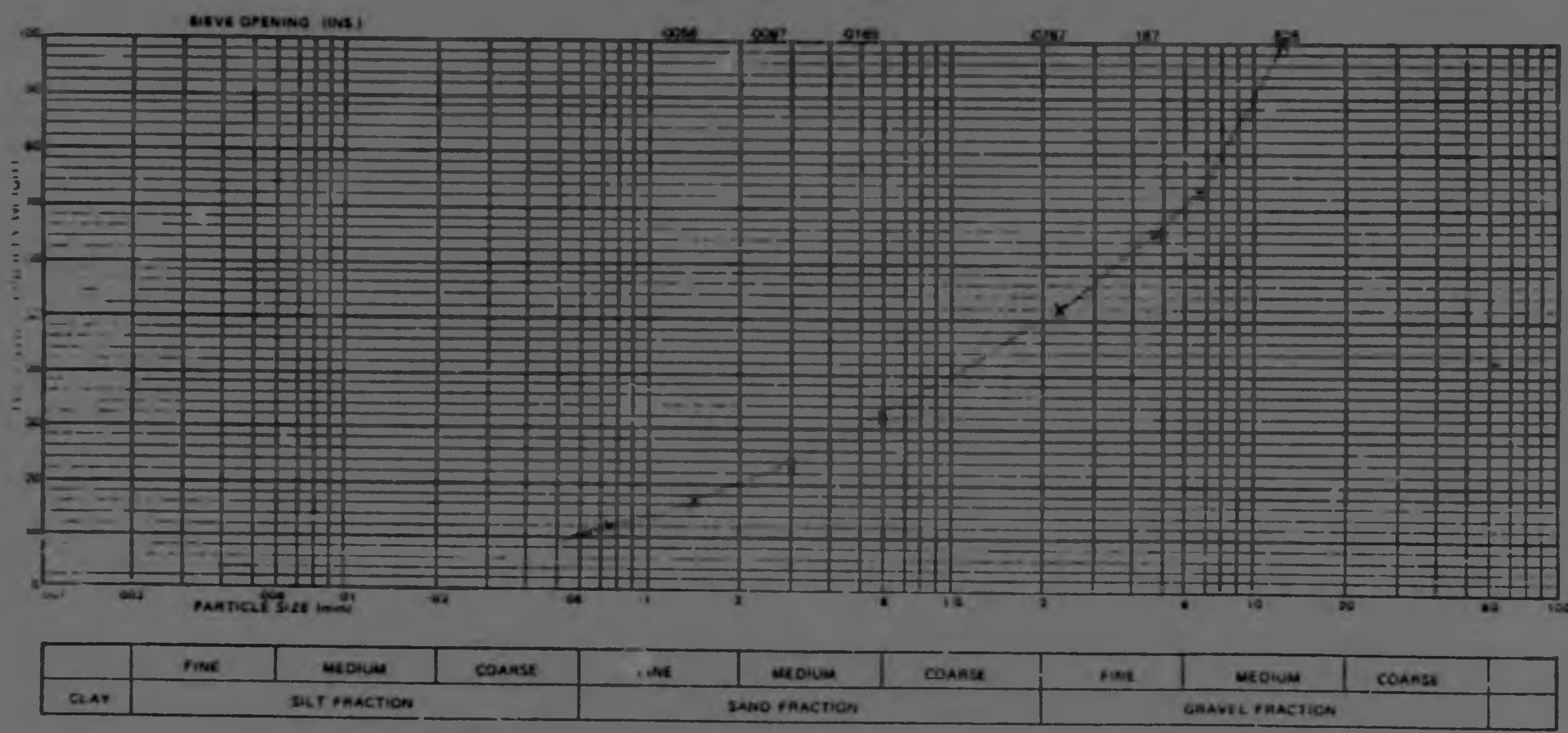

FIGURE C3(d) : Percent finer by weight, Kleinsee 2

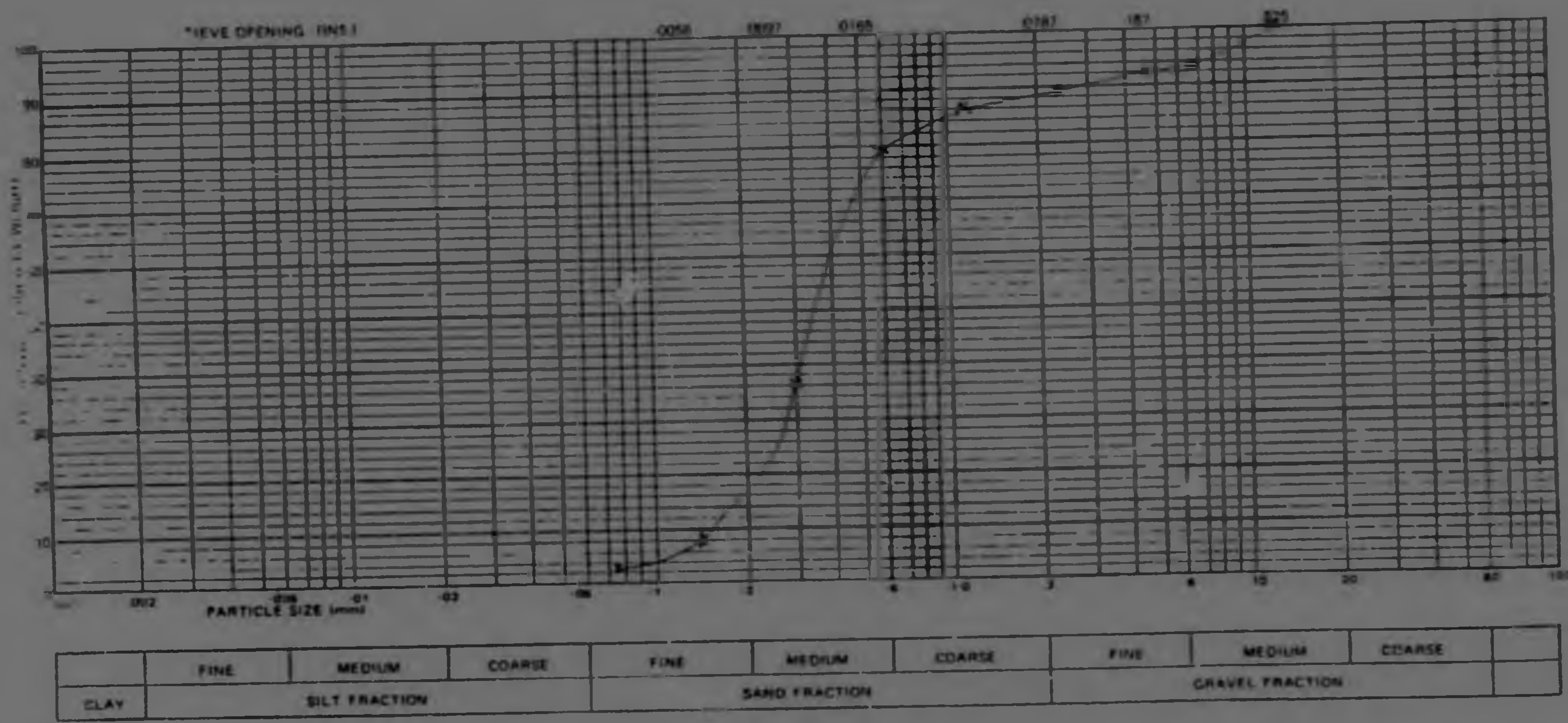

FIGURE C3(e) : Percent finer by weight, Kleinsee 3

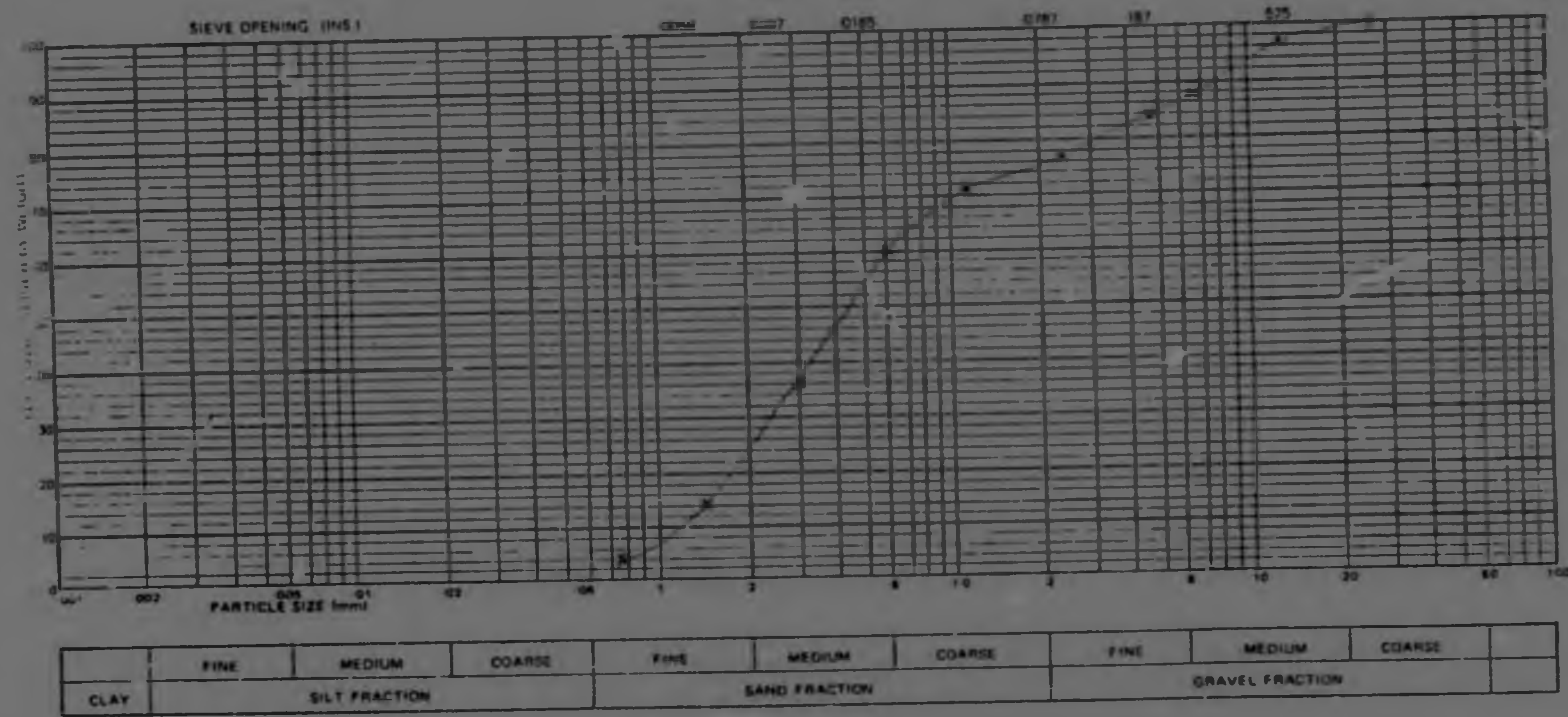

FIGURE C3(f) : Percent finer by weight, Twe[illegible]

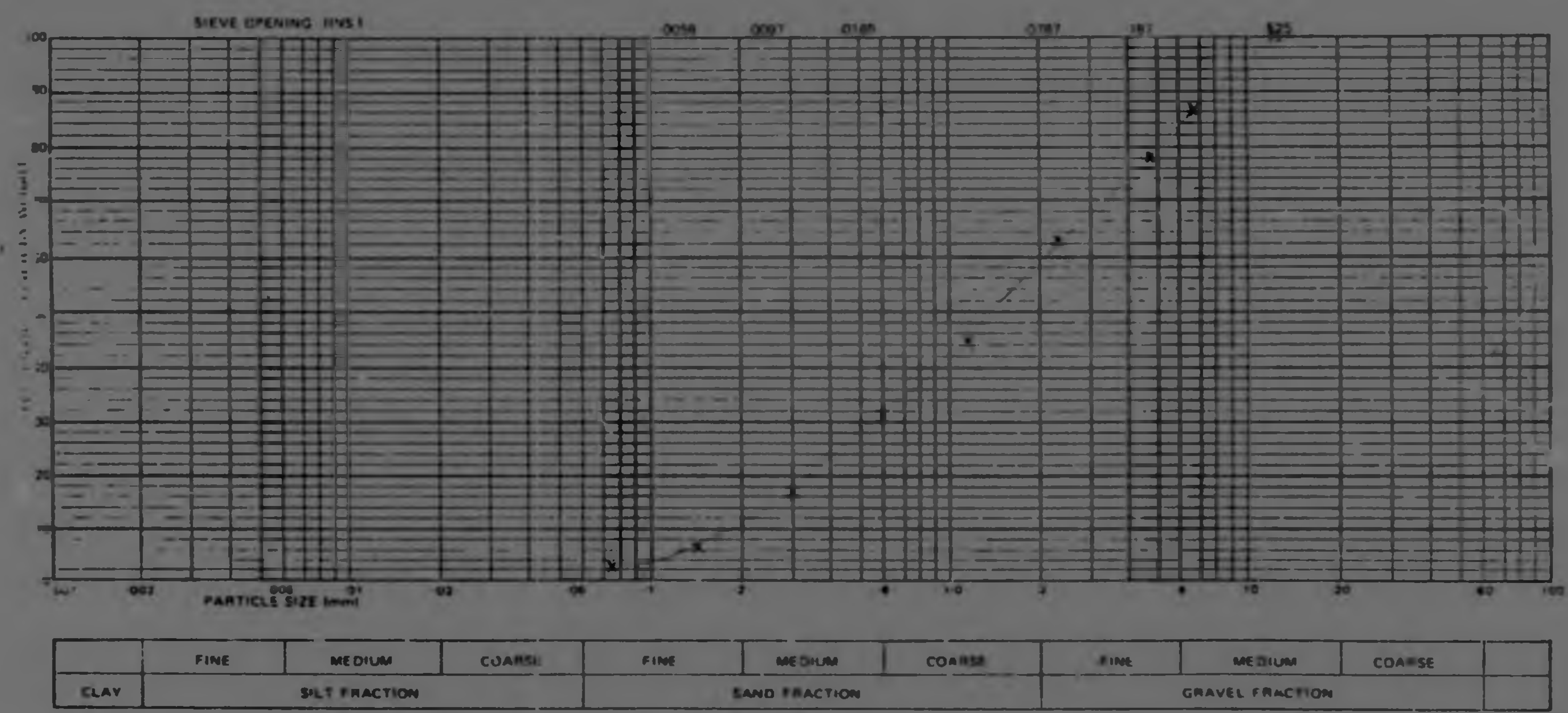

FIGURE C3(g) : Percent finer by weight, Koingnaas